Západočeská univerzita v Plzni
Fakulta aplikovaných věd

ZPŘESNĚNÍ PARAMETRŮ TÍHOVÉHO POLE ZEMĚ MODELOVÁNÍM VLIVU ZBYTKOVÝCH TERÉNNÍCH HMOT

Ing. Mgr. Martin Kadlec

disertační práce
k získání akademického titulu doktor
v oboru Geomatika

Školitel: Prof. Ing. Pavel Novák, Ph.D.

Katedra: Katedra matematiky

Plzeň 2011

University of West Bohemia
Faculty of Applied Sciences

REFINING GRAVITY FIELD PARAMETERS BY RESIDUAL TERRAIN MODELLING

Ing. Mgr. Martin Kadlec

Dissertation thesis in partial fulfillment of requirements
for
the degree of Doctor of Philosophy
in the subject of Geomatics

Supervisor: Prof. Ing. Pavel Novák, Ph.D.

Department: Department of Mathematics

Plzeň 2011

Declaration

I hereby declare that this Ph.D. thesis is completely my own work and that I used only the cited sources.

.....

Martin Kadlec

Acknowledgments

I would like to express my gratitude to my supervisor Pavel Novák for his support and inspiration without which this work would have been simply impossible.

I would like to thank my wife Martina for her support and love.

I would like to thank also our daughter Michaela, whose smile helped me many times during finishing this thesis.

Last, but not least, I would like to thank to my parents for their support during my studies.

Anotace

Tato disertační práce popisuje určení parametrů tíhového pole Země metodou kombinace dat z tíhových modelů s nižším prostorovým rozlišením a gravitačního účinku terénních hmot popsaných digitálním modelem terénu s vysokým prostorovým rozlišením.

V teoretické části nejprve popisujeme způsob výpočtu vybraných parametrů tíhového pole Země, kterými jsou gravitační potenciál a jeho první a druhá radiální derivace, respektive z nich odvozené veličiny výšková anomálie, tíhové zrychlení a gradient tíhového zrychlení. Kromě vztahů pro výpočet parametrů z globálních modelů tíhového pole Země se práce podrobně věnuje výpočtu gravitačních parametrů z terénních hmot. Terénní hmoty jsou rozložené na jedno základní geometricky jednoduché těleso, které generuje většinu gravitačního signálu, a na terénní efekt, který vyjadřuje vliv variace výšek v okolí výpočetního bodu.

Zvláštní pozornost je věnovaná geometrii zvoleného základního jednoduchého tělesa. Doposud se v geodézii volilo těleso tvaru nekonečné desky nebo kulové slupky. V práci ukazujeme, že pro výpočet lokálních efektů jsou taková tělesa nekompatibilní s terénním efektem, a odvozujeme gravitační potenciál a jeho první a druhou derivaci pro desku a kulovou slupku, které jsou omezené do určité vzdálenosti od výpočetního bodu.

Odvozené vztahy jsou dále použity pro výpočet zbytkového gravitačního účinku terénu, který je ze své podstaty lokálně omezený. Zbytkový gravitační účinek terénu představuje gravitační účinek těch hmot, které nejsou zahrnuty v tíhovém modelu s nižším prostorovým rozlišením. Protože se prostorové rozlišení tíhových modelů stále zvyšuje, klesá maximální nutná vzdálenost pro výpočet terénní korekce a místo vztahů pro neomezenou desku a kulovou

slupku nastupují vztahy odvozené v této práci.

Při výpočtu zbytkového gravitačního účinku terénu je nutné efekt jednoduchého tělesa a terénní opravy vypočítat dvakrát - od hodnot spočítaných z detailního modelu terénu musíme odečíst hodnoty již obsažené v tíhovém modelu. Při tomto postupu může nastat situace, že gravitační efekt je nutné spočítat uvnitř terénních hmot, což vyžaduje použití zobecněných vzorců nebo aplikaci tzv. harmonické korekce. V práci jsou originálně odvozeny všechny potřebné vztahy i pro tuto situaci, i když v závěru práce ukazujeme, že pro globální modely tíhového pole Země ve formě rozvoje potenciálu do řady kulových funkcí se tyto korekce aplikovat nemají.

V závěrečné praktické části práce spočítáme popsanou kombinační metodou tři parametry tíhového pole země pro území České republiky: tíhovou anomálii, gravitační zrychlení a gradient gravitačního zrychlení. V každém z těchto parametrů se jednotlivé složky kombinovaného postupu (složka z tíhového modelu, z jednoduchého tělesa a terénní oprava) projevují s jinou váhou, což umožňuje podrobně ověřit jejich význam a přesnost. Všechny tři vypočtené parametry jsou testované na měřických bodech (body GNSS/nivelace, gravimetrické body a gradiometrické body). Výsledky spočítané kombinační metodou prokazatelně zpřesňují výpočet tíhového zrychlení a gradientu oproti výsledkům spočítaným pouze z globálního modelu, u tíhové anomálie nelze o možném zpřesnění spolehlivě rozhodnout, protože přesnost vypočtených parametrů je zřejmě větší než přesnost měření na bodech GNSS/nivelace.

Annotation

This thesis deals with the determination of the gravity field of the earth by a combination of data from gravity models with lower resolution with gravity induced by terrain described by digital elevation model with high spatial resolution.

In the theoretical chapters we describe methods of evaluation for selected gravity field parameters, which are gravitational potential and its first and second radial derivative and also some derived parameters: height anomaly, gravity attraction and gravity gradient. Required formulas are derived for evaluation of these parameters from global geopotential models, but the biggest effort is dedicated to evaluation of the gravitational effect of terrain masses. Terrain is decomposed to one simple geometric body, which generates most of the effect, and terrain effect, which reflects the effect of variable elevation nearby the computational point.

Particular attention is devoted to the shape of the simple body. So far was used in geodesy an infinite slab or spherical shell. In this work we show that for the calculation of local effects such bodies are incompatible with terrain effect and we derive the gravitational potential and its derivatives to second order of a plate and a spherical shell, which are limited to a certain distance from the computational point.

Derived relations are then used to calculate the effect of the residual terrain masses, which are inherently limited locally. The residual terrain effect is the gravitational effect of those masses, that are not included in the gravity model with a lower spatial resolution. Because the spatial resolution of gravity models is still increasing, the maximum distance required to calculate the terrain correction is decreasing and we should use gravitational effects of

bodies which are derived in this work rather then effects of unlimited slab or shell.

When calculating the residual terrain effect, it is necessary to evaluate the effect of chosen simple body and terrain corrections twice — from the values computed from detailed DEM should be subtracted values of masses already contained in the gravity model. In this procedure, it may happen that gravitational effect is necessary to calculate inside the masses, which requires the use of generalized formulas or the application of the harmonic correction. In this thesis are derived all relations necessary for this situation, even if we show at the end that these corrections do not apply for global geopotential models given in a form of spherical harmonics coefficients.

In the final part of the thesis we calculate three parameters of the gravity field for the area of the Czech Republic by the proposed combined method. These parameters are gravity anomaly, gravitational acceleration and gravity gradient. In each of these parameters, the individual components of the combined procedure (the gravity model component, component of a simple body and terrain correction) play a different role, which allows to verify their relevance and accuracy. All three calculated parameters are tested at surveying points (GNSS/leveling points, gravimetric points and gradiometric points). Gravity acceleration and gravity gradients are proven to be calculated more accurately using our combinational method compared to values computed only form global geopotential models. For the gravity anomaly is not possible to reliably determine the improvement because the accuracy of calculated parameters is probably greater than the accuracy of GNSS/leveling points.

Contents

List of Figures

List of Tables

List of acronyms and abbreviations

Bpv Baltic Vertical Datum — After Adjustment (from Czech *Výškový systém baltský - po vyrovnání*)

CGS Czech Gravimetric Network (from Czech *Česká gravimetrická síť*)

CSNS Czech National Leveling Network (from Czech *Česká státní nivelační síť*)

DEM Digital Elevation Model

EGM96 Global geopotential model up to degree 360 published by NASA Goddard Space Flight Center in 1996 [Lemoine et al., 1998]

EGM08 Global geopotential model up to degree 2160 published by USA National Geospatial-Intelligence Agency in 2008 [Pavlis et al., 2008]

ETRS European Terrestrial Reference System

GGM Global Geopotential Model given by a set of Stokes coefficients and constants a, GM

GRS80 Geodetic Reference System 1980 [Moritz, 1980b]

ICGEM International Center for Global Gravity Field Models

IERS International Earth Rotation and Reference Systems Service

IUGG International Union of Geodesy and Geophysics

MES Mean Elevation Surface

NGA National Geospatial-Intelligence Agency of the USA

RTE Residual Terrain Effect

RTM Residual Terrain Modeling

S-JTSK Datum of Uniform Trigonometric Cadastral Network (from Czech *Souřadnicový systém Jednotné trigonometrické sítě katastrální*)

S-Gr95 Gravity System 1995

SRTM Shuttle Radar Topography Mission

SRTM3 Global DEM from SRTM with spatial resolution $3'' \times 3''$

TC Terrain Correction (negative terrain effect)

TE Terrain Effect

VÚGTK Research Institute of Geodesy, Topography and Cartography (from Czech *Výzkumný ústav geodetický, topografický a kartografický*)

WGS84 World Geodetic System 1984 [WGS84, 2010]

ZČU University of West Bohemia (from Czech *Západočeská univerzita v Plzni*)

ZÚ Czech Land Survey Office (from Czech *Zeměměřický úřad*)

Symbols

a	semi-major axis of an ellipsoid of revolution
b	semi-minor axis of an ellipsoid of revolution
c_n	gravity anomaly degree variance
C_{nm}	spherical harmonic coefficient
$\bar{C}_{nm}$	fully normalized spherical harmonic coefficient
Δg	gravity anomaly
e	first numerical eccentricity of an ellipsoid of revolution
E	Eötvös unit $[E] = [10^{-9} s^{-2}]$
f	flattening of an ellipsoid of revolution
g	magnitude of gravity vector
g_r	radial component of the gravity gradient
G	universal gravitational constant
GM	geocentric gravitational constant
h	height of terrain
h^g	height of mean elevation surface
J_2	dynamical form factor of an ellipsoid of revolution
ℓ	spatial distance

m	order of spherical harmonic expansion
M	total mass of the earth
n	degree of spherical harmonic expansion
N	prime vertical radius of curvature of an ellipsoid of revolution
N	maximal degree of spherical harmonic expansion
$P_n(t)$	Legendre polynomial
$\bar{P}_n(t)$	fully normalized Legendre polynomial
$P_{nm}(t)$	associated Legendre function of the first kind
$\bar{P}_{nm}(t)$	fully normalized associated Legendre function of the first kind
r	radius (spherical coordinate)
R	radius of a reference sphere
R_m	mean radius of the earth
S_{nm}	spherical harmonic coefficient
$\bar{S}_{nm}$	fully normalized spherical harmonic coefficient
T	disturbing gravitational potential
U	normal gravity potential
V_n	normal gravitational potential
V_r	first radial derivative of normal gravitational potential
V_{rr}	second radial derivative of normal gravitational potential
V	gravitational potential
W	gravity potential

δg	gravity disturbance
Δg	gravity anomaly
ϵ_o	mean omission error
γ	normal gravity
γ_a	normal gravity at the equator
γ_b	normal gravity at the poles
ζ	height anomaly
θ	spherical co-latitude (polar distance)
λ	longitude
φ	geodetic latitude
ψ	spherical distance between computation and integration points
ψ_0	maximal integration radius
Ψ	centrifugal potential
ρ	mean rock mass density
ω	mean angular velocity of the earth

Constants

IERS constants

symbol	*description*	*value*	*units*
G	universal gravitational constant	6.673×10^{-11}	$m^3 kg^{-1} s^{-2}$
W_0	gravity potential at the mean see level	62636856.0	$m^2 s^{-2}$
ω	mean angular velocity of the earth	7.292115×10^{-5}	$rad\ s^{-1}$

Table 1: IERS constants [McCarthy and Petit, 2004]

Other constants

symbol	*description*	*value*	*units*
ρ	mean mass rock density	2670	$kg\ m^{-3}$

Table 2: Physical constants [Heiskanen and Moritz, 1967]

WGS84 constants

symbol	*description*	*value*	*units*
a	semi-major axis	6378137	m
b	semi-minor axis	6356752.31414	m
R_m	mean earth radius	6371000	m
e^2	first eccentricity squared	$6.69437999014 \times 10^{-3}$	–
f	flattening	1/298.257222101	–
ω	angular velocity of the earth	7292115×10^{-11}	s^{-1}
GM	earth's gravitational constant	3986004.418×10^8	$m^3 s^{-2}$
γ_a	normal gravity at the equator	9.7803253359	ms^{-2}
γ_b	normal gravity at the poles	9.8321849378	ms^{-2}
J_2	dynamical form factor	0.00108263	–

Table 3: WGS84 parameters

Chapter 1

Introduction

1.1 Introduction

Almost all geodetic measurements depend on the earth's gravity field. Therefore, the *physical geodesy*, which deals with the description of the external gravity field of the earth, is an important part of geodesy. Models of the earth's external gravity field then serve not only in geodesy, but provide useful information about the interior of the earth also for other geosciences.

The gravity field of the earth can be split into two components: gravitational component and centrifugal component. Computation of the centrifugal component requires only knowledge of the position of the evaluational point and the angular velocity of the earth and can be nowadays handled with sufficient accuracy. On the other hand, the gravitational part remains challenging because the direct evaluation by the well known Newton's law of gravitation cannot be performed due to the lack of information about geometry and density of masses inside the earth. Instead, the gravitational models are based on various observations which are performed on the surface of the earth or above it. These observations include namely terrestrial and satellite gravimetry, satellite gradiometry and satellite altimetry.

The gravitational field is a potential field which implies that the natural quantity that can be used for description of the gravitational field is the gravitational potential. Using the potential theory, the gravitational potential outside the masses of the earth can be developed into series of spherical harmonic functions which are represented by a set of spherical harmonic coefficients. Such set of coefficients together with parameters GM (geocentric gravitational constant) and a (semi-major axis of reference ellipsoid) are called a global geopotential model (GGM). The main advantage of representing the gravitational potential as GGM is that using only one set of

parameters, one can compute many gravity field parameters such as gravity, gravity gradient, quasigeoid height or deflections of the vertical anywhere outside the earth. Because any model can be only an approximation of the reality, the theoretically unlimited harmonic series is cut off at some degree N and harmonic coefficients of higher degrees are neglected. The parameter N should be carefully selected so that it corresponds to the accuracy of the observations: choosing too small value causes too high omission (truncation) error whereas choosing too large N requires storing too many harmonic coefficients and consumes too much computational time without providing more accurate result. Despite the theoretical discussion about the convergence of the series ([Moritz, 1980a], [Shen, 2009]) there are nowadays no serious practical issues with it.

The progress in the spatial resolution and accuracy of GGM can be simply illustrated by the increasing N: first GGMs in 1960-1970 have N between 8 - 24, OSU78 GGM published in 1978 has $N = 180$ and EGM96 released in 1996 has $N = 360$. Detailed overview of historical models can be found at the web pages of the International Center for Global Gravity Field Models (ICGEM) [ICGEM, 2008] or in [Rapp, 1998]. The latest widely used and generally accepted GGM is the Earth Gravitational Model EGM08, which has been released by the USA National Geospatial-Intelligence Agency. EGM08 is complete to spherical harmonic degree and order 2159, and contains additional coefficients extending to degree 2190 and order 2159. The degree and order correspond to spatial resolution of $30' \times 30'$ (approximately 900 m at the equator).

Data used in the development of EGM08 were various physical quantities coming from many sources in the world. The final Stokes coefficients of EGM08 were computed from a global dataset of $5' \times 5'$ gravity anomalies

on the surface of the earth, which were downward continued to an ellipsoid where the harmonic analysis was performed. Even though the final model is represented by a set of spherical harmonic coefficients, the harmonic analysis was performed on an ellipsoid using ellipsoidal harmonic functions. The main advantage of ellipsoidal harmonics is that the distance between the surface of the earth and a reference ellipsoid is much smaller than distance between the surface of the earth and a reference sphere which significantly reduces errors caused by the unstable nature of the downward continuation of high resolution gravity anomalies. The ellipsoidal harmonic coefficients were then transformed into spherical harmonic coefficients which are well known to the geodetic community and can be manipulated by many widely used software packages.

The dataset of surface $5' \times 5'$ gravity anomalies was related to the global digital elevation model DTM2006.0, which served not only as a common surface for all gravity anomalies, but was used consistently in the computation of all terrain-related quantities necessary for the pre-processing of gravity data and for the development and subsequent use of EGM08 [Pavlis et al., 2006]. The gravity anomalies came from various sources that included according to [Pavlis et al., 2008] the Arctic gravity project, many national gravity databases of terrestrial and aerial gravimetry and satellite altimetry. Where no better sources were available, filling procedure based on evaluation of gravity from topography was used. The coefficients of lower degrees are based on a Grace only gravity field model ITG-GRACE03S [Mayer-Gürr, 2009] including its complete error covariance matrix to $N = 180$. Least-Squares Adjustment was used in order to combine the GRACE-only information with the coefficients implied solely by the database of gravity anomalies [Pavlis et al., 2008].

The final model EGM08 was independently tested shortly after its release by a Joint Working Group between the International Gravity Field Service and the International Association of Geodesy entitled "Evaluation of Global Earth Gravity Models". The first results of the EGM08 evaluation tests were presented by the working group members during the IAG international symposium "Geoid, Gravity and Earth Observation" in June 2008 in Chania, Greece. 25 peer-reviewed evaluation papers about the testing results were afterwards published in a special issue of Newton's Bulletin [Huang and Kotsakis, 2009]. This issue of Newton's Bulletin is the most comprehensive study of the accuracy of EGM08. It contains testing of the geoid computed from EGM08 at a global level (comparison with sea surface topography and geoids computed from other GGMs) and also testing at a national/regional level by comparison of the EGM08 geoid with GNSS/leveling observations. Terrestrial or aerial gravity anomalies were also tested in some countries, even though most of available gravity anomalies, contrary to GNSS/leveling observations, were used in the development of EGM08 and therefore testing gravity anomalies cannot be considered as an independent test. But it can at least show how accurate are gravity anomalies computed from the model with comparison with original input data and therefore validate the development process.

The testing results have shown very good quality of EGM08 particularly in Europe, where were available high quality gravity anomalies for the development of the model. The standard deviation of differences between quasigeoid or geoid heights and values observed at GNSS/leveling points was in order of centimeters for Europe: for example in Germany the standard deviation was 3.8 cm [Gruber, 2009], in Sweden 2.7 cm [Ågren, 2009] and in the Czech Republic 3.3 cm [Novák et al., 2009a]. In the other continents the

standard deviations were significantly higher, but still good when the quality and quantity of available input terrestrial gravity anomalies and also the quality of the testing points (possible systematic errors in leveling networks) is taken into account. The reported standard deviation for Australia was 17.3 cm [Claessens et al., 2009] and for South Africa 35 cm [Merry, 2009]. For USA, T. Gruber reported standard deviation 33.4 cm [Gruber, 2009] and M. Burša similar value 28.3 cm which are quite bad results, but D.R. Roman notes that the coordinates of GNSS/leveling points were updated in last years and some trends were removed and he reports the standard deviation 6.9 cm for the continental part of USA [Roman et al., 2009], which is good result for such a huge area.

Gravity anomalies computed from EGM08 were also compared with gravity anomalies evaluated from terrestrial or aerial gravimetric measurements. In Sweden, the standard deviation was 10 mGal [Ågren, 2009], in South America 20.43 mGal [Blitzkow and de Matos, 2009], in China from 12.5 mGal to 27 mGal [Li et al., 2009] (results were provided per provinces), but in Australia only 5 mGal (terrestrial gravimetric observations) or 4 mGal (airborne gravity observations) [Claessens et al., 2009]. In Florida, where were used for comparison gravity anomalies from aerial gravimetry, the standard deviation was 2.3 mGal [Roman et al., 2009].

This overview shows two interesting facts. The first fact is that the best results were obtained for aerial gravity anomalies in Florida and Australia, even though the accuracy of terrestrial gravity measurements is by orders better than accuracy of aerial gravimetry. The second interesting fact is that there is no correlation between quality of geoid heights and gravity anomalies: for example the standard deviation for geoid in Australia was 17.3 cm and for gravity anomalies 5 mGal, whereas in Sweden the standard deviations

were 2.7 cm for geoid and 10 mGal for gravity anomalies. Our hypothesis is that the issue is the accuracy of gravity anomalies computed from EGM08 which are significantly affected by a so-called omission error.

Each quantity computed from GGM suffers from *commission error*, which is caused by errors in observations which are propagated into Stokes coefficients, and *omission error*, which is caused by limited resolution which is expressed by maximal degree of GGM. The commission error is an inherent part of any GGM and can be hardly reduced. But the omission error represents the content which is missing in GGM and which can be added to quantities computed from GGM from some other sources. Such source is usually a terrain model, because the terrain generates the main part of the high-frequency content of the gravitational field, which is missing in GGM. Therefore, the effect of terrain masses can be evaluated separately using digital elevation model (DEM) and added to the reference part of the signal computed from GGM.

The good agreement between aerial and EGM08 gravity anomalies can be caused by the fact, that the aerial gravity anomalies do not contain such a strong signal in the highest frequencies as terrestrial data and the spectra of EGM08 gravity anomalies and aerial gravity anomalies are more similar. The aerial gravity suffers also from the omission error in the highest frequencies. The highest frequencies do not have to be either removed from aerial gravimetry or added to EGM08 to obtain comparable data as it is in terrestrial gravimetry.

The wide range of reported standard deviations between terrestrial gravity anomalies and gravity anomalies computed from EGM08 can have the same reason — the spectral inconsistency. Authors who have applied terrain corrections to reduce the omission error got lower standard deviations, i.e.

4.9 mGal in [Claessens et al., 2009], authors who have evaluated only the EGM08 gravity anomalies without terrain corrections got higher standard deviation, i.e. in 10.1 mGal in [Ågren, 2009], who explicitly remarks that his differences in gravity anomalies do contain the omission error. In [Li et al., 2009], a terrain reduction was applied, but the standard deviation is only about 12.5–27 mGal. We think that in this case the terrain reduction was overestimated, because a so called topographic-isostatic reduction has been applied as it is reported in [Li et al., 2009]. For such reduction, the topographic reduction is usually evaluated for larger areas around the gravity station, which can be also wrong, because it generates also a medium-frequency signal which is already in EGM08 and cannot be added again.

We have reviewed the studies of the accuracy of EGM08 to show that the EGM08 is accurate enough to generate high-quality low-frequency and medium-frequency gravitational signal. If we were able to add also a high-quality high-frequency content computed as a signal generated by terrain nearby the evaluation point, we would be able to model gravity field quantities with considerably better accuracy than from EGM08 itself. This do not hold only for gravity anomalies, the omission error affects any quantity computed from EGM08.

Our goal is to develop a method for predicting height anomalies, gravity anomalies and gravity gradient from EGM08 and high-resolution digital elevation models. This idea is not new and some studies have already tested similar approaches. For gravity anomalies, Forsberg in [Forsberg, 2009] reported the standard deviation 3.5 mGal between observed and modeled gravity anomalies after applying terrain corrections. Without the terrain corrections, the standard deviation was 11.6 mGal. The effects on height anomalies are studied in [Hirt et al., 2010] and [Jekeli et al., 2009] and the effects on

deflections of the vertical in [Hirt, 2010]. [Omang et al., 2010] has studied the effect of terrain and harmonic corrections on the accuracy of height anomalies and gravity anomalies. Zhu has studied the effect on gravity gradient in [Zhu, 2007] and [Zhu and Jekeli, 2009]. This short overview of recent publications on this topic shows that the chosen topic is highly actual in geodesy.

The gravitational effect of the terrain can be modeled either directly, for example by right rectangular prisms, or indirectly by splitting the topography to one simple geometric body, which generates most of the effect, and terrain effect, which reflects the effect of variable elevation nearby the computational point. When using the indirect approach, the split has to be done two times, once for the real terrain and once for the mean elevation surface. Both methods have their advantages and both are widely practically used. This topic is very wide and details can be found in [Heck and Seitz, 2007] or [Tsoulis et al., 2009]. We are focusing on the latter method in this thesis.

The issue is that also the global geopotential model already contains gravity signal generated by topography, which can be evaluated twice if it is not treated properly. Instead of evaluation of the effect of all topography nearby the computational point, we should evaluate only that part of topography, which is not covered by GGM. This is ensured by using two DEM: one of the highest possible resolution and accuracy, and second one of the same resolution as the GGM. The terrain between these two surfaces is called residual terrain and its effect is called residual terrain effect [Forsberg, 1984] and the method is called residual terrain modeling (RTM).

1.2 Goals

The main goal is to develop a method for precise computation of height anomalies, gravity anomalies and gravity gradient from GGM and DEM. To fulfil the main goal, we will perform these steps:

- Evaluate the omission error of EGM08 model for various quantities to get a rough estimate how much can the high-frequency component computed from the topography improve the EGM08 results. The terrain implied signal cannot do more than reduce the omission error.
- Develop a method based on RTM method for evaluation of gravity field quantities from EGM08 GGM in both spherical and planar approximations.
- Consider the effect of the harmonic reduction problem [Forsberg, 2009], [Omang et al., 2010].
- Evaluate selected gravity field quantities by the developed method in the Czech Republic and compare them with observed values.

Two particular issues require special attention. The first one is the extent of the simple geometric body, which was mentioned above. The second issue is the harmonic reduction problem.

So far was used in geodesy an infinite slab or spherical shell as the simple geometric body, which generates most of the topography effect. In this work we show that for the calculation of local effects such bodies are incompatible with terrain effect. We derive the gravitational potential and its derivatives to second order of a plate and a spherical shell, which are limited to a certain distance from the computational point so they are compatible with the classic terrain correction.

The second issue is the harmonic correction problem. We assume that the global gravity model contains effect of the mean elevation surface. If we want to evaluate some quantity above the mean elevation surface, we can just model the topography above and evaluate its effect. The situation differs for points under the mean elevation surface. Because the global model contains the effect of mean surface, we are evaluating the required quantity inside mean elevation surface, i.e. inside masses. This problem was pointed out already in [Forsberg, 1984]. In this work the problem is solved by introducing the so called harmonic correction for gravity anomalies. However, the harmonic correction was developed only for gravity anomaly and no other corrections were derived for other gravity field quantities. This problem becomes again important after release of EGM08, which gives more focus on RTM, because of high resolution and accuracy. Recently, the problem was recalled in [Forsberg, 2009] (the problem is pointed out, but not solved) and [Omang et al., 2010]. Our goal was to derive computational formulas, which evaluate the terrain effect and handle also the harmonic correction. We have succeeded and formulas for potential and its first and second derivatives are derived, but we are showing that there is no need for such correction when using global geopotential model in a form of expansion of the geopotential into spherical harmonics.

This work is organized as follows: The first chapter is the introduction you are now reading. The second chapter "Gravity modeling" describes modeling of gravity field quantities from global geopotential models and from topography. It contains also a short introduction to basic theory. In the section "Gravitational effects of topography" are derived some new formulas for the gravitational effect of the limited Bouguer plate and shell. In the third chapter, which deals with the residual terrain modeling, are the

formulas developed in Chapter 2 applied for residual terrain modeling using limited Bouguer plate and shell and including the harmonic correction. Most of derived relations are authors original work. The fourth chapter contains evaluation of our method for the area of the Czech Republic. We are evaluating three parameters of the earth's gravity field: gravity anomaly, gravitational acceleration and gravity gradient. All three calculated parameters are then tested at surveying points (GNSS/leveling points, gravimetric points and gradiometric points). The final Chapter 5 contains summary and conclusions.

Chapter 2

Gravity modeling

2.1 Basic theory

In this section, we will shortly describe used reference coordinate systems and the normal gravity field. We are not providing detailed description of basic geodetic theory as it can easily be found in books such as [Hoffmann-Wellenhof and Moritz, 2005]. We would like to remind also the list of used symbols and abbreviations at the beginning of this thesis, which can make its reading easier.

2.1.1 Coordinate systems

We will use several coordinate systems in this thesis. The geodetic coordinates represent a particular type of ellipsoidal coordinates which are used in geodesy usually for large-area and global problems. We will use them for evaluation of quantities from GGM (even though they will be transformed into spherical coordinates as EGM08 is based on spherical harmonic expansion). For derivation of terrain induced gravitational effect, we will use spherical and planar approximation, therefore we will introduce also Cartesian and spherical coordinates. Finally, for derivation of the gravitational effect of the Bouguer plate we will use the cylindrical coordinate system.

Geodetic coordinates

The triplet of coordinates φ, λ, h is a triplet of geodetic coordinates

φ geodetic latitude
λ longitude
h geodetic height.

Cartesian coordinates

The triplet of coordinates x, y, z is used for right-handed rectangular coordinate (Cartesian) system with origin in the earth's mass center and with z-axis coincidenting with the earth's mean axis of rotation. The x-axis is parallel to the meridian plane.

Spherical coordinates

The triplet of coordinates r, θ, λ are spherical coordinates

r radius (geocentric distance)
θ polar distance – spherical co-latitude
λ longitude.

Cylindrical coordinates

The triplet of coordinates r, α, z are cylindrical coordinates

r radius
α azimuth
z height.

A cylindrical coordinate system can be shortly described using the Cartesian system as a system that specifies point positions by the distance r from the reference z axis (not from the origin as in spherical coordinates), the azimuth α to projection of the point P to plane xy (measured from x axis), and the distance z from plane xy.

The ambiguity between spherical and cylindrical radii r should not occur as the cylindrical radius r will be used only in derivation of the gravitational potential of a cylinder.

2.1.2 Normal gravity field

The normal gravity field is a gravity field generated by a reference ellipsoid of revolution. It approximates the real gravity field of the earth quite well and therefore it is often used in geodesy. We will need some relations related to normal gravity field in this thesis, particularly in the last chapter, where normal gravity field parameters will be combined with disturbing or anomalous parameters calculated from EGM08.

The normal potential U can be computed by the series [Heiskanen and Moritz, 1967]

$$U(r,\theta) = \frac{GM}{r}\left[1 - \sum_{n=1}^{N=\infty} J_{2n}\left(\frac{a}{r}\right)^{2n} P_{2n}\left(\cos\theta\right)\right], \tag{2.1}$$

where $P_{2n}(\cos\theta)$ are Legendre polynomials and coefficients J_{2n} are given by

$$J_{2n} = (-1)^{n+1}\frac{3e^{2n}}{(2n+1)(2n+3)}(1 - n + 5nJ_2e^{-2}). \tag{2.2}$$

Practically, we stop the summation at $n = 10$ because the series converges very fast.

The normal gravity γ at the surface of the reference ellipsoid is computed by Somigliana formula [Heiskanen and Moritz, 1967]

$$\gamma(\varphi) = \frac{a\gamma_a\cos^2\varphi + b\gamma_b\sin^2\varphi}{\sqrt{a^2\cos^2\varphi + b^2\sin^2\varphi}}, \tag{2.3}$$

and above the ellipsoid as [Heiskanen and Moritz, 1967]

$$\gamma(\varphi,h) = \gamma(\varphi)\left[-\frac{2}{a}\left(1 + f + m - 2f\sin^2\varphi\right)h + \frac{3}{a^2}h^2\right]. \tag{2.4}$$

2.2 Gravity prediction from GGM

2.2.1 Global geopotential models

Global geopotential models (GGM) are used for large-scale problems including the determination of satellite orbits, inertial navigation and development of other geophysical and geodynamic models. From GGM can be evaluated a global geoid (quasigeoid) that can be used as a global vertical reference system [Torge, 2001]. In this thesis, the most recent GGM called EGM08 will be used to calculate the reference part of gravity field quantities. The overall description of GGMs (and particularly EGM08) including their history and important properties was provided in section 1.1.

The following sections contain review of some fundamental facts about spherical harmonics and show basic equations for evaluation of the gravity potential W, gravity g and vertical gravity gradient g_r.

2.2.2 Spherical harmonics

Scalar function f harmonic outside a geocentric sphere of radius R can be expressed in spherical coordinates for any $r > R$ as [Heiskanen and Moritz, 1967]

$$f(r,\theta,\lambda) = \frac{1}{r}\sum_{n=0}^{\infty}\left(\frac{R}{r}\right)^n \sum_{m=0}^{n}(C_{nm}\cos m\lambda + S_{nm}\sin m\lambda)P_{nm}(\cos\theta), \quad (2.5)$$

where C_{nm} and S_{nm} are coefficients of the expansion and $P_{nm}(t)$ are associated Legendre functions of the first kind. Instead of $P_{nm}(t)$, in geodesy are used fully normalized associated Legendre functions of the first kind $\bar{P}_{nm}(t)$ [Torge, 2001]

$$\bar{P}_{nm}(t) = \sqrt{k(2n+1)\frac{(n-m)!}{(n+m)!}}P_{nm}(t) \quad (2.6)$$

where $k = 1$ for $m = 0$ and $k = 2$ for $m > 0$.

$$f(r,\theta,\lambda) = \frac{1}{r}\sum_{0}^{\infty}\left(\frac{R}{r}\right)^n \sum_{m=0}^{n}(\bar{C}_{nm}\cos m\lambda + \bar{S}_{nm}\sin m\lambda)\bar{P}_{nm}(\cos\theta). \quad (2.7)$$

Its derivatives $\frac{\partial f}{\partial r}$, $\frac{\partial f}{\partial \theta}$ and $\frac{\partial f}{\partial \lambda}$ are given by

$$\frac{\partial f}{\partial r} = \frac{1}{r^2}\sum_{n=0}^{\infty}(n+1)\left(\frac{R}{r}\right)^n \sum_{m=0}^{n}\left(\bar{C}_{nm}\cos m\lambda + \bar{S}_{nm}\sin m\lambda\right)\bar{P}_{nm}(\cos\theta), \quad (2.8)$$

$$\frac{\partial f}{\partial \theta} = -\frac{\sin\theta}{r}\sum_{n=0}^{\infty}\left(\frac{R}{r}\right)^n \sum_{m=0}^{n}\left(\bar{C}_{nm}\cos m\lambda + \bar{S}_{nm}\sin m\lambda\right)\cdot\bar{P}'_{nm}(\cos\theta), \quad (2.9)$$

$$\frac{\partial f}{\partial \lambda} = \frac{1}{r}\sum_{n=0}^{\infty}\left(\frac{R}{r}\right)^n \sum_{m=0}^{n} m\left(\bar{S}_{nm}\cos m\lambda - \bar{C}_{nm}\sin m\lambda\right)\bar{P}_{nm}(\cos\theta), \quad (2.10)$$

where

$$\bar{P}'_{nm}(t) = \frac{d}{dt}\bar{P}_{nm}(t), \quad (2.11)$$

is the first derivative of the fully normalized associated Legendre function with respect to its parameter t. In (2.9), we need the derivative with respect to argument $t = \cos\theta$ which is by the chain rule

$$\frac{d}{d\theta}\bar{P}_{nm}(\cos\theta) = -\bar{P}'_{nm}(\cos\theta)\sin\theta \quad (2.12)$$

The second radial derivative of the function f is given by

$$\frac{\partial^2 f}{\partial r^2} = \frac{1}{r^3}\sum_{n=0}^{N}(n+2)(n+1)\left(\frac{R}{r}\right)^n \sum_{m=0}^{n}\left(\bar{C}_{nm}\cos m\lambda + \bar{S}_{nm}\sin m\lambda\right)\bar{P}_{nm}(\cos\theta) \quad (2.13)$$

2.2.3 Evaluation of potentials V, W and T

The gravitational potential V can be evaluated from GGM by summation of series, see (2.5)

$$V(r,\theta,\lambda) = \frac{GM}{r}\sum_{n=0}^{N}\left(\frac{a}{r}\right)^n \sum_{m=0}^{n}\left(\bar{C}_{nm}\cos m\lambda + \bar{S}_{nm}\sin m\lambda\right)\bar{P}_{nm}(\cos\theta), \quad (2.14)$$

where N is maximal degree of given GGN.

The gravity potential W can be expressed by adding the centrifugal potential $\Phi(r, \theta)$ which is given by [Heiskanen and Moritz, 1967]

$$\Phi(r, \theta) = \frac{1}{2}\omega^2 r^2 \sin^2 \theta, \tag{2.15}$$

where ω is the mean angular velocity of the earth, so W becomes

$$W(r, \theta, \lambda) = \frac{GM}{r} \sum_{n=0}^{N} \left(\frac{a}{r}\right)^n \sum_{m=0}^{n} \left(\bar{C}_{nm} \cos m\lambda + \bar{S}_{nm} \sin m\lambda\right) \bar{P}_{nm}(\cos \theta) + \\ + \frac{1}{2}\omega^2 r^2 \sin^2 \theta. \tag{2.16}$$

For derivation of the disturbing gravity potential T, we have to introduce normal gravity field and the potential of this field, see subsection 2.1.2 The normal gravity field is a generated by a level ellipsoid of total mass M which is rotating along its semi-minor axis with the mean angular velocity ω. Potential U of such a gravity field is uniquely determined only by four constants (e.g., semi-major and semi-minor axes a, b, M and ω [Heiskanen and Moritz, 1967]). The normal gravity potential can be divided (as well as the gravity potential W) to gravitational and centrifugal parts

$$U = V_n + \Phi, \tag{2.17}$$

where V_n is the normal gravitational potential.

V_n is a harmonic function outside the reference ellipsoid and can be expanded into series of spherical harmonics of the form

$$V_n(r, \theta) = \frac{GM}{r} \sum_{n=0}^{\infty} \left(\frac{a}{r}\right)^n \bar{J}_n \bar{P}_n(\cos \theta), \tag{2.18}$$

where only even degree coefficients $\bar{J}_n$ are non-zero. It can be computed from the above mentioned four constants [Heiskanen and Moritz, 1967]. The

series converges very rapidly and only 5 non-zero $\bar{J}_n$ coefficients ($N = 10$) are usually taken into account.

The normal gravity potential U differs from (2.18) again only by adding the centrifugal potential Φ

$$U(r, \theta, \lambda) = \frac{GM}{r} \sum_{n=0}^{\infty} \left(\frac{a}{r}\right)^n \bar{J}_n \bar{P}_n(\cos\theta) + \frac{1}{2}\omega^2 r^2 \sin^2\theta. \tag{2.19}$$

Disturbing gravity potential T

The disturbing gravity potential is defined as

$$T = W - U. \tag{2.20}$$

Neither W nor U can be expressed in spherical harmonics, because they both contain Φ and therefore are not harmonic. But T can be easily expressed as

$$T = V - V_n, \tag{2.21}$$

where both V and V_n can be expanded into spherical harmonics as was shown before in equations (2.14) and (2.18). If the earth's gravitational constant GM and semi-major axes a of GGM and of the reference ellipsoid defining the normal field are equal, the series for V and V_n can be computed in one step introducing new set of Stokes's coefficients

$$\begin{aligned} \Delta\bar{C}_{nm} &= \bar{C}_{nm} - \bar{J}_n \quad && \text{for } m = 0 \\ \Delta\bar{C}_{nm} &= \bar{C}_{nm} && \text{for } m \neq 0 \\ \Delta\bar{S}_{nm} &= \bar{S}_{nm} \end{aligned} \tag{2.22}$$

If the constants differ, either the coefficients $\bar{C}_{nm}$ and $\bar{S}_{nm}$ or $\bar{J}_n$ have to be accordingly rescaled, for details see [Heiskanen and Moritz, 1967].

2.2.4 Gravity g

Gravity g, gravity anomaly Δg and gravity disturbance δg are examples of quantities related to first order radial derivative of the potential V_r. From GGM are usually computed only disturbing or anomalous quantities Δg and δg, but we will show also computational formula for g itself, without any reduction by normal field. Later in this thesis, we will test quantities computed from EGM08 and supported by terrain induced gravitation on gravity stations in the Czech Republic, where we have g as a main parameter. We have decided to evaluate g also from EGM08 and test this quantity instead of Δg. Evaluation of g is more challenging, because it would not hide any single error (for example in heights), which could be hidden when using smooth quantities as Δg. Because evaluation of g from GGM is not common, we provide at this place its more comprehensive description than for other quantities.

Basic relations

The gravity vector $\mathbf{g}$ is defined as

$$\mathbf{g} = \text{grad } W \tag{2.23}$$

where W is the potential of the gravity field of the earth. The gradient can be expressed in spherical coordinates as

$$\text{grad } W = \frac{1}{r}\frac{\partial W}{\partial \theta}\mathbf{e}_\theta + \frac{1}{r\sin\theta}\frac{\partial W}{\partial \lambda}\mathbf{e}_\lambda + \frac{\partial W}{\partial r}\mathbf{e}_\mathbf{r}, \tag{2.24}$$

where $(\mathbf{e}_\theta, \mathbf{e}_\lambda, \mathbf{e}_\mathbf{r})$ is a triplet of unity vectors in θ, λ and r directions.

The magnitude of the gravity vector g (called also simply *gravity*) is given as

$$g = |\mathbf{g}|. \tag{2.25}$$

Inserting (2.24) into (2.25) yields

$$g = \sqrt{\left(\frac{1}{r}\frac{\partial W}{\partial \theta}\right)^2 + \left(\frac{1}{r\sin\theta}\frac{\partial W}{\partial \lambda}\right)^2 + \left(\frac{\partial W}{\partial r}\right)^2}. \tag{2.26}$$

Gravity g can be expressed also as [Heiskanen and Moritz, 1967]

$$g = -\frac{\partial W}{\partial H}, \tag{2.27}$$

where ∂H is the differential element of the orthometric height H (which is measured along the plumb line but has the opposite direction).

The direction of the real plumb line is usually unknown. Two approximations of the direction of the plumb line may be introduced into (2.27): a spherical approximation or an ellipsoidal approximation.

In the spherical approximation, the plumb line is approximated by the normal to the geocentric sphere (radius) r

$$g = -\frac{\partial W}{\partial H} \approx -\frac{\partial W}{\partial r}, \tag{2.28}$$

so g is computed as a radial derivative of W.

In the ellipsoidal approximation, the plumb line is approximated by the ellipsoidal normal n

$$g = -\frac{\partial W}{\partial H} \approx -\frac{\partial W}{\partial n}. \tag{2.29}$$

The gravity g in the **spherical approximation** is given by

$$g \approx -\frac{\partial W}{\partial r} = -\frac{\partial (V+\Psi)}{\partial r} = -\frac{\partial V}{\partial r} - \frac{\partial \Psi}{\partial r}, \tag{2.30}$$

which becomes

$$g \approx \frac{GM}{r^2}\sum_{n=0}^{N}(n+1)\left(\frac{a}{r}\right)^n \sum_{m=0}^{n}\left(\bar{C}_{nm}\cos m\lambda + \bar{S}_{nm}\sin m\lambda\right)\bar{P}_{nm}(\cos\theta) - \omega^2 r\sin^2\theta. \tag{2.31}$$

The series for evaluating g in the **ellipsoidal approximation** is according to [Wenzel, 1999]

$$g \approx -\frac{\partial W}{\partial n} = \frac{GM}{r^2}\sum_{n=0}^{N}\left(\frac{a}{r}\right)^n \sum_{m=0}^{n}\left(\bar{C}_{nm}\cos m\lambda + \bar{S}_{nm}\sin m\lambda\right)\cdot$$
$$\cdot\left(\sin(\varphi+\theta)(n+1)\bar{P}_{nm}(\cos\theta) + \cos(\varphi+\theta)\sin(\theta)\bar{P}'_{nm}(\cos\theta)\right) + \quad (2.32)$$
$$- \omega^2 r\sin^2\theta$$

where φ is the ellipsoidal (geodetic) latitude and $\bar{P}'_{nm}(\cos\theta)$ is given by (2.12)

GGM itself can be used for even better approximation of the plumb line. Let us call the method **GGM approximation**. We start again with

$$g = \sqrt{\left(\frac{1}{r}\frac{\partial W}{\partial\theta}\right)^2 + \left(\frac{1}{r\sin\theta}\frac{\partial W}{\partial\lambda}\right)^2 + \left(\frac{\partial W}{\partial r}\right)^2}, \quad (2.33)$$

where $\frac{\partial W}{\partial\theta}$ and $\frac{\partial W}{\partial\lambda}$ are given by

$$\frac{\partial W}{\partial\theta} = -\frac{GM\sin\theta}{r}\sum_{n=0}^{N}\left(\frac{a}{r}\right)^n\sum_{m=0}^{n}\left(\bar{C}_{nm}\cos m\lambda + \bar{S}_{nm}\sin m\lambda\right)\cdot\bar{P}'_{nm}(\cos\theta) +$$
$$+\omega^2 r^2\sin\theta\cos\theta, \quad (2.34)$$
$$\frac{\partial W}{\partial\lambda} = \frac{GM}{r}\sum_{n=0}^{N}\left(\frac{a}{r}\right)^n\sum_{m=0}^{n} m\left(\bar{S}_{nm}\cos m\lambda - \bar{C}_{nm}\sin m\lambda\right)\bar{P}_{nm}(\cos\theta), \quad (2.35)$$

and $\frac{\partial W}{\partial r}$ is given by

$$\frac{\partial W}{\partial r} = -\frac{GM}{r}\sum_{n=0}^{N}(n+1)\left(\frac{a}{r}\right)^n\sum_{m=0}^{n}\left(\bar{C}_{nm}\cos m\lambda + \bar{S}_{nm}\sin m\lambda\right)\bar{P}_{nm}(\cos\theta) +$$
$$+ \omega^2 r\sin^2\theta. \quad (2.36)$$

2.2.5 Vertical gravity gradient g_r

The vertical gravity gradient is defined as

$$g_r = \frac{\partial g}{\partial H} \quad (2.37)$$

where H is height, which in (2.37) represents direction of the plumb line. We can again introduce the spherical, ellipsoidal or GGM approximation, but in the case of vertical gravity gradient the radial part is determining so we will use only the spherical approximation

$$g_r \approx \frac{\partial g}{\partial r} \approx \frac{\partial^2 W}{\partial r^2}. \tag{2.38}$$

In terms of spherical harmonics we have

$$\frac{\partial^2 W}{\partial r^2} = \frac{GM}{r^3} \sum_{n=0}^{N} \left((n+2)(n+1) \left(\frac{a}{r} \right)^n \cdot \right.$$
$$\left. \cdot \sum_{m=0}^{n} \left(\bar{C}_{nm} \cos m\lambda + \bar{S}_{nm} \sin m\lambda \right) \bar{P}_{nm}(\cos\theta) \right) + \omega^2 \sin^2\theta.$$

2.2.6 Omission errors

Each GGM is limited to certain maximal degree N. If we compute any quantity from GGM, we may be interested in what additional information is available in the higher degree potential coefficients [Rapp, 1973]. The missing information is called the omission or truncation error and can be estimated using anomaly degree variance models. In this subsection, we will show estimates of the omission errors for quantities computed in this thesis from EGM08.

The mean omission error for gravity anomaly $\epsilon_o(\Delta g)$ can be computed by summation of the series above the maximal degree N

$$\epsilon_o(\Delta g) = \sum_{n=N+1}^{\infty} c_n \tag{2.39}$$

where c_n are gravity anomaly degree variances [Torge, 2001]

$$c_n = \left(\frac{GM}{R} \right)^2 \left(\frac{(n-1)}{R} \right)^2 \sum_{m=0}^{n} (\bar{C}_{nm}^2 + \bar{S}_{nm}^2). \tag{2.40}$$

To calculate mean omission error for other quantities, gravity anomaly degree variances can be recalculated. For height anomaly we get [Sjöberg, 2011]

$$\epsilon_o(\zeta) = \left(\frac{1}{\gamma}\right)^2 \left(\frac{R}{(n-1)}\right)^2 \sum_{n=N+1}^{\infty} c_n \tag{2.41}$$

where we have reordered the expression on the right side of the equation to emphasize the transformation of c_n to disturbing potential degree variances (the second bracketed term) and transformation to height anomalies (the first bracketed term). Similarly, the mean omission error for second radial derivative of the disturbing potential $\epsilon_o(T_{rr})$ can be expressed as

$$\epsilon_o(T_{rr}) = \left(\frac{(n+1)(n+2)}{R^2}\right)^2 \left(\frac{R}{(n-1)}\right)^2 \sum_{n=N+1}^{\infty} c_n \tag{2.42}$$

Because we do not know Stokes coefficients $\bar{C}_{nm}$, $\bar{S}_{nm}$ for degree $n > N$, we cannot calculate c_n and the mean omission errors directly. Instead, we should use some model of degree variances.

The first model we use is the standard Tscherning–Rapp model [Tscherning and Rapp, 1974]

$$c_n = A\frac{(n-1)}{(n-2)(n+B)}\left(\frac{R_B}{R}\right)^{2(n+2)} \tag{2.43}$$

where parameters $R = 6371000$ m, $A = 425.28$ mGal^2, $B = 24$ and $R_B = R - 1225$ m were adopted from [Ågren, 2004]. Even though this model is quite old, it is still widely used and generally accepted.

The second model is a model derived by Flury in [Flury, 2006]. This model is based on the analysis of gravity anomalies from 13 test regions in various geographical areas and geophysical settings, using various power spectrum computation approaches and should be valid for wavelengths between 0.7

and 100 km, which corresponds to degree variance spectra range from degree 400 to 57,000 [Flury, 2006]. The degree variance model reads

$$c_n = \frac{6.8 \times 10^7 \ mGal^2}{(n + 0.5)^{3.09}} \tag{2.44}$$

The estimates of mean omission errors for model Tscherning–Rapp are shown in Table 2.1 and for model Flurry (2006) in Table 2.2. The summation of infinite series was stopped at degree 100000.

N	$\epsilon_o(\zeta)$ $[m]$	$\epsilon_o(\Delta g)$ $[mGal]$	$\epsilon_o(T_{rr})$ $[E]$
180	0.23	25.2	83.6
360	0.10	20.1	82.6
1800	0.03	12.6	77.3
2160	0.02	11.1	75.0
3600	0.01	7.1	64.9

Table 2.1: Omission error model Tscherning/Rapp for maximum degree N

N	$\epsilon_o(\zeta)$ $[m]$	$\epsilon_o(\Delta g)$ $[mGal]$	$\epsilon_o(T_{rr})$ $[E]$
180	0.21	24.2	512.8
360	0.09	19.8	512.7
1800	0.03	15.0	512.2
2160	0.02	14.2	511.9
3600	0.01	12.1	510.9

Table 2.2: Omission error model Flurry (2006) for maximum degree N

The omission error for height anomaly is very similar for both models and we can conclude that omission error for height anomalies computed

from EGM08 is $\epsilon_o(\zeta) \approx 3\ cm$. The omission error for gravity anomaly is slightly higher in the model Flurry (2006), particularly for higher degrees. For EGM08, $\epsilon_o(\Delta g)$ can be expected in range $10 - 15$ mGal. We should remark that Flury used refined Bouguer anomalies and RTM anomalies to derive his model instead of free-air gravity anomalies. Because refined Bouguer anomalies are smoother than free-air gravity anomalies, we would expect $\epsilon_o(\Delta g)$ from model Flury to be lower than from model Tscherning–Rapp, but the opposite was true.

In case of $\epsilon_o(T_{rr})$ the results are very different. The mean value of the gravity gradient on the surface of the earth is 3080 E so the difference between estimated omission errors 75.0 E and 511.9 E for the disturbing quantity is relatively very high. We can only conclude that in both models, increasing N has only very little effect on the accuracy of T_{rr} and the omission error remains high.

Estimates of omission errors provided in this subsection will be compared with generated terrain induced signal, which is supposed to generate the missing signal, in the last chapter of this thesis.

2.3 Gravitational effects of topography

2.3.1 Bouguer layer and terrain correction

This section deals with evaluation of the gravitational signal from topography. We will study the effect of topography on three different gravity field quantities: the gravitational potential V and its first and second order radial derivatives $\partial V/\partial r$, $\partial^2 V/\partial r^2$.

The term "topography" represents all masses between the reference level (geoid, quasigeoid, ellipsoid) and the surface of the earth. The effect of topography can be studied either globally (all topographical masses over the whole earth are taken into account) or locally (only masses up to some distance from a computational point are taken into account). We will focus on evaluation of the effect of the local masses, because our aim is to combine a short-wavelength signal from topography with a long-wavelength signal from GGM, which already contains effect of distant masses.

The total gravitational effect of topography for a particular point P with height $h(P)$ can be divided into two parts: the effect of Bouguer layer and the terrain correction. The Bouguer layer is a layer of constant height $h(P)$ above the reference surface and the terrain correction is the part of topography above or below the Bouguer layer. The shape of the Bouguer layer depends on approximation of the reference level and the point P level (horizon). In planar approximation, the Bouguer layer becomes a Bouguer plate — an unlimited plate of thickness $h(P)$. In the spherical approximation, the Bouguer layer becomes a spherical shell of thickness $h(P)$, which is called the Bouguer shell.

This section is organized as follows: Subsections 2.3.2 – 2.3.5 describe the effect of the Bouguer plate and the Bouguer shell. The following subsections are dedicated to the evaluation of the terrain correction. The prism

and tesseroid modeling methods are described and a combined method is introduced. These subsections are based on an article [Tsoulis et al., 2009], but contrary to the mentioned article, where only the terrain corrections for V_r is evaluated, we evaluate also the terrain correction for V and V_{rr} in this thesis.

During the derivation, we are sometimes use approximation and neglect some parts of expression. The effect of each neglected term was carefully considered during the derivation, either analytically using the Wolfram Mathematica software package for manipulating algebraic expressions or numerically in more complicated cases. Unfortunately it was not possible to explain each algebraic step in detail. To support the credibility of derived expressions, we provide some plots and tables with numerical comparison of all important approximate formulas with their exact counterparts.

2.3.2 Limited Bouguer plate

Geometry of the plate

The Bouguer plate is usually defined as an unlimited planar layer of constant density ρ with thickness h (see Figure 2.1). However, sometimes it may be useful to limit the radius of the Bouguer plate and use only a cylinder instead of the unlimited plate, which is traditionally used in geodesy, e.g. [Heiskanen and Moritz, 1967]. We will use terms *unlimited Bouguer plate* for an unlimited plate (which can be considered as a cylinder with infinite radius) and *limited Bouguer plate* for a cylinder with finite radius R.

Let us start with the limited Bouguer plate that has a shape of the cylinder. We want to derive the gravitational potential and its first and second derivatives for an evaluation point P lying anywhere on the vertical axis of

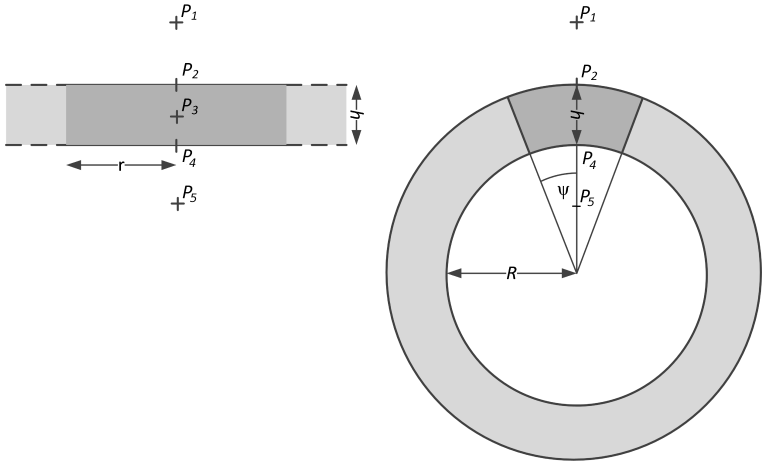

Figure 2.1: *Bouguer plate and shell.* The unlimited (light gray) and limited (dark gray) Bouguer plate and Bouguer shell.

the Bouguer plate (see Figure 2.2): above the plate (point $P_1(z > 0)$), on the top of the plate ($P_2(z = 0)$), inside the plate (point $P_3(0 < z < -h)$) on the bottom of the plate (point $P_4(z = -h)$) or under the plate ($P_5(z < -h)$). Because at least one of the second derivatives of the gravitational potential is expected to be a discontinuous function [Heiskanen and Moritz, 1967] at points P_2 and P_4, we will keep the methodology used in [Burša, 2004] : first we will express the potential for points P_1, P_3 and P_5 which are outside or inside the cylinder. Then we can express the potential on the cylinder as the limit case of these potentials. For V and V_r, the limits from both left and right should be equal at these points. For V_{rr}, its limits from left and right will differ. Note that contrary to the derivations shown in [Burša, 2004] and [Heiskanen and Moritz, 1967] we use a slightly different position of the cylinder. In our case, the center of the coordinate system lies on the top of the cylinder, see figure 2.2. This has two advantages: First, the derived

formulas are simpler. Second, we will combine obtained formulas with terrain corrections, where point P lies on the top of the cylinder and it should be in the center of the coordinate system (to keep consistency with usual expression for terrain corrections).

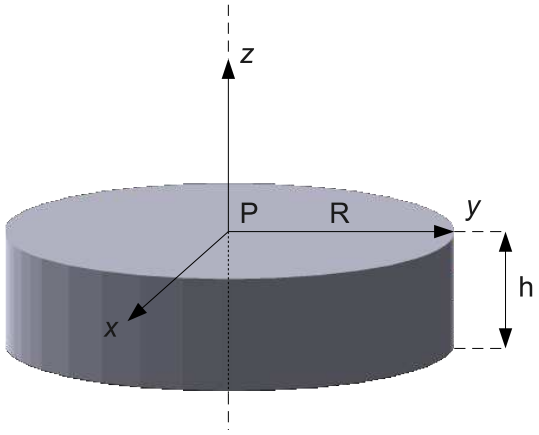

Figure 2.2: *Limited Bouguer plate (cylinder)*

Gravitational potential V

The gravitational potential at the point $P(z)$ lying anywhere on the z axis is given by

$$V(P) = G\rho \int_0^{2\pi} \int_0^R \int_{-h}^0 \sqrt{r'^2 + (z - z')^2} r' dz' dr' d\alpha'. \tag{2.45}$$

Potential for the point P_1 above the cylinder is given by solution of the integral (2.45) under condition $z > 0$. The result is

$$V(P_1) = G\rho\pi \left(R^2 \log \frac{\ell_h + h + z}{z + \ell_0} - h^2 + h\left(\ell_h - 2z\right) + z\left(\ell_h - \ell_0\right) \right) \tag{2.46}$$

where ℓ_h and ℓ_0 are substitutions for

$$\ell_h = \sqrt{R^2 + (h+z)^2} \tag{2.47}$$

$$\ell_0 = \sqrt{R^2 + z^2} \tag{2.48}$$

To get the potential at the point P_3 inside the cylinder, we should solve the integral (2.45) under condition $z < 0 \wedge z > -h$. We get

$$V(P_3) = G\rho\pi\left(R^2 \log \frac{\ell_h + h + z}{z + \ell_0} - h^2 + h(\ell_h - 2z) - 2z^2 + z(\ell_h - \ell_0)\right). \tag{2.49}$$

The potential at the point P_5 under the cylinder is given by solving the integral (2.45) under condition $z < -h$. We obtain

$$V(P_5) = G\rho\pi\left(R^2 \log \frac{\ell_h + h + z}{z + \ell_0} + h^2 + h\,(\ell_h + 2z) + z\,(\ell_h - \ell_0)\right). \tag{2.50}$$

Because the gravitational potential is a continuous function throughout the space, the potential on the top of the cylinder (point P_2) can be evaluated by introducing $z = 0$ into (2.46) or by introducing $z = 0$ into (2.49). Both results are after few simple manipulations equal. Finally, the potential in the point P_2 is

$$V(P_2) = G\rho\pi\left(R^2 \log \frac{\sqrt{h^2 + R^2} + h}{R} - h^2 + h\sqrt{h^2 + R^2}\right) \tag{2.51}$$

Similarly, the potential at the bottom of the cylinder (point P_4) can be obtained either by introducing $z = -h$ into (2.49) or by introducing $z = -h$ into (2.50). The result is

$$V(P_4) = G\rho\pi\left(R^2 \log \frac{R}{\sqrt{h^2 + R^2} - h} + h^2 + h\sqrt{h^2 + R^2}\right). \tag{2.52}$$

All formulae (2.46), (2.51), (2.49), (2.52) and (2.50) can be generalized to form

$$V = G\rho\pi\left(R^2 \log \frac{\ell_h + h + z}{z + \ell_0} - (h+z)|h+z| + z|z| + z\ell_h + h\ell_h - z\ell_0\right), \tag{2.53}$$

which holds for any point lying on the vertical axis z of the cylinder.

First radial derivative V_r

In the planar approximation, $V_r = V_z$ for the point P lying on the z axis. Because we have a general formula for the gravitational potential for any point P on the axis of the cylinder, we can easily derive the formula for its derivative in z direction. The derivative of term (2.53) is

$$V_r = G\rho\pi\Bigg(R^2\frac{z+\ell_0}{\ell_h+h+z}\left(\frac{\ell_h'+1}{z+\ell_0}-\frac{(\ell_0'+1)\,(\ell_h+h+z)}{(z+\ell_0)^{\,2}}\right)-|h+z| \\ -(h+z)|h+z|'+z|z|'+|z|+z\ell_h'+h\ell_h'+\ell_h-z\ell_0'-\ell_0\Bigg), \tag{2.54}$$

where symbol $|\cdot|'$ denotes the derivative of the absolute value function and

$$\ell_h' = \frac{\partial \ell_h}{\partial z} = \frac{h+z}{\ell_h}, \tag{2.55}$$

$$\ell_0' = \frac{\partial \ell_h}{\partial z} = \frac{z}{\ell_0}. \tag{2.56}$$

The Equation (2.54) can be simplified to

$$V_r = \frac{G\rho\pi}{\ell_0\ell_h}\Bigg(\ell_h\left(-R^2-z^2\right)+\ell_0^2\Big(-h\ell_h|h+z|'+z\ell_h|z|'-z\ell_h|h+z|'+ \\ |z|\ell_h-\ell_h|h+z|+h^2+2hz+\ell_h^2+R^2+z^2\Big)\Bigg). \tag{2.57}$$

Now we can again introduce ℓ_h and ℓ_0 and get after few steps

$$V_r = G\rho\pi\left(-(h+z)|h+z|'+z|z|'-|h+z|+|z|+2\ell_h-2\ell_0\right). \tag{2.58}$$

The disadvantage of this equation is the fact that $\partial|f(z)|/\partial z \equiv |f(z)|'$ is not defined for $f(z)=0$. In other cases (when $f(z)\neq 0$), the derivative $|f(z)|'$ is the signum function. We will denote the signum function as $[f(z)]$.

For $f(z) = 0$, $[f(z)] = 0$ while $|f(z)|'$ is not defined. The cases $z = 0$ and $z + h = 0$ will be now considered separately. For $z = 0$ (P on the top of the cylinder), the situation is easy because the term $z|z|' = 0$, so we can use $[z]$ instead of $|z|'$ also in this case. For $z + h = 0$ the situation is the same, the term $(h + z)|h + z|' = 0$ and we can again use $[h + z]$ instead of $|h + z|'$. The final equation, that holds for any z, is

$$V_r = G\rho\pi \left(z[z] - (h + z)[h + z] - |h + z| + |z| + 2\ell_h - 2\ell_0\right). \tag{2.59}$$

An explicit formula for any point P on the vertical axis of the cylinder after replacing ℓ_h and ℓ_0 by Equations (2.47) and (2.48) is

$$\begin{aligned} V_r = G\rho\pi\Big(& z[z] - (h + z)[h + z] - |h + z| + |z| \\ & + 2\sqrt{(h + z)^2 + R^2} - 2\sqrt{R^2 + z^2}\Big). \end{aligned} \tag{2.60}$$

All five special cases for points $P_1 - P_5$ are

$$V_r(P_1) = -2\pi G\rho \left(-\sqrt{h^2 + 2hz + R^2 + z^2} + h + \sqrt{R^2 + z^2}\right), \tag{2.61}$$

$$V_r(P_2) = -2\pi G\rho \left(-\sqrt{h^2 + R^2} + h + R\right), \tag{2.62}$$

$$V_r(P_3) = -2\pi G\rho \left(-\sqrt{h^2 + 2hz + R^2 + z^2} + h + \sqrt{R^2 + z^2} + 2z\right), \tag{2.63}$$

$$V_r(P_4) = -2\pi G\rho \left(\sqrt{R^2 + h^2} - R - h\right), \tag{2.64}$$

$$V_r(P_5) = -2\pi G\rho \left(-\sqrt{h^2 + 2hz + R^2 + z^2} - h + \sqrt{R^2 + z^2}\right). \tag{2.65}$$

Second radial derivative V_{rr}

The second radial derivative V_{rr} will be again computed as V_{zz}. Deriving (2.59) gives us

$$\begin{aligned} V_{rr} = G\rho\pi\Big(& - |h + z|' + |z|' - h[h + z]' - z[h + z]' - [h + z] \\ & + z[z]' + [z] + 2\ell_h' - 2\ell_0'\Big). \end{aligned} \tag{2.66}$$

We will substitute (2.55) and (2.56) into (2.66) obtaining

$$V_{rr} = G\rho\pi\Big(- |h+z|' + |z|' - h[h+z]' - z[h+z]' - [h+z] + z[z]' + [z] + 2\frac{h+z}{\ell_h} - 2\frac{z}{\ell_0}\Big). \tag{2.67}$$

The functions $|h+z|'$, $|z|'$, $[h+z]'$ and $[z]'$ again do not exist for $z = 0$ or $z + h = 0$. Contrary to the previous case, these singularities cannot be removed. This is expected, because it is well known from the potential theory that the second derivative in the normal direction is not continuous on the boundary of the attracting body (here cylinder).

For the point on the top of the cylinder ($z = 0$) the limits are

$$\lim_{z\to 0^-} V_{rr}(P_2) = 2G\rho\pi\frac{\left(h - 2\sqrt{R^2+h^2}\right)}{\sqrt{R^2+h^2}}, \tag{2.68}$$

$$\lim_{z\to 0^+} V_{rr}(P_2) = 2G\rho\pi\frac{h}{\sqrt{R^2+h^2}}, \tag{2.69}$$

and for the point on the bottom of the cylinder ($z = -h$) the limits are

$$\lim_{z\to 0^-} V_{rr}(P_4) = 2G\rho\pi\frac{h}{\sqrt{R^2+h^2}}, \tag{2.70}$$

$$\lim_{z\to 0^+} V_{rr}(P_4) = 2G\rho\pi\frac{\left(h - 2\sqrt{R^2+h^2}\right)}{\sqrt{R^2+h^2}}. \tag{2.71}$$

We are interested in the external gravity field so more important limits are the limits from outer space $\lim_{z\to 0^+} V_{rr}(P_4)$ given by equation (2.69) and $\lim_{z\to 0^-} V_{rr}(P_4)$ given by Equation (2.70).

For the remaining points outside or inside the plate (P_1, P_3 and P_5),

Euqtion (2.67) can be simplified to

$$\begin{aligned} V_{rr} &= 2G\rho\pi \left([z] - [h+z] + \frac{h+z}{\ell_h} - \frac{z}{\ell_0} \right) \\ &= 2G\rho\pi \left([z] - [h+z] + \frac{h+z}{\sqrt{(h+z)^2 + R^2}} - \frac{z}{\sqrt{R^2+z^2}} \right). \end{aligned} \tag{2.72}$$

Explicit formulas for P_1, P_3 and P_5 are

$$V_{rr}(P_1) = 2\pi G\rho \left(\frac{h+z}{\sqrt{(h+z)^2 + R^2}} - \frac{z}{\sqrt{R^2+z^2}} \right), \tag{2.73}$$

$$V_{rr}(P_3) = 2\pi G\rho \left(\frac{h+z}{\sqrt{(h+z)^2 + R^2}} - \frac{z}{\sqrt{R^2+z^2}} - 2 \right), \tag{2.74}$$

$$V_{rr}(P_5) = 2\pi G\rho \left(\frac{h+z}{\sqrt{(h+z)^2 + R^2}} - \frac{z}{\sqrt{R^2+z^2}} \right). \tag{2.75}$$

2.3.3 Unlimited Bouguer plate

The potential V and its derivatives V_r, V_{rr} can be derived as limits of equations for the limited plate where $R \to \infty$. The limit of Equation (2.53) for the potential V is

$$\lim_{R\to\infty} V = \infty. \tag{2.76}$$

The limit of the formula in Euqtion (2.59) for the attraction is

$$\lim_{R\to\infty} V_r = -2G\rho\pi \left(|h+z| - |z| \right). \tag{2.77}$$

Expressions for points P_i are

$$V_r(P_1) = V_r(P_2) = -2\pi G\rho h, \tag{2.78}$$

$$V_r(P_3) = -2\pi G\rho(h+2z), \tag{2.79}$$

$$V_r(P_4) = V_r(P_5) = 2\pi G\rho h. \tag{2.80}$$

The attraction V_r for points above or under the infinite plate do not depend on the position of the point above (under) the Bouguer plate, but only on the thickness of the plate [Burša, 2004].

The second radial derivative is given for points that are not on the boundary of the plate by letting $R \to \infty$ in the formula of Equation (2.67). It is

$$\lim_{R\to\infty} V_{rr} = 2G\rho\pi \left(-2[h+z] + 2[z]\right). \tag{2.81}$$

The result of this formula depends only on the position of the evaluation point: for the points P_1, and P_5 we have

$$V_{rr}(P_1) = V_{rr}(P_5) = 0 \tag{2.82}$$

and for point the P_3 we have

$$V_{rr}(P_3) = -4\pi G\rho \tag{2.83}$$

The function is again not continuous at the points P_2 and P_4.

2.3.4 Limited Bouguer shell

Gravitational potential V

The geometry of the limited Bouguer shell is shown at Figure 2.1. However, we use a more general notation: the inner radius will be denoted as r_1 (it corresponds to R at Figure 2.1) and the outer radius as r_2 (it is $R + h$ in Figure 2.1). We use this notation to emphasize that the relations are valid generally for any r_1, r_2 and r. Some special cases for $r_1 = R$, where R is radius of the earth and h is a thickness of the Bouguer layer, will also be shown. Relations for the latter case are sometimes simpler, because some terms can be safely neglected.

The potential V at the point $(r, \psi = 0)$ is given by

$$V = G\rho \int_0^{2\pi} \int_0^{\psi_0} \int_{r_1}^{r_2} \frac{1}{\ell} r'^2 \sin\psi' dr' d\psi' d\alpha', \tag{2.84}$$

where

$$\ell = \sqrt{r^2 + r'^2 - 2rr'\cos\psi'}. \tag{2.85}$$

After integration over α' we get

$$V = 2\pi G\rho \int_0^{\psi_0} \int_{r_1}^{r_2} \frac{1}{\ell} r'^2 \sin\psi' dr' d\psi', \tag{2.86}$$

and after integration over ψ' we get

$$V = \frac{2\pi G\rho}{r} \int_{r_1}^{r_2} (\ell_0 - |r - rr|) r' dr', \tag{2.87}$$

where

$$\ell_0 = \sqrt{r^2 + r'^2 - 2rr'\cos\psi_0}. \tag{2.88}$$

After integration over r', we get for $r \geq r_2$ [Martinec, 1998], [Heck and Seitz, 2007]

$$V = 2\pi G\rho \left(\frac{r'^3}{3r} - \frac{r'^2}{2} \right) \Bigg|_{r'=r_1}^{r'=r_2} + 2\pi G\rho \Bigg(\frac{\ell_0^3}{3r} + \frac{1}{2}\ell_0 \cos\psi_0 (r' - r\cos\psi_0) + \frac{1}{2} r^2 \cos\psi_0 \sin^2\psi_0 \log(\ell_0 + r' - r\cos\psi_0) \Bigg) \Bigg|_{r'=r_1}^{r'=r_2}, \tag{2.89}$$

and for $r \leq r_1$

$$V = -2\pi G\rho \left(\frac{r'^3}{3r} - \frac{r'^2}{2} \right) \Bigg|_{r'=r_1}^{r'=r_2} + 2\pi G\rho \Bigg(\frac{\ell_0^3}{3r} + \frac{1}{2}\ell_0 \cos\psi_0 (r' - r\cos\psi_0) + \frac{1}{2} r^2 \cos\psi_0 \sin^2\psi_0 \log(\ell_0 + r' - r\cos\psi_0) \Bigg) \Bigg|_{r'=r_1}^{r'=r_2}. \tag{2.90}$$

Equations (2.89) and (2.90) do not hold for points inside the shell. To derive a general formula that holds for any r, we split the integral in Equation (2.87) into two parts $V = V_1 + V_2$ where V_1 is given by

$$V_1 = \frac{2\pi G\rho}{r}\int_{r_1}^{r_2} \ell_0 r' dr' = 2\pi G\rho\left(\frac{1}{2}r^2\sin^2\psi_0\cos\psi_0\log\left(\frac{r_2+\ell_2-r\cos\psi_0}{r_1+\ell_1-r\cos\psi_0}\right)\right.$$
$$\left. + \frac{\ell_2^3-\ell_1^3}{3r} + \frac{1}{2}\cos\psi_0\left(\ell_2\left(r_2-r\cos\psi_0\right)-\ell_1\left(r_1-r\cos\psi_0\right)\right)\right), \tag{2.91}$$

where

$$\ell_1 = \sqrt{r^2+r_1^2-2rr_1\cos\psi_0}, \tag{2.92}$$
$$\ell_2 = \sqrt{r^2+r_2^2-2rr_2\cos\psi_0}, \tag{2.93}$$

and V_2 is given by

$$V_2 = \frac{2\pi G\rho}{r}\int_{r_1}^{r_2} -|r-rr|r'dr'$$
$$= 2\pi G\rho\frac{(r-r_1)\left|r-r_1\right|(r+2r_1)-(r-r_2)\left|r-r_2\right|(r+2r_2)}{6r}. \tag{2.94}$$

The first part V_1 of the solution (2.91) has the same form as in (2.89) and (2.90) but the second part V_2 is more general. For $r \geq r_2$ it becomes

$$V_2 = 2\pi G\rho\frac{2(r_2^3-r_1^3)+3r(r_1^2-r_2^2)}{6r} \tag{2.95}$$

so it is equal to the respective part of (2.89). For $r_1 < r < r_2$ it becomes

$$V_2 = 2\pi G\rho\frac{-2r^3+3r\left(r_1^2+r_2^2\right)-2\left(r_1^3+r_2^3\right)}{6r}m \tag{2.96}$$

and for $r < r_1$ it becomes

$$V_2 = 2\pi G\rho\frac{2(r_1^3-r_2^3)+3r(r_2^2-r_1^2)}{6r}. \tag{2.97}$$

so it is equal to the respective part of (2.90). The final general formula, that holds for any r, is

$$V = 2\pi G\rho\Bigg(\frac{(r_1 - r)\,|r - r_1|\,(r + 2r_1) + (r - r_2)\,|r - r_2|\,(r + 2r_2)}{6r} + \frac{1}{2}r^2 \sin^2\psi_0 \cos\psi_0 \log\left(\frac{r_2 + \ell_2 - r\cos\psi_0}{r_1 + \ell_1 - r\cos\psi_0}\right) + \frac{\ell_2^3 - \ell_1^3}{3r} + \frac{1}{2}\cos\psi_0\,(\ell_2\,(r_2 - r\cos\psi_0) - \ell_1\,(r_1 - r\cos\psi_0))\Bigg). \quad (2.98)$$

The formula in Equation (2.98) can be used for evaluation of the potential of a Bouguer layer in a spherical approximation as will be shown later in this thesis. However, the relation is quite complicated. We will be particularly interested in its form for the point P_2, i.e., the point lying on the top of the limited Bouguer shell. We will now derive a simpler expression for V under assumptions $r_1 = R$, $h > 0$, $r_2 = R + h$, $r = R + h$, $\psi_0 < 1^\circ$ and $R \gg h$.

We will first introduce $r_1 = R$, $r_2 = R + h$, $r = R + h$ into (2.92) and (2.93). We get

$$\ell_1 = \sqrt{R^2 + (h + R)^2 - 2R(h + R)\cos\psi_0}, \quad (2.99)$$

and

$$\ell_2 = \sqrt{-2(h + R)^2\,(\cos\psi_0 - 1)}. \quad (2.100)$$

Both formulas can be further simplified. Neglecting the curvature of the limited shell, we get for ℓ_1 expression

$$\ell_1 \approx \sqrt{R^2 \sin^2\psi_0 + h^2} \approx \sqrt{R^2\psi_0^2 + h^2}. \quad (2.101)$$

The Distance ℓ_2 defined by (2.93) can be simplified to even simpler form

$$\ell_2 \approx (R + h)\psi_0. \quad (2.102)$$

Now we will insert $r_1 = R$, $h > 0$, $r_2 = R + h$, $r = R + h$ into (2.98). We get

$$\begin{aligned} V =& \frac{1}{3}\pi G\rho\Bigg(- \frac{h^2(h+3R)}{h+R} + \frac{2\left(\ell_2^3 - \ell_1^3\right)}{h+R} \\ &+ 3(h+R)^2 \sin^2\psi_0 \cos\psi_0 \log\left(\frac{-(h+R)\cos\psi_0 + h + R + \ell_2}{-(h+R)\cos\psi_0 + R + \ell_1}\right) \\ &+ 3\cos\psi_0\left(\ell_1\left((h+R)\cos\psi_0 - R\right) - \ell_2(h+R)\left(\cos\psi_0 - 1\right)\right)\Bigg). \end{aligned} \tag{2.103}$$

We put $\cos\psi_0 = 1$ because $\psi_0 < 1^\circ$. We have

$$V = \frac{1}{3}\pi G\rho\left(\frac{2\left(\ell_2^3 - \ell_1^3\right)}{h+R} - \frac{h^3 + 3Rh^2}{h+R} + 3(h+R)^2 \sin^2\psi_0 \log\frac{\ell_2}{\ell_1 - h} + 3h\ell_1\right). \tag{2.104}$$

We neglect the first term because it is much smaller than the others. After simple algebra we get the final expression for the potential at the point P_2 lying on the top of a limited Bouguer shell under the conditions $\psi_0 < 1^\circ$ and $R \gg h$

$$V(P_2) = \pi G\rho\left(-\frac{h^3}{3R} - h^2 + h\ell_1 + (h+R)^2 \sin^2\psi_0 \log\frac{\ell_2}{\ell_1 - h}\right) \tag{2.105}$$

where ℓ_1 and ℓ_2 can be computed by using either the original formulas (2.92) and (2.93) or by the simplified formulas (2.101) and (2.102).

First radial derivative V_r

V_r is given as radial derivative of the formula (2.98)

$$\begin{aligned} V_r =& \frac{1}{3}\pi G\rho\Bigg(\frac{\left(r^2 + r_2 r - 2r_2^2\right)\left[r - r_2\right] - \left(r^2 + r_1 r - 2r_1^2\right)\left[r - r_1\right]}{r} \\ &+ \frac{|r - r_2|\left(r^2 + 2r_2^2\right) - |r - r_1|\left(r^2 + 2r_1^2\right)}{r^2} \end{aligned}$$

$$+ 3r^2 \sin^2\psi_0 \cos\psi_0 \left(\frac{(r_1+\ell_1)\cos\psi_0 - r}{\ell_1\left(-r\cos\psi_0 + r_1 + \ell_1\right)} - \frac{(r_2+\ell_2)\cos\psi_0 - r}{\ell_2\left(-r\cos\psi_0 + r_2 + \ell_2\right)} \right)$$
$$+ 3\cos\psi_0 \left(\frac{\left(r\cos\psi_0 - r_1\right)\left(r - r_1\cos\psi_0\right)}{\ell_1} - \frac{\left(r\cos\psi_0 - r_2\right)\left(r - r_2\cos\psi_0\right)}{\ell_2} \right)$$
$$+ 3\cos^2\psi_0\left(\ell_1 - \ell_2\right) + \frac{6\left(\ell_1\left(r_1\cos\psi_0 - r\right) + \ell_2\left(r - r_2\cos\psi_0\right)\right)}{r}$$
$$+ \frac{2\left(\ell_1^3 - \ell_2^3\right)}{r^2} + 6r\sin^2\psi_0\cos\psi_0 \log\left(\frac{-r\cos\psi_0 + r_2 + \ell_2}{-r\cos\psi_0 + r_1 + \ell_1} \right) \Bigg), \qquad (2.106)$$

where the derivative of the absolute value function $|\cdot|'$ was again replaced by the signum function $[\,\cdot\,]$.

We will use the limited shell usually for $\psi_0 < 1°$. In such case, we can slightly simplify the expression in Equation (2.106) putting $\cos\psi_0 = 1$ and $\sin\psi_0 = \psi_0$. We get

$$V_r = \frac{\pi G\rho}{3}\Bigg(3r^2\left(\frac{1}{\ell_1} - \frac{1}{\ell_2}\right)\psi_0^2 + \frac{2\left(\ell_1^3 - \ell_2^3\right)}{r^2} + 6r\psi_0^2 \log\left(\frac{-r + r_2 + \ell_2}{-r + r_1 + \ell_1} \right)$$
$$+ 3\left(\frac{\left(r - r_1\right)^2}{\ell_1} - \frac{\left(r - r_2\right)^2}{\ell_2} + \ell_1 - \ell_2 \right) + \frac{6\left(\left(r_1 - r\right)\ell_1 + \left(r - r_2\right)\ell_2\right)}{r} \Bigg)$$
$$- \frac{\pi G\rho}{3r^2}\Big(\left(r^2 + 2r_1^2\right)|r - r_1| - \left(r^2 + 2r_2^2\right)|r - r_2|$$
$$+ r\left(\left(r^2 + r_1 r - 2r_1^2\right)[r - r_1] - \left(r^2 + r_2 r - 2r_2^2\right)[r - r_2] \right) \Big) \qquad (2.107)$$

The solution (2.107) works only for $\psi_0 < 1°$, but it is still valid for any r, r_1 and r_2. Now we will derive one more particular solution for the specific position of the evaluation point on the top of the shell $V_r(P_2)$. We simplify (2.106) by using assumptions $r_1 = R$, $h > 0$, $r_2 = R + h$, $r = R + h$, $\psi_0 < 1°$ and $R \gg h$. Substituting $r_1 = R$, $r_2 = R + h$, $r = R + h$ into (2.106) gives

$$V_r = \frac{1}{3}\pi G\rho\Bigg(\frac{-\left((R+h)^2 + R(R+h) - 2R^2\right)}{(R+h)} + \frac{-|h|\left((R+h)^2 + 2R^2\right)}{(R+h)^2} +$$
$$3(R+h)^2\sin^2\psi_0\cos\psi_0 \cdot$$

$$\left(\frac{(R+\ell_1)\cos\psi_0-(R+h)}{\ell_1\left(-(R+h)\cos\psi_0+R+\ell_1\right)}-\frac{((R+h)+\ell_2)\cos\psi_0-(R+h)}{\ell_2\left(-(R+h)\cos\psi_0+(R+h)+\ell_2\right)}\right)+$$
$$3\cos\psi_0\left(\frac{\left((R+h)\cos\psi_0-R\right)\left((R+h)-R\cos\psi_0\right)}{\ell_1}-\right.$$
$$\left.\frac{\left((R+h)\cos\psi_0-(R+h)\right)\left((R+h)-(R+h)\cos\psi_0\right)}{\ell_2}\right)$$
$$+3\cos^2\psi_0\left(\ell_1-\ell_2\right)+\frac{2\left(\ell_1^3-\ell_2^3\right)}{(R+h)^2}$$
$$+\frac{6\left(\ell_1\left(R\cos\psi_0-(R+h)\right)+\ell_2\left((R+h)-(R+h)\cos\psi_0\right)\right)}{(R+h)}$$
$$+6(R+h)\sin^2\psi_0\cos\psi_0\log\left(\frac{-(R+h)\cos\psi_0+(R+h)+\ell_2}{-(R+h)\cos\psi_0+R+\ell_1}\right)\Bigg). \tag{2.108}$$

Because $\psi_0 < 1^\circ$, we put all $\cos\psi_0 = 1$

$$V_r=\frac{1}{3}\pi G\rho\left(\frac{-\left((R+h)^2+R(R+h)-2R^2\right)}{(R+h)}+\frac{-|h|\left((R+h)^2+2R^2\right)}{(R+h)^2}+\right.$$
$$3(R+h)^2\sin^2\psi_0\cdot$$
$$\left(\frac{(R+\ell_1)-(R+h)}{\ell_1\left(-(R+h)+R+\ell_1\right)}-\frac{((R+h)+\ell_2)-(R+h)}{\ell_2\left(-(R+h)+(R+h)+\ell_2\right)}\right)+$$
$$3\left(\frac{\left((R+h)-R\right)\left((R+h)-R\right)}{\ell_1}-\right.$$
$$\left.\frac{\left((R+h)-(R+h)\right)\left((R+h)-(R+h)\right)}{\ell_2}\right)+3\left(\ell_1-\ell_2\right)+\frac{2\left(\ell_1^3-\ell_2^3\right)}{(R+h)^2}$$
$$+\frac{6\left(\ell_1\left(R-(R+h)\right)+\ell_2\left((R+h)-(R+h)\right)\right)}{(R+h)}$$
$$\left.+6(R+h)\sin^2\psi_0\log\left(\frac{-(R+h)+(R+h)+\ell_2}{-(R+h)+R+\ell_1}\right)\right). \tag{2.109}$$

The first two fractions in (2.109) are

$$\frac{-\left((R+h)^2+R(R+h)-2R^2\right)}{(R+h)}+\frac{-|h|\left((R+h)^2+2R^2\right)}{(R+h)^2}=$$

$$\frac{-(R+h)\left((R+h)^2+R(R+h)-2R^2\right)-h\left((R+h)^2+2R^2\right)}{(R+h)^2}=$$
$$\frac{-2h(3R^2+Rh+h^2)}{(R+h)^2}. \tag{2.110}$$

In the nominator, only the term with R^2 is important because $R \gg h$. For the same reason, the denominator can be simplified to R^2. We get

$$\frac{-2h(3R^2+Rh+h^2)}{(R+h)^2} \approx \frac{-6hR^2}{R^2} = -6h. \tag{2.111}$$

The third and fourth fractions in (2.109) are

$$\left(\frac{(R+\ell_1)-(R+h)}{\ell_1\left(-(R+h)+R+\ell_1\right)}-\frac{((R+h)+\ell_2)-(R+h)}{\ell_2\left(-(R+h)+(R+h)+\ell_2\right)}\right)=$$
$$\frac{\ell_1-h}{\ell_1(\ell_1-h)}-\frac{\ell_2}{\ell_2^2}=\frac{1}{\ell_1}-\frac{1}{\ell_2}. \tag{2.112}$$

The fifth and sixth fractions in (2.109) become

$$3\left(\frac{h^2}{\ell_1}-0\right). \tag{2.113}$$

The term $3(\ell_1-\ell_2)$ remains unchanged whereas the seventh and eighth fractions can be omitted because their denominators are much bigger then nominators. The last term which is

$$6(R+h)\sin^2\psi_0\log\left(\frac{-(R+h)+(R+h)+\ell_2}{-(R+h)+R+\ell_1}\right)=$$
$$6(R+h)\sin^2\psi_0\log\left(\frac{\ell_2}{\ell_1-h}\right) \tag{2.114}$$

can be also omitted.

We have $\sin^2\psi_0 \approx 0.0003$ and also $\log\left(\frac{\ell_2}{\ell_1-h}\right)$ is almost zero, so the final product can be also omitted (regardless the part $6(R+h)$), because the remaining terms are by orders of magnitude larger.

Putting all particular results together we get

$$V_r(P_2) \approx \pi G\rho \left(\frac{h^2}{\ell_1} + (h+R)^2 \sin^2(\psi_0) \left(\frac{1}{\ell_1} - \frac{1}{\ell_2} \right) + \ell_1 - \ell_2 - 2h \right), \tag{2.115}$$

where ℓ_1 and ℓ_2 can be computed using either original formulas (2.92) and (2.93) or by simplified formulas (2.101) and (2.102).

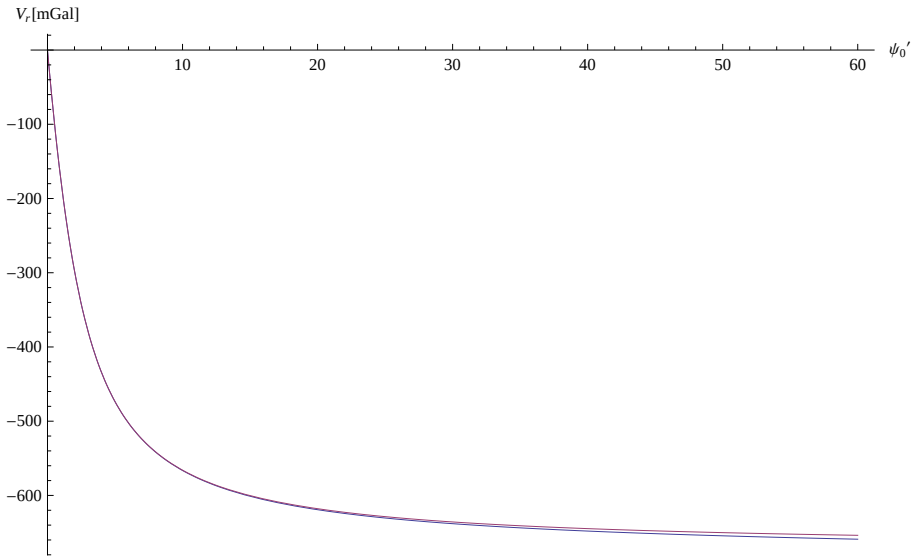

Figure 2.3: *V_r for limited cylinder.* Difference between original (blue line) and simplified function (violet line) V_r for $\psi_0 \in (0, 60')$, $h = 6000$ m, $R = R_m$

Differences between the original function and simplified function are plotted in Figure 2.3. We should emphasize that the simplified relations are accurate enough for practical evaluation of the gravitational effect. They should be avoided only in special cases, for example when we want to evaluate differences between effects of various shapes of Bouguer layers, because the differences between various shapes itself are not big and they are often

caused by these small terms. Neglecting terms (even though they are small) can result in effect that is neither spherical nor limited. Simplifying the equations too much will finally result in keeping only the largest part, which represents the effect of the unlimited Bouguer plate.

Second radial derivative V_{rr}

V_{rr} is given as a radial derivative of the formula (2.106). We will split V_{rr} into two parts

$$V_{rr} = V_{rr}^1 + V_{rr}^2 \tag{2.116}$$

where

$$\begin{aligned}
V_{rr}^1 = \pi G\rho\Bigg(&\frac{4\left(\ell_1\left(r - r_1\cos\psi_0\right) + \ell_2\left(r_2\cos\psi_0 - r\right)\right)}{r^2}\\
&+r^2\sin^4\psi_0\cos\psi_0\left(\frac{r_2\left(r\cos\psi_0+\ell_2\right)+\ell_2^2-r^2}{m_2^2\ell_2^2} - \frac{r_1\left(r\cos\psi_0+\ell_1\right)+\ell_1^2-r^2}{m_1^2\ell_1^2}\right)\\
&+r^2\sin^2\psi_0\cos\psi_0\frac{\left(r - r_2\cos\psi_0\right)\left(\left(r_2+\ell_2\right)\cos\psi_0 - r\right)}{m_2\ell_2^3}\\
&-r^2\sin^2\psi_0\cos\psi_0\frac{\left(r - r_1\cos\psi_0\right)\left(\left(r_1+\ell_1\right)\cos\psi_0 - r\right)}{m_1\ell_1^3}\\
&+4r\sin^2\psi_0\cos\psi_0\left(\frac{\left(r_1+\ell_1\right)\cos\psi_0 - r}{m_1\ell_1} - \frac{\left(r_2+\ell_2\right)\cos\psi_0 - r}{m_2\ell_2}\right)\\
&+2\sin^2\psi_0\cos\psi_0\log\left(\frac{m_2}{m_1}\right) - \frac{4\left(\ell_1^3-\ell_2^3\right)}{3r^3}\\
&+\cos\psi_0\Bigg(\frac{\left(r\cos\psi_0 - r_2\right)\left(r - r_2\cos\psi_0\right)^2}{\ell_2^3} - \frac{\left(r\cos\psi_0 - r_1\right)\left(r - r_1\cos\psi_0\right)^2}{\ell_1^3}\\
&+\frac{3r\left(\ell_2-\ell_1\right)\cos\psi_0 + \left(r_2\ell_1 - r_1\ell_2\right)\left(\cos\left(2\psi_0\right)+2\right)}{\ell_1\ell_2}\Bigg)\\
&+\frac{2\left(\ell_1(r - r_2\cos\psi_0)^2 - \ell_2(r - r_1\cos\psi_0)^2\right)}{r\ell_1\ell_2} + \frac{2\left(\ell_2-\ell_1\right)}{r}\Bigg),
\end{aligned} \tag{2.117}$$

and

$$V_{rr}^2 = -\frac{\pi G\rho}{3r^3}\Bigg(r^2\left((r^2+r_1r-2r_1^2)|r-r_1|'' - (r^2+r_2r-2r_2^2)|r-r_2|''\right) + 2r\left((r^2+2r_1^2)|r-r_1|' - (r^2+2r_2^2)|r-r_2|'\right) + 4\left(r_2^2\,|r-r_2| - r_1^2\,|r-r_1|\right)\Bigg). \tag{2.118}$$

In (2.117) we have introduced substitutions

$$m_1 = r_1 + \ell_1 - r\cos\psi_0, \tag{2.119}$$

$$m_2 = r_2 + \ell_2 - r\cos\psi_0. \tag{2.120}$$

The first part V_{rr}^1 of the solution V_{rr} is valid for any $r > 0$, but the second part V_{rr}^2 is again not continuous at points $P_2(r = r_2)$ and $P_4(r = r_1)$.

Simplifying the formula (2.118) for point P_1 under condition $r > r_2 > r_1$ gives

$$V_{rr}^2(P_1) = -4\pi G\rho\frac{(r_1^3 - r_2^3)}{3r^3}. \tag{2.121}$$

Simplifying (2.118) for point P_3 under condition $r_2 > r > r_1$ gives

$$V_{rr}^2(P_3) = -4\pi G\rho\frac{(r^3 + r_1^3 + r_2^3)}{3r^3}, \tag{2.122}$$

and simplifying (2.118) for point P_5 under condition $r_2 > r_1 > r$ gives

$$V_{rr}^2(P_5) = -4\pi G\rho\frac{(r_2^3 - r_1^3)}{3r^3}. \tag{2.123}$$

Solution in points P_2 and P_4 can be obtained as limits of the formulas in Equations (2.121), (2.122) and (2.123). We get

$$\lim_{r\to r_2^-} V_{rr}^2(P_2) = V_{rr}^2(P_3(r = r_2)) = -4\pi G\rho\frac{(r_1^3 + 2r_2^3)}{3r_2^3}, \tag{2.124}$$

$$\lim_{r\to r_2^+} V_{rr}^2(P_2) = V_{rr}^2(P_1(r = r_2)) = -4\pi G\rho\frac{(r_1^3 - r_2^3)}{3r_2^3}, \tag{2.125}$$

and

$$\lim_{r\to r_1^-} V_{rr}^2(P_4) = V_{rr}(P_5(r=r_1)) = -4\pi G\rho\frac{(r_2^3-r_1^3)}{3r_1^3}, \tag{2.126}$$

$$\lim_{r\to r_1^+} V_{rr}^2(P_4) = V_{rr}(P_3(r=r_1)) = -4\pi G\rho\frac{(r_2^3+2r_1^3)}{3r_1^3}. \tag{2.127}$$

The differences of limits from left and from right when going from outside to inside of the shell are

$$\lim_{r\to r_2^+} V_{rr}^2(P_2) - \lim_{r\to r_2^-} V_{rr}^2(P_2) = 4\pi G\rho, \tag{2.128}$$

$$\lim_{r\to r_1^-} V_{rr}^2(P_4) - \lim_{r\to r_1^+} V_{rr}^2(P_4) = 4\pi G\rho, \tag{2.129}$$

as was expected.

For points P_1, P_3 and P_5 where the function V_{rr}^2 is continuous, we have a general solution

$$V_{rr}^2 = -\frac{\pi G\rho}{3r^3}\Bigg(2r\left((r^2+2r_1^2)[r-r_1] - (r^2+2r_2^2)[r-r_2]\right) + 4\left(r_2^2\,|r-r_2| - r_1^2\,|r-r_1|\right)\Bigg). \tag{2.130}$$

The most important case is again $V_{rr}(P_2)$. However, at this point V_{rr} is not continuous. Because we are interested in the external gravity field, we will study the limit $\lim_{r\to r_2^+} V_{rr}(P_2)$. In the following text we will not repeat the limit from right every time and only the expression $V_{rr}(P_2)$ is used as the abbreviation for limit from right. According to (2.116), the solution consists of two parts: V_{rr}^1 given by (2.117) and V_{rr}^2 given by (2.124). Such a general solution is again quite complicated and can be simplified for assumptions $r_1 = R$, $h > 0$, $r_2 = R + h$, $r = R + h$, $\psi_0 < 1^\circ$ and $R \gg h$. Such assumptions represent a typical limited Bouguer shell and the application shown later in this thesis will fulfill such conditions.

First, we can omit the term V_{rr}^2 because it is much smaller than V_{rr}^1. Using substitutions $r_1 = R$, $r_2 = R + h$ and $r = R + h$ the term V_{rr}^1 becomes

$$
\begin{aligned}
V_{rr}^1(P_2) = \frac{1}{3}\pi G\rho\Bigg(& 3(h+R)^2 \sin^4\psi_0 \cos\psi_0 \cdot \\
& \Bigg(\frac{(h+R)\left((h+R)\cos\psi_0 + \ell_2\right) - (h+R)^2 + \ell_2^2}{m_2^2 \ell_2^2} \\
& - \frac{R\left((h+R)\cos\psi_0 + \ell_1\right) - (h+R)^2 + \ell_1^2}{m_1^2 \ell_1^2} \Bigg) \\
& + 6(h+R)\sin^2\psi_0 \cos\psi_0 \Bigg(\frac{2\left(-h + R\cos\psi_0 - R + \ell_1 \cos\psi_0\right)}{m_1 \ell_1} \\
& - \frac{2\left((h+R)\cos\psi_0 - h - R + \ell_2\cos\psi_0\right)}{m_2 \ell_2} \Bigg) \\
& + 3(h+R)^2 \sin^2\psi_0 \cos\psi_0 \\
& \Bigg(\frac{\left(\cos\psi_0 + h + R - h - R\right)\right)\left(\cos\psi_0\left(h + R + \ell_2\right) - h - R\right)}{m_2 \ell_2^3} \\
& - \frac{\left(h - R\cos\psi_0 + R\right)\left(-h + \left(R + \ell_1\right)\cos\psi_0 - R\right)}{m_1 \ell_1^3} \Bigg) \\
& + \frac{6\left(\ell_1\left(-(h+R)\cos\psi_0 + h + R\right)^2 - \ell_2\left(h - R\cos\psi_0 + R\right)^2\right)}{\ell_1 \ell_2 (h+R)} \\
& + \frac{12\left(\ell_1\left(h - R\cos\psi_0 + R\right) - \ell_2\left(-(h+R)\cos\psi_0 + h + R\right)\right)}{(h+R)^2} \\
& + 3\cos\psi_0 \Bigg(- \frac{\left((h+R)\cos\psi_0 - R\right)\left(h - R\cos\psi_0 + R\right)^2}{\ell_1^3} \\
& + \frac{3\left(\ell_2 - \ell_1\right)(h+R)\cos\psi_0 + \left(\cos\left(2\psi_0\right) + 2\right)\left(\ell_1(h+R) - R\ell_2\right)}{\ell_1 \ell_2} \\
& + \frac{\left(-(h+R)\cos\psi_0 + h + R\right)^2\left((h+R)\cos\psi_0 - h - R\right)}{\ell_2^3} \Bigg) \\
& + \frac{6\left(\ell_2 - \ell_1\right)}{h+R} - \frac{4\left(\ell_1^3 - \ell_2^3\right)}{(h+R)^3} + 6\log\left(\frac{m_2}{m_1}\right)\sin^2\psi_0\cos\psi_0 \Bigg). \qquad (2.131)
\end{aligned}
$$

We can omit a lot of terms in Equation (2.131) for similar reasons as

in (2.109). We do not provide detailed explanation of each particular step, but to support our steps, we will show the difference between original and approximated function for set of reasonable parameters. After neglecting very small terms we get

$$
\begin{aligned}
V_{rr}^{1}(P_2) \approx \frac{1}{3}\pi G\rho\Bigg(& 3(h+R)^2 \sin^2\psi_0 \cos\psi_0 \cdot \\
& \Bigg(\frac{(\cos\psi_0 + h + R - h - R))\left(\cos\psi_0\left(h+R+\ell_2\right) - h - R\right)}{m_2\ell_2^3} - \\
& \frac{\left(h - R\cos\psi_0 + R\right)\left(-h + (R+\ell_1)\cos\psi_0 - R\right)}{m_1\ell_1^3}\Bigg) + \\
& 3\cos\psi_0\Bigg(- \frac{\left((h+R)\cos\psi_0 - R\right)\left(h - R\cos\psi_0 + R\right)^2}{\ell_1^3} + \\
& \frac{3\left(\ell_2 - \ell_1\right)(h+R)\cos\psi_0 + \left(\cos\left(2\psi_0\right) + 2\right)\left(\ell_1(h+R) - R\ell_2\right)}{\ell_1\ell_2} + \\
& \frac{\left(-(h+R)\cos\psi_0 + h + R\right)^2\left((h+R)\cos\psi_0 - h - R\right)}{\ell_2^3}\Bigg)\Bigg).
\end{aligned}
\tag{2.132}
$$

Putting $\cos\psi_0 = 1$ and $\sin\psi_0 = \psi_0$ and simplifying all nominators yields a much simpler expression

$$
V_{rr}^{1}(P_2) \approx \frac{1}{3}\pi G\rho\left(3\left(\frac{3h}{\ell_1} - \frac{h^3}{\ell_1^3}\right) - \frac{3h(h+R)^2\left(\ell_1 - h\right)\psi_0^2}{m_1\ell_1^3}\right) \tag{2.133}
$$

and after replacing $m_1 = \ell_1 - h$ we get the final expression

$$
V_{rr}(P_2) \approx V_{rr}^{1}(P_2) \approx \pi G\rho\left(-\frac{h^3}{\ell_1^3} - \frac{h(h+R)^2\psi_0^2}{\ell_1^3} + \frac{3h}{\ell_1}\right). \tag{2.134}
$$

Almost no differences between original function and simplified version are illustrated in Figure 2.4.

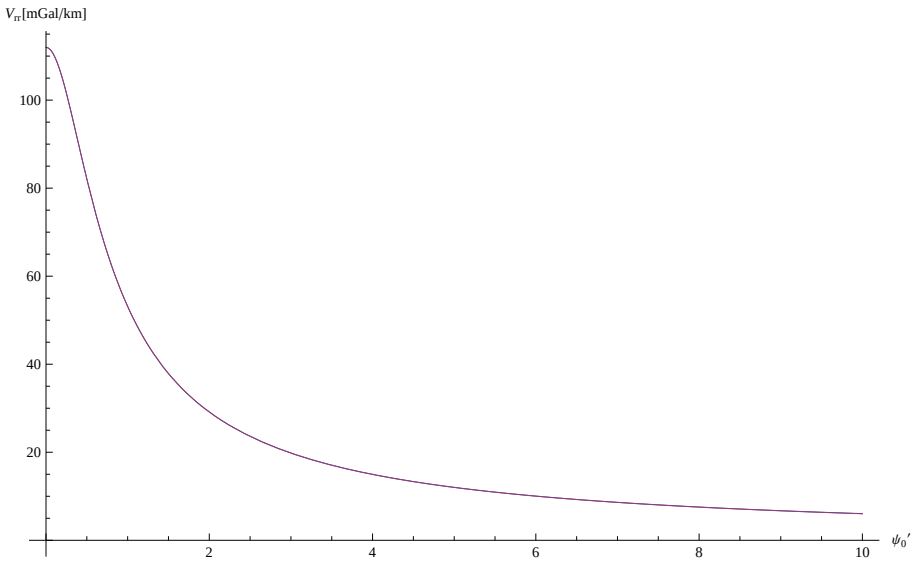

Figure 2.4: *$V_r r$ for limited cylinder.* Original (blue line) and simplified functions (violet line) V_{rr} for $\psi_0 \in (0, 10')$, $h = 1000$ m, $R = R_m$. The lines coincident.

2.3.5 Unlimited Bouguer shell

Gravitational potential V

The potential can easily be derived by introducing $\psi = \pi$ into (2.98). We get

$$V(P) = \frac{\pi G\rho}{3r}\Big(\left(r^2 + r_2 r - 2r_2^2\right)|r - r_2| - \left(r^2 + r_1 r - 2r_1^2\right)|r - r_1| - 2r_1^3 - 3rr_1^2 + 2r_2^3 + 3rr_2^2 \Big) \tag{2.135}$$

Equation (2.135) is again a general formula that holds for any $r > 0$. In special cases we have (cf. [Vaníček et al., 2001], [Heck and Seitz, 2007])

$$V(P_1) = \frac{4\pi G\rho}{3r}\left(r_2^3 - r_1^3\right), \tag{2.136}$$

$$V(P_2) = \frac{4\pi G\rho}{3r_2}\left(r_2^3 - r_1^3\right), \tag{2.137}$$

$$V(P_3) = \frac{2\pi G\rho}{3r}\left(3r_2^2 r - r^3 - 2r_1^3\right), \tag{2.138}$$

$$V(P_4) = 2\pi G\rho\left(r_2^2 - r_1^2\right), \tag{2.139}$$

$$V(P_5) = 2\pi G\rho\left(r_2^2 - r_1^2\right). \tag{2.140}$$

First radial derivative V_r

By introducing $\psi = \pi$ into (2.106) or by derivative of Equation (2.135) we get

$$V_r(P) = \frac{\pi G\rho}{3r^2}\Big(\left(r^2 + r_2 r - 2r_2^2\right) r[r - r_2] - \left(r^2 + r_1 r - 2r_1^2\right) r[r - r_1] + (r^2 + 2r_2^2)|r - r_2| - (r^2 + 2r_1^2)|r - r_1| - 2(r_2^3 - r_1^3)\Big). \tag{2.141}$$

In special cases (points $P_1 - P_5$) we get

$$V_r(P_1) = \frac{4}{3}\pi G\rho \frac{r_1^3 - r_2^3}{r^2}, \tag{2.142}$$

$$V_r(P_2) = \frac{4}{3}\pi G\rho \frac{r_1^3 - r_2^3}{r_2^2}, \tag{2.143}$$

$$V_r(P_3) = \frac{4}{3}\pi G\rho \frac{r_1^3 - r^3}{r^2}, \tag{2.144}$$

$$V_r(P_4) = 0, \tag{2.145}$$

$$V_r(P_5) = 0. \tag{2.146}$$

Inserting $r_1 = R$ and $r_2 = R + h$ in (2.143) yields

$$V_r(P_2) = \frac{4}{3}\pi G\rho \frac{R^3 - R^3 - 3R^2h - 3Rh^2 - h^3}{(R+h)^2}. \tag{2.147}$$

This equation can be approximated for $R \gg h$ so we get the well known formula [Vaníček et al., 2001]

$$V_r(P_2) \approx \frac{4}{3}\pi G\rho \frac{-3R^2h}{R^2} = -4\pi G\rho h. \tag{2.148}$$

Second radial derivative V_{rr}

The radial derivative of (2.141) yields

$$\begin{aligned} V_{rr} = -\frac{2\pi G\rho}{3r^3}\Big(&- 2r_1^2\,|r - r_1| + 2r_2^2\,|r - r_2| + r^3[r - r_1] - r^3[r - r_2] \\ &+ 2r_1^2 r[r - r_1] - 2r_2^2 r[r - r_2] + 2r_1^3 - 2r_2^3\Big). \end{aligned} \tag{2.149}$$

We have as usually replaced $|\cdot|'$ by signum function $[\cdot]$ and left out terms containing $[\cdot]'$. This is a general solution for the points P_1, P_3 and P_5. We

can rewrite this formula for each individual case as follows:

$$V_{rr}(P_1) = -\frac{8\pi G\rho}{3r^3}\left(r_1^3 - r_2^3\right), \tag{2.150}$$

$$V_{rr}(P_3) = -\frac{4\pi G\rho}{3r^3}\left(r^3 + 2r_1^3\right), \tag{2.151}$$

$$V_{rr}(P_5) = 0. \tag{2.152}$$

$$\tag{2.153}$$

At the points P_2 and P_4 the function V_{rr} is not continuous, but it is continuous from left and from right, so we can insert $r = r_2$ into (2.150) or (2.151) having

$$\lim_{r\to r_2^+} V_{rr}(P_2) = -\frac{8\pi G\rho}{3r_2^3}\left(r_1^3 - r_2^3\right), \tag{2.154}$$

$$\lim_{r\to r_2^-} V_{rr}(P_2) = -\frac{4\pi G\rho}{3r_2^3}\left(r_2^3 + 2r_1^3\right), \tag{2.155}$$

and $r = r_1$ into (2.151) or (2.152) having

$$\lim_{r\to r_1^+} V_{rr}(P_4) = -\frac{4\pi G\rho}{3r^3}\left(r^3 + 2r_1^3\right), \tag{2.156}$$

$$\lim_{r\to r_1^-} V_{rr}(P_4) = 0. \tag{2.157}$$

2.3.6 Numerical examples

We will show the differences between the limited shell, unlimited shell, limited plate and unlimited plate on three examples. The geometry of the Bouguer shell and plate is illustrated at Figure 2.5.

The first example is a an example with simple numerical values. The size of the shell is given by values $r_1 = 5.5$ m, $r_2 = 7$ m, $\psi_0 = 0.5$ rad. Dimensions of the corresponding Bouguer plate were chosen to have a similar shape and volume as the spherical shell: $R = \psi_0(r_1 + r_2)/2$ and $h = r_2 - r_1$. Numerical values are $R = 3.125$ m and $h = 1.5$ m. The resulting potential V and

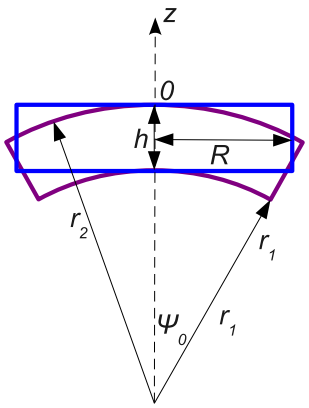

Figure 2.5: *Bouguer plate and shell.* Geometry of the limited Bouguer plate (blue shape) and the limited Bouguer shell (violet shape).

its first and second radial derivatives for a point $P(r),\ r \in \langle 1; 11\rangle$, which is under, inside and above the shell, is plotted in Figure 2.6 by blue lines. Corresponding values under, inside and above the Bouguer plate $P(z),\ z \in \langle -6; 4\rangle$, are shown in the same figure by violet lines. Orange dashed lines and red points show the boundary of the plate $z = -h,\ z = 0$ that corresponds to boundaries of the shell r_1 and r_2.

The second example is a Bouguer shell with dimensions $r_1 = R_m$, $r_2 = R_m + 750$ m and $\psi_0 = 1°$. Corresponding Bouguer plate has dimensions $R = 111201$ m and $h = 750$ m. These values approximately corresponds to the maximal elevation of the residual terrain between DEMs SRTM3 and DTM2006 if the terrain correction is computed up to the distance $1°$.

The third example is a Bouguer shell with dimensions $r_1 = R_m$, $r_2 = R_m + 750$ m and $\psi_0 = 5'$. The corresponding Bouguer plate has dimensions $R = 9266.79$ m and $h = 750$ m. Values are similar as in the second example, but ψ_0 now corresponds to the terrain correction evaluated up to the spherical

distance $5'$. We have evaluated the effect for the limited plate and shell by exact formulas (Table 2.5) and also by simplified formulas which were derived from exact formulas by neglecting small terms (Table 2.6). The results are almost identical as was expected.

Figure 2.7 shows V, V_r and V_{rr} for the layer of thickness $h = 750$ m as a function of ψ_0. Examples 2 and 3 are particular solutions shown in Figure 2.7 for $\psi_0 = 1^\circ$ and $\psi_0 = 5'$.

quantity, units	unlimited		limited	
	plate	shell	plate	shell
V $[m^2 s^{-2}]$	∞	0.00002	4.18397×10^{-6}	3.99834×10^{-6}
V_r $[mGal]$	-0.16795	-0.26907	-0.12973	-0.14107
V_{rr} $[mGal/km]$	0	76.8763	48.4522	75.4271

Table 2.3: *Example 1: Effects of the Bouguer plate and shell.*
Shell geometry: $r_1 = 5.5$ m, $r_2 = 7$ m, $\psi_0 = 0.5$ rad.

quantity, units	unlimited		limited	
	plate	shell	plate	shell
V $[m^2 s^{-2}]$	∞	10700.3	93.0687	93.0648
V_r $[mGal]$	-83.9763	-167.933	-83.6931	-84.416
V_{rr} $[mGal/km]$	0	0.0527	0.7552	0.7815

Table 2.4: *Example 2: Effects of the Bouguer plate and shell.*
Shell geometry: $r_1 = R_m, r_2 = R_m + 750$ m, $\psi_0 = 1^\circ$.

We will use all derived formulas to predict the gravitational potential, gravity and gravity gradient at points on the surface of the earth. Therefore,

quantity, units	unlimited		limited	
	plate	shell	plate	shell
$V\ [m^2s^{-2}]$	∞	10700.3	7.47549	7.47528
$V_r\ [mGal]$	−83.9763	−167.933	−80.5836	−80.6353
$V_{rr}\ [mGal/km]$	0	0.0527	9.0325	9.0565

Table 2.5: *Example 3. Effects of Bouguer plate and shell (exact solution)* Shell geometry: $r_1 = R_m, r_2 = R_m + 750$ m, $\psi_0 = 5'$. Values were evaluated using exact formulas without neglecting any terms.

quantity, units	unlimited		limited	
	plate	shell	plate	shell
$V\ [m^2s^{-2}]$	∞	10700.3	7.47549	7.47528
$V_r\ [mGal]$	−83.9763	−167.933	−80.5836	−80.6353
$V_{rr}\ [mGal/km]$	0	0.0527	9.0325	9.0565

Table 2.6: *Example 3. Effects of Bouguer plate and shell (simplified solution).* Shell geometry: $r_1 = R_m, r_2 = R_m + 750$ m, $\psi_0 = 5'$.

the most important case is when the point is located on the top of the surface (point P_2). The gravitational potential and its derivatives for such a point for all three examples are shown in Tables 2.3, 2.4 and 2.5. The second order derivatives, which are not continuous functions, are computed as limits going from the outer space to the interior of the plate or shell. The results can be interpreted as follows:

- In case of the gravitational potential, differences between limited and unlimited layers are always important. Moreover, the unlimited Bouguer plate generates an infinite gravitational potential (cf. [Vaníček et al.,

2001]).

- For V_r, there are big differences between the unlimited plate and the unlimited shell, which is twice as big. This difference has also been studied many times and is known as a difference between planar and spherical approximation. Similar behavior have also limited plate and shell. The effect of the limited plate converges fast to the effect of the unlimited plate. The effect of the limited shell converges to the effect of the unlimited shell as well, but the convergence is much slower, as is illustrated on Figures 2.8 and 2.9 for the Bouguer layer of thickness $h = 100$ m.

- In forward modeling, the terrain correction is usually computed by integration only to some distance ψ_{max} from the computational point. Such terrain correction is then often combined with the effect of the unlimited Bouguer plate. The lower is the distance ψ_{max}, the bigger is the difference between unlimited and limited Bouguer plate (cf. second rows columns 1 and 3 in tables 2.3, 2.4 and 2.5). With increasing accuracy and resolution of GGMs, the integration distance ψ_{max} becomes smaller. But for such small distances ψ_{max}, the limited Bouguer plate effect should be preferred to an unlimited plate that is usually used nowadays. This is even more important for V_{rr} and small radius ψ_{max} and it is absolutely necessary in the case of the potential V. Another option (but much more complicated) how to reduce the large effect of unlimited shell is to reduce such an effect by the far zone terrain correction ([Novák et al., 2001], [Mikuška et al., 2006]).

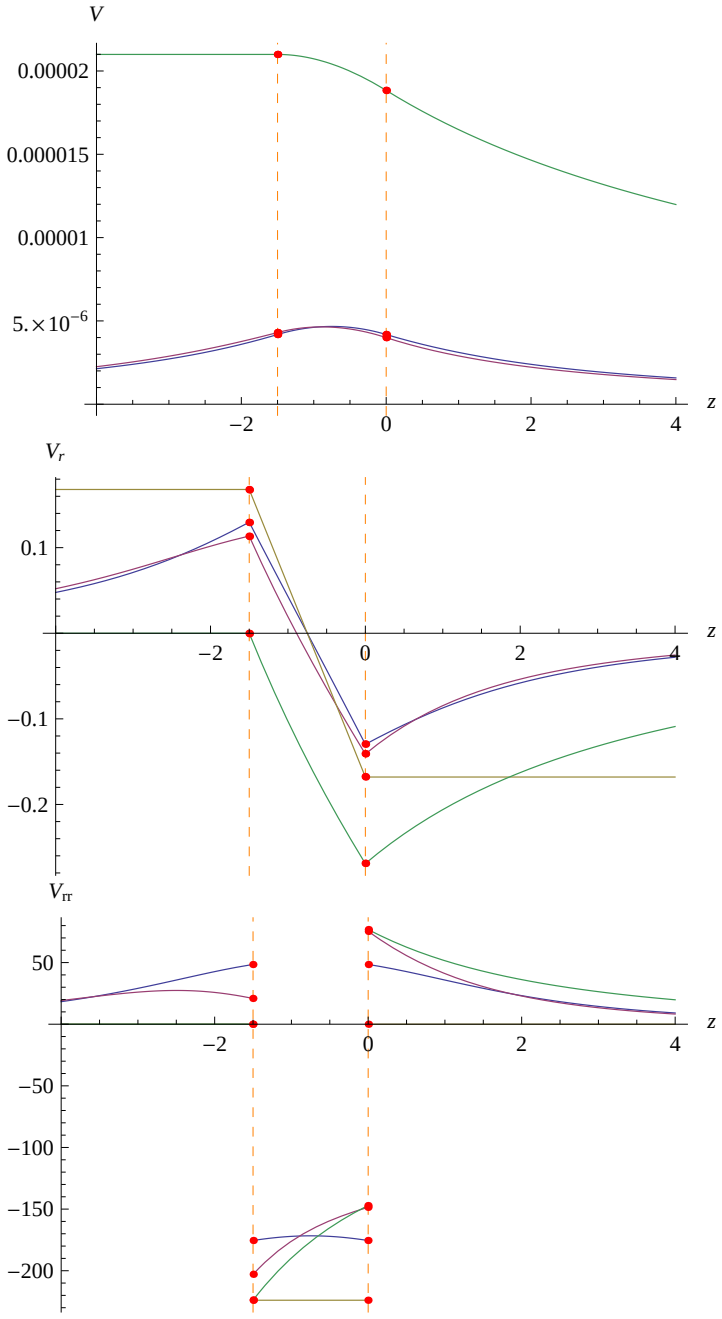

Figure 2.6: *Example 1: Comparison of the Bouguer plate and shell.* V $[m^2/s^2]$, V_r $[mGal]$ and V_{rr} $[mGal/km]$ of the limited Bouguer plate (blue), the limited Bouguer shell (violet), unlimited Bouguer plate (brown) and unlimited Bouguer shell (green).

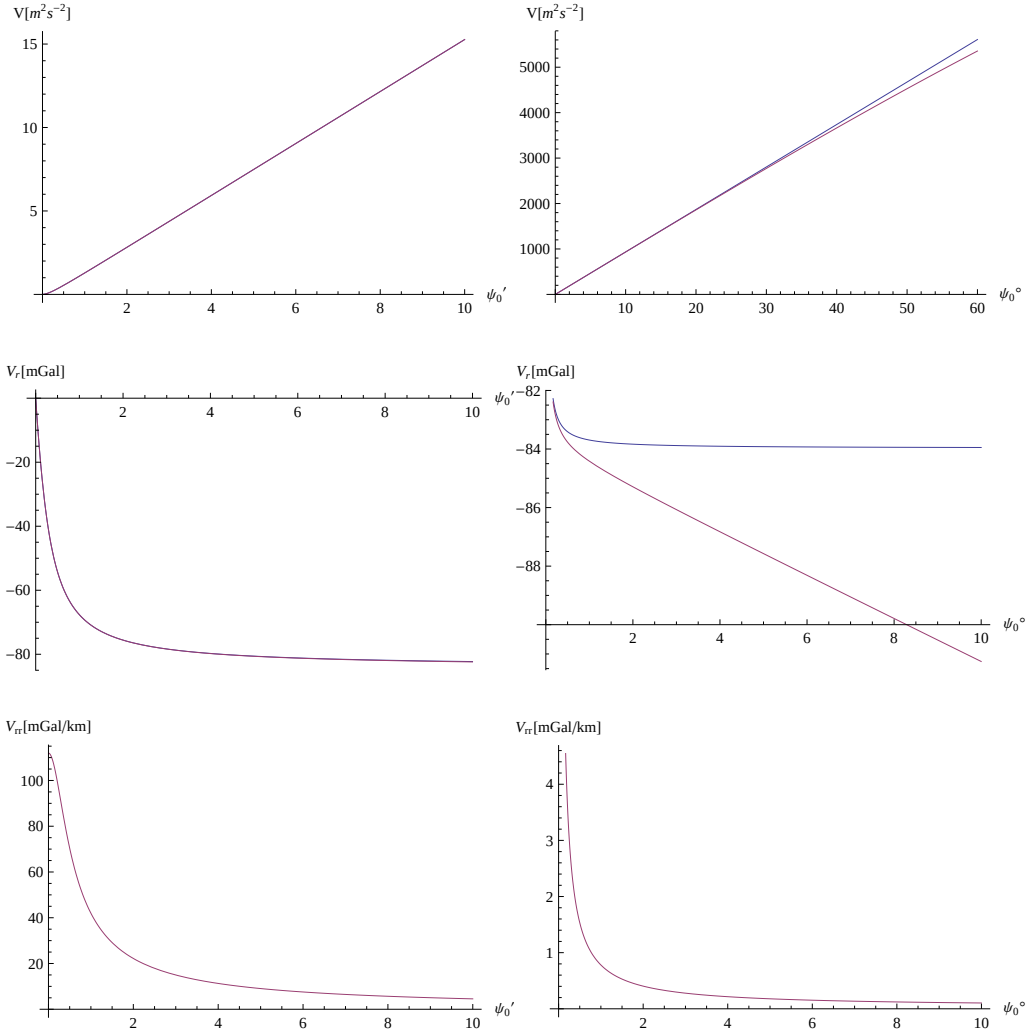

Figure 2.7: *Dependence of V, V_r and V_{rr} on the radius of the Bouguer layer.* The radius is defined either by the angle ψ_0 of the limited Bouguer shell ($r_1 = R_m$, $r_2 = R_m + 750$ m, violet line) or corresponding radius R of limited Bouguer plate (thickness $h = 750$ m, blue line). Note that lines often coincide. Left plots are detail for $\psi_0 \in \langle 0; 10' \rangle$, right plots are plots up to $10°$ (or $60°$ for V). Values are evaluated on the top of the Bouguer plate or shell (and on their vertical axes). Second derivatives are limits from the outer space.

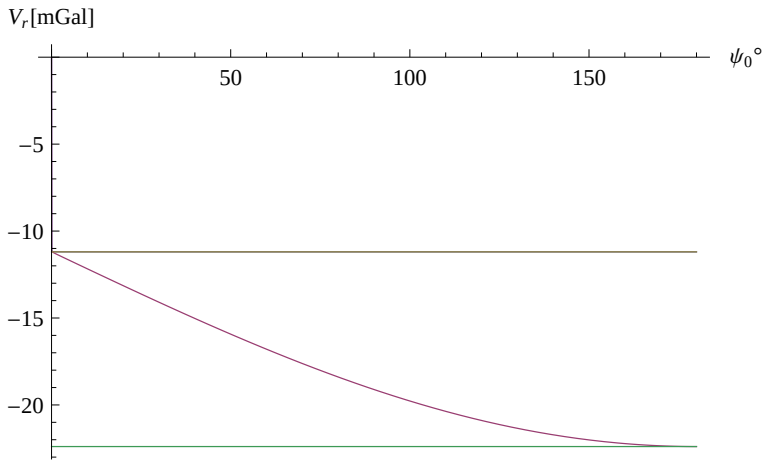

Figure 2.8: *V_r for Bouguer layers.* V_r for the limited Bouguer plate (blue), limited Bouguer shell (violet), unlimited Bouguer plate (brown) and unlimited Bouguer shell (green). The effect of limited Bouguer plate first coincides with the effect of the limited Bouguer shell and then with the effect of the unlimited Bouguer plate, so it is overlapped on this figure. See Figure 2.9 for details.

Tables 2.3, 2.4 and 2.5 illustrate also a known fact that the potential V increases with the volume of the Bouguer layer. The shape (plate or shell) does not play such an important role in this case, but the size does (thickness h and either the radius R or angle ψ_0).

For V_r, the situation differs. There is only a small difference between V_r generated by the unlimited plate and the plate or shell limited to $\psi_0 = 1°$ (see the second row of Table 2.4, columns 1, 3 and 4). But the difference is much larger when the plate or shell is limited to $\psi_0 = 5'$ (see the second row of Table 2.5, columns 1, 3 and 4). This fact should be taken into account when combining terrain corrections, that were computed only to some small integration radius, with the effect of the Bouguer plate or shell. In the case

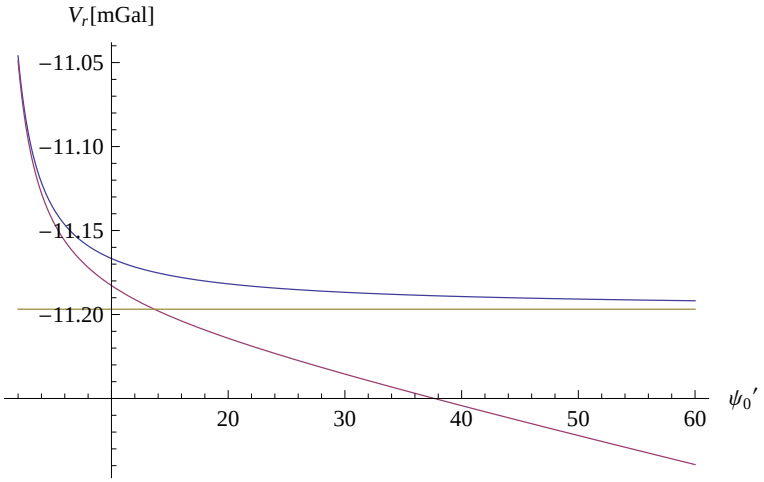

Figure 2.9: *V_r for Bouguer layers — detail.* V_r for the limited Bouguer plate (blue), limited Bouguer shell (violet) and unlimited Bouguer plate (brown). This detail for $\psi_0 \in (2'; 60')$ shows convergence of the limited Bouguer shell to the unlimited Bouguer shell, which is not clearly visible on Figure 2.8.

of the unlimited Bouguer shell, the effect is approximately twice as large as in the other cases and it is necessary to fix it by introduction of far-zone terrain effects.

The absolute value of V and V_r increases with the size of the Bouguer layer. The behavior of V_{rr} is completely different: for unlimited plate it is always 0 (this corresponds to the fact that V_r is constant above the plate). For the unlimited shell, V_{rr} is not zero, but a very small number (V_r is not constant but almost constant above the shell). For the limited shell and limited plate, V_{rr} increases with decreasing ψ_0 in case of the shell or R in case of the plate. The dependence on the radius (angle) is very strong and acts inversely (smaller radius, bigger effect) as one could expect.

2.3.7 Terrain effects

Terrain effect (TE) is an effect of the terrain on the gravitational potential of the earth or on its functional. The terrain is defined [Tsoulis et al., 2009] as the part of topography which rises above or below the local horizon of a particular point P located on the surface of the earth. The surface of the earth is approximated by digital elevation models (DEM), which are provided in various forms (grids, coefficients of a spherical or ellipsoidal harmonic expansion of a smoothed surface, scattered points, triangulated irregular network – TIN etc.). Heights in any model can be given above the geoid (orthometric heights), quasi-geoid (normal heights) or the reference ellipsoid (geodetic heights). Because the terrain is described by relative elevation of the topography with respect to the point P and because we will compute the terrain effect only up to the spherical distance of order of tens of arc minutes, we can neglect differences between various types of heights and use spherical approximation, where both the reference height level and the local horizon are approximated by the geocentric spheres. In the close neighborhood of the point P, the planar approximation may be also used. In the planar approximation, both the reference level of heights and the local horizon are approximated by parallel planes. Both approximation can be used only up to a certain distance from the computation point. A couple of kilometers and several degrees of arc represent the most commonly accepted values for the transition from planar to spherical and from spherical to some higher (e.g., ellipsoidal) approximation, respectively ([Tsoulis, 2003], [Novák et al., 2001], [Novák and Grafarend, 2005]).

There are many different modeling methods used to describe the terrain geometrically and usually several strategies on how to compute the gravitational effect for the respective modeling method numerically. Generally, all

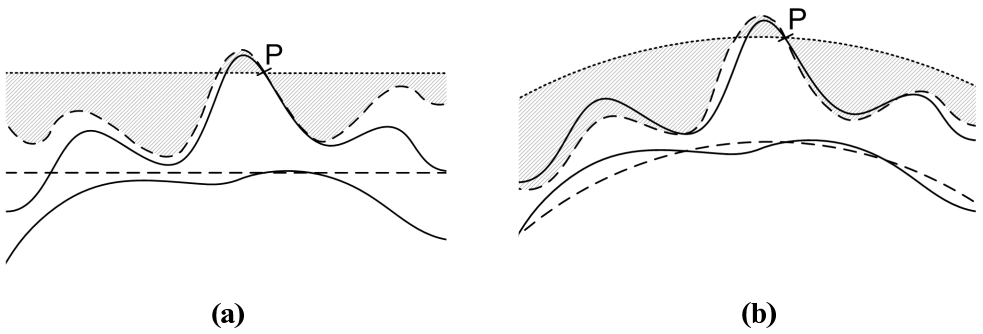

Figure 2.10: *(a) Planar and (b) spherical approximation of the terrain.* Solid lines — real reference level (e.g., geoid) and real terrain, dashed lines — planar (spherical) reference level and planar (spherical) approximation of terrain, dashed lines — point level in planar and spherical approximation.

methods divide the terrain into some simple volume elements such as right-rectangular prisms, spherical or ellipsoidal tesseroids. These mass elements correspond to the chosen approximation method utilizing the height data of the available DEM as numerical values that define their geometric shape. In some cases the terrain effect, that is obtained from these volume elements, can be computed analytically – if a closed expression for the gravitational signal of the respective mass element exists – or numerically by using some approximate formulas through standard numerical integration procedures. The final numerical value expressing the terrain-induced gravitational attraction computed at a certain computation point P results from the summation of individual contributions of the volume elements. The procedure is based on a well-known super-positioning principle of the potential theory [Blakely, 1996].

2.3.8 TE in spherical approximation

The gravitational potential in spherical coordinates is given by

$$V(r,\varphi,\lambda) = G\rho \iint\limits_{\sigma} \left[\int\limits_{r'} \frac{1}{\ell} r'^2 dr' \right] d\sigma, \tag{2.158}$$

where ℓ is the spatial distance between computational point $P(r,\varphi,\lambda)$ and integration point $P'(r',\varphi',\lambda')$

$$\ell = \sqrt{r^2 + r'^2 - 2rr'\cos\psi} \tag{2.159}$$

and $\cos\psi$ is cosine of the spherical distance between radius vectors of the point $P(r,\varphi,\lambda)$ and $P'(r',\varphi',\lambda')$ given by

$$\cos\psi = \sin\varphi\sin\varphi' + \cos\varphi\cos\varphi'\cos(\lambda-\lambda') \tag{2.160}$$

and where the infinite surface element $d\sigma = \cos\varphi' d\varphi' d\lambda'$ or as

$$V(r,\varphi,\lambda) = G\rho \iiint\limits_{\Omega} \frac{1}{\ell} d\Omega \tag{2.161}$$

where the infinite volume element $d\Omega = r'\cos\varphi' dr' d\varphi' d\lambda'$.

The potential of a particular tesseroid of a constant mass density ρ is given by

$$V(r,\varphi,\lambda) = G\rho \int\limits_{\lambda_1}^{\lambda_2}\int\limits_{\varphi_1}^{\varphi_2}\int\limits_{r_1}^{r_2} \frac{1}{\ell} r'^2 \cos\varphi' dr' d\varphi' d\lambda' \tag{2.162}$$

The first radial derivative of the potential $\partial V(r,\varphi,\lambda)/\partial r$ is given by any of relations

$$\frac{\partial V}{\partial r} = G\rho \int\limits_{\lambda_1}^{\lambda_2}\int\limits_{\varphi_1}^{\varphi_2}\int\limits_{r_1}^{r_2} \frac{r - r'\cos\psi}{\ell^3} r'^2 \cos\varphi' dr' d\varphi' d\lambda', \tag{2.163}$$

$$\frac{\partial V}{\partial r} = G\rho \iint\limits_{\sigma} \left[\int\limits_{r'} \frac{r - r'\cos\psi}{\ell^3} r'^2 dr' \right] d\sigma, \tag{2.164}$$

$$\frac{\partial V}{\partial r} = G\rho \iiint\limits_{\Omega} \frac{r - r' \cos\psi}{\ell^3} d\Omega. \tag{2.165}$$

The second radial derivative of the potential $\partial^2 V/\partial r^2$ is given by any of relations

$$\frac{\partial^2 V}{\partial r^2} = G\rho \int\limits_{\lambda_1}^{\lambda_2} \int\limits_{\varphi_1}^{\varphi_2} \int\limits_{r_1}^{r_2} \frac{2r'^2 - 4\cos\psi r r' + (3\cos^2\psi - 1)r^2}{\ell^5} r'^2 \cos\varphi' dr' d\varphi' d\lambda', \tag{2.166}$$

$$\frac{\partial^2 V}{\partial r^2} = G\rho \iint\limits_{\sigma} \left[\int\limits_{r'} \frac{2r'^2 - 4\cos\psi r r' + (3\cos^2\psi - 1)r^2}{\ell^5} r'^2 dr' \right] d\sigma, \tag{2.167}$$

$$\frac{\partial^2 V}{\partial r^2} = G\rho \iiint\limits_{\Omega} \frac{2r'^2 - 4\cos\psi r r' + (3\cos^2\psi - 1)r^2}{\ell^5} d\Omega. \tag{2.168}$$

None of integrals in Equations (2.162)–(2.168) can be solved analytically. However, there are several numerical methods how to evaluate these integrals (the list is not complete):

THS method — Tesseroids by Heck-Seitz method: expansion of the integration kernel into the Taylor series up to order 0 or 2 and analytical integration of the approximated kernel [Heck and Seitz, 2007].

TMV method — Tesseroids by Martinec-Vaníček method: analytical solution of the inner integral (integration variable r') and numerical quadrature of the resulting surface integral.

3D Gauss-Legendre quadrature — this method is a standard numerical procedure for evaluation of volume integrals, applications in terrain effect computations in geodesy were studied, e.g., in [Ardalan and Safari, 2004] or [Wild-Pfeiffer, 2008].

2.3.9 TMV method

The solution of the inner indefinite integral in Equation (2.158) is

$$\int \frac{r'^2}{\ell} dr' = \mathcal{K} = \frac{1}{2}\left((r' + 3r\cos\psi)\ell + r^2(3\cos^2\psi - 1)\log|2(\ell + r' - r\cos\psi)|\right), \tag{2.169}$$

where

$$\ell = \sqrt{r^2 + r'^2 - 2rr'\cos\psi}, \tag{2.170}$$

and the solution of the respective definite integral with boundaries r_1, r_2 is

$$\int_{r_1}^{r_2} \frac{r'^2}{\ell} dr' = \mathcal{K}\Big|_{r'=r_1}^{r'=r_2} = \frac{1}{2}\left(r^2\left(1 - 3\cos^2\psi\right)\log\left(\frac{\ell(r_1) - r\cos(\psi) + r_1}{\ell(r_2) - r\cos(\psi) + r_2}\right) + 3r\cos\psi\left(\ell(r_2) - \ell(r_1)\right) - r_1\ell(r_1) + r_2\ell(r_2)\right) \tag{2.171}$$

, where

$$\ell(r_1) = \sqrt{r^2 + r_1^2 - 2rr_1\cos\psi}, \tag{2.172}$$

$$\ell(r_2) = \sqrt{r^2 + r_2^2 - 2rr_2\cos\psi}, \tag{2.173}$$

so the final surface integral is given by

$$V(r,\varphi,\lambda) = G\rho\int_{\lambda_1}^{\lambda_2}\int_{\varphi_1}^{\varphi_2}\mathcal{K}\Big|_{r'=r_1}^{r'=r_2}\cos\varphi' d\varphi' d\lambda'. \tag{2.174}$$

Similarly, the radial derivative of the potential V_r (attraction) is given by

$$V_r(r,\varphi,\lambda) = G\rho\int_{\lambda_1}^{\lambda_2}\int_{\varphi_1}^{\varphi_2}\mathcal{K}_r\Big|_{r'=r_1}^{r'=r_2}\cos\varphi' d\varphi' d\lambda', \tag{2.175}$$

where

$$\mathcal{K}_r = 3\ell\cos\psi + \frac{\ell r'}{r} - \frac{r'^3}{\ell r} + \frac{1}{2}r\left(3\cos^2\psi - 1\right) + r\left(3\cos^2(\psi) - 1\right)\log(\ell - r\cos(\psi) + r'), \tag{2.176}$$

so that

$$\mathcal{K}_r\Big|_{r'=r_1}^{r'=r_2} = 3\cos\psi(\ell(r_2)-\ell(r_1)) + \frac{\ell(r_2)r_2}{r} - \frac{\ell(r_1)r_1}{r} - \frac{{r_2}^3}{\ell(r_2)r} + \frac{{r_1}^3}{\ell(r_1)r} + r\left(3\cos^2(\psi)-1\right)\log\left(\frac{\ell(r_2)-r\cos\psi+r_2}{\ell(r_1)-r\cos\psi+r_1}\right). \quad (2.177)$$

The second radial derivative V_{rr} is given by

$$V_{rr}(r,\varphi,\lambda) = G\rho\int_{\lambda_1}^{\lambda_2}\int_{\varphi_1}^{\varphi_2}\mathcal{K}_{rr}\Big|_{r'=r_1}^{r'=r_2}\cos\varphi' d\varphi' d\lambda', \quad (2.178)$$

where kernel K_{rr} is given by [Makhloof and Ilk, 2008]

$$\mathcal{K}_{rr} = \frac{(r'\cos\psi - r)((r'^2+3r^2)\cos\psi + rr'(1-6\cos^2\psi))}{\ell^3} + (3\cos^2\psi-1)\log|r'-r\cos\psi+\ell| + \frac{2r'+6r\cos\psi-9r'\cos^2\psi}{\ell}, \quad (2.179)$$

so that $\mathcal{K}_{rr}\Big|_{r'=r_1}^{r'=r_2}$ is after few manipulations [Wild-Pfeiffer, 2008]

$$\mathcal{K}_{rr}\Big|_{r'=r_1}^{r'=r_2} = \frac{1}{r^2}\left(r^2\left(3\cos^2(\psi)-1\right)\log\left(\frac{\ell(r_2)+r_2-r\cos\psi}{\ell(r_1)+r_1-r\cos\psi}\right) + 3r\cos\psi\left(\ell(r_2)-\ell(r_1)\right) - \frac{(r^2-r_1^2)r_1^3}{2\ell^3(r_1)} + \frac{r_2^3(r^2-r_2^2)}{2\ell^3(r_2)} + \frac{r_1^3}{2\ell(r_1)} - \frac{r_2^3}{2\ell(r_2)} + r_2\ell(r_2) - r_1\ell(r_1)\right). \quad (2.180)$$

2.3.10 TE in planar approximation

The gravitational potential V of a prism at the point $P(x,y,z)$ is given by the Newtonian volume integral

$$V(P) \;=\; G\varrho\int_{x_1}^{x_2}\int_{y_1}^{y_2}\int_{z_1}^{z_2}\frac{1}{\ell}dx'dy'dz', \quad (2.181)$$

where $(x_i,\ y_i,\ z_i)$ with $i = 1, 2$ are the coordinates of the prism's corners with respect to the local Cartesian coordinate system, $dx'dy'dz'$ is the infinitesimal volume element, and

$$\ell = \sqrt{(x - x')^2 + (y - y')^2 + (z - z')^2}, \tag{2.182}$$

is the Euclidean distance between the computation point $P(x, y, z)$ and an gravitating particle coordinated by (x', y', z').

There are three basic methods how to evaluate the terrain effect in planar approximation:

PAN method — Analytical integration. The analytical solution of (2.181) exists and can be expressed as a closed form formula [Mader, 1951], [Nagy et al., 2000], [Nagy et al., 2002].

PMM method — MacMillan's solution. Development of the kernel function $1/\ell$ into the Taylor series and solution of the integral with kernel approximated by series to certain degree [Macmillan, 1930], [Anderson, 1976], [Tsoulis, 1999b].

FFT methods — Evaluation of terrain effect is a time-consuming task. In the past, it was very difficult to calculate terrain corrections for larger areas from detailed DEM. A group of methods based on Fast Fourier Transform was developed to solve the task using much less computational time. But these methods are based on some approximations and it is also difficult to cut off the effect at the chosen distance from the computational point, which is necessary for combination of the signal with other gravity data. A review of FFT methods for evaluation of gravity gradients can be found in [Zhu, 2007].

We will review the PAN method in the next subsection, because it provides the most accurate solution. Description of the other methods can be found in cited publications.

2.3.11 PAN method

The closed analytical expression for the gravitational potential of a right-rectangular prism computed at the point $P(x, y, z)$ is given among others by [Mader, 1951]

$$V(P) = G\rho \sum_{i,j,k}^{2} (-1)^{i+j+k} \left(\Delta x_i \Delta y_j \ln \left| \frac{\Delta z_k + \ell_{ijk}}{\ell_{ij}} \right| + \Delta y_j \Delta z_k \ln \left| \frac{\Delta x_i + \ell_{ijk}}{\ell_{jk}} \right| + \Delta x_i \Delta z_k \ln \left| \frac{\Delta y_j + \ell_{ijk}}{\ell_{ik}} \right| - \frac{1}{2} \left(\Delta x_i^2 \arctan \frac{\Delta y_j \Delta z_k}{\Delta x_i \ell_{ijk}} + \Delta y_j^2 \arctan \frac{\Delta x_i \Delta z_k}{\Delta y_j \ell_{ijk}} + \Delta z_k^2 \arctan \frac{\Delta x_i \Delta y_j}{\Delta z_k \ell_{ijk}} \right) \right), \tag{2.183}$$

where (x_i, y_j, z_k) are corners of the prism and where

$$\Delta x_i = (x - x_i), \quad \Delta y_i = (y - y_i), \quad \Delta z_i = (z - z_i), \tag{2.184}$$

$$\ell_{ijk} = \sqrt{(x - x_i)^2 + (y - y_j)^2 + (z - z_k)^2} = \sqrt{\Delta x_i^2 + \Delta y_j^2 + \Delta z_k^2}, \tag{2.185}$$

$$\ell_{ij} = \sqrt{\Delta x_i^2 + \Delta y_j^2}, \quad \ell_{ik} = \sqrt{\Delta x_i^2 + \Delta z_k^2}, \quad \ell_{jk} = \sqrt{\Delta y_j^2 + \Delta z_k^2}. \tag{2.186}$$

The vertical derivative $V_r \approx V_z$ is given by expression

$$V_z(P) = G\rho \sum_{i,j,k}^{2} (-1)^{i+j+k} \left(\Delta y_j \ln \left| \frac{\Delta x_i + \ell_{ijk}}{\ell_{jk}} \right| + \Delta x_i \ln \left| \frac{\Delta y_j + \ell_{ijk}}{\ell_{ik}} \right| - \Delta z_k \arctan \frac{\Delta x_i \Delta y_j}{\Delta z_k \ell_{ijk}} \right). \tag{2.187}$$

The second vertical derivative $V_{rr} \approx V_{zz}$ is given by formula [Rózsa and Tóth, 2005], [Wild-Pfeiffer, 2008]

$$V_{zz}(P) = G\rho \sum_{i,j,k}^{2} (-1)^{i+j+k} \left(- \arctan \frac{\Delta x_i \Delta y_i}{\Delta z_i \ell_{ijk}} \right). \tag{2.188}$$

It is necessary to remark that equations for V, V_z and V_{zz} are not valid in some cases, e.g., when the computation point coincides with an edge of the prism or when the orthogonal projection of point P falls into some face of the prism. All singularities that may occur are described and solved in [Tsoulis, 1999a].

Detailed comparison of THS and PAN methods for V and V_r is provided by Heck and Seitz in [Heck and Seitz, 2007]. They conclude that the THS method is an efficient method, but in the neighborhood of the computational point, the PSA method should be rather used. We have proposed in [Tsoulis et al., 2009] a method combining PSA in the direct vicinity of the computational point with TMV. We have shown that this method is both numerically efficient and accurate.

Chapter 3

Combination of GGM and DEM

3.1 Residual terrain modeling

3.1.1 Idea of RTM

Any global geopotential model suffers from missing the high frequency content of the gravitational field (omission error). Because the high frequency content is generated namely by the terrain near the evaluation point, the gravitational effect effect of terrain masses can be evaluated separately using DEM and added to the reference part of the signal computed from the global model. For example, the gravity anomaly Δg can be approximated as

$$\Delta g \approx \Delta \tilde{g} = \Delta g^g + \Delta g^{rtm} \tag{3.1}$$

where Δg^g is the reference part of the gravity anomaly computed from GGM and Δg^{rtm} is a residual terrain part of the gravity anomaly computed from DEM (terrain effect). Δg^ϵ is an error of the approximation of the true gravity anomaly Δg by $\Delta \tilde{g}$

$$\Delta g^\epsilon = \Delta g - \Delta \tilde{g} = \Delta g - \Delta g^g - \Delta g^{rtm} \tag{3.2}$$

Δg^ϵ is affected mainly by

a) commission error of Δg^g (caused by errors in GGM coefficients),

b) errors in Δg^{rtm} (caused by limited knowledge of geometry and density of terrain masses and by method of evaluation),

c) missing ultra-high frequency spectral content (caused by limited resolution of DEM),

d) non-seamless spectral separation between Δg^g and Δg^{rtm},

e) errors in upward/downward continuation of Δg from mean surface to actual topography.

We will show in the following sections method for very accurate prediction of height anomaly ζ, gravity g and gravity gradient g_r by a combination method using EGM08 and terrain induced gravity signal.

The biggest issue we are facing is the fact that the gravitational signal of the topography contributes to all frequencies of the gravitational potential. But EGM08 itself already incudes the gravitational effect of the global topography. For a spectrally seamless combination of Δg^g and Δg^{rtm}, Δg^{rtm} (and the other RTM quantities) should contain only frequencies that are higher than maximal frequency of EGM.

This may be done using a *residual terrain modeling (RTM) method*. This method was first described for gravity anomalies in [Forsberg, 1984]. We will shortly review this method according to [Forsberg, 1984] and [Forsberg, 1994] and then generalize this method for another gravity field quantities (such as the potential V, height anomaly ζ and second radial derivative $\partial^2 V/\partial r^2$) and improve it for a better fit with EGM08.

3.1.2 Mean elevation surface

The idea behind RTM is that in addition to a real topography surface (approximated by the best available DEM) we use a mean elevation surface (MES) that corresponds to GGM, i.e., has the same spatial resolution, and we reduce all gravitational terrain effects by effects generated by MES, which is expected already to be included in GGM. MES can be given either as a spherical harmonic expansion of the global topography to the same degree and order as EGM or by a suitable filtering of local terrain heights [Forsberg,

1994]. Example of a real topography and MES is shown at figure 3.1.

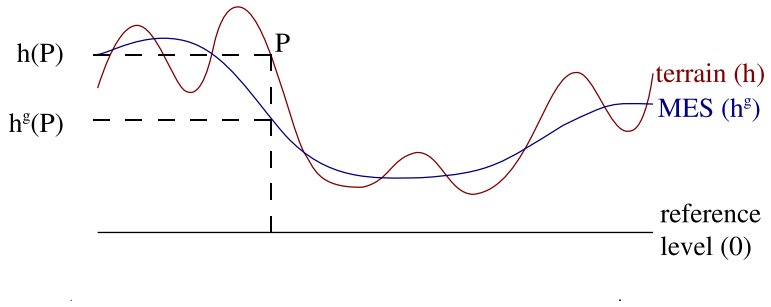

Figure 3.1: *Real terrain and mean elevation surface (MES)*

Contrary to the classic terrain effect, which represents the gravitational effect of masses between a constant elevation level of a point P and the actual topographical surface (see Figure 3.3), the residual terrain effect represents the effect of masses between MES and actual topography (see Figure 3.2). The RTM density anomalies make a balanced set of positive and negative density anomalies, representing areas where the topography is either above or below MES. Therefore the gravitational effect of the RTM density anomalies will in general cancel out in zones at larger distances from a computational point (e.g., a distance 2-3 times the resolution of MES), which makes RTM reductions easy to work with in practise [Forsberg, 1994]. For EGM08 this means that the terrain correction can safely be evaluated only up to the spherical distance $10'$, that is the central Europe about 12 km in east-west direction and 18 km in south-north direction.

RTM has two properties which will be now explained in more detail. The first one is the so-called harmonic correction. The second is the problem of a too large effect generated by the unlimited Bouguer layers.

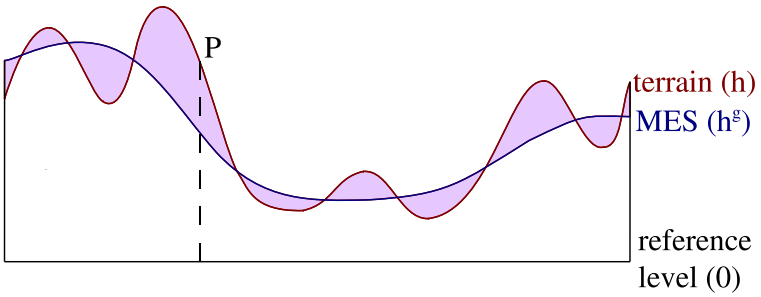

Figure 3.2: *Residual terrain effect (RTM)*

3.1.3 Harmonic correction

The gravitational effect of the residual terrain (see Figure 3.2) can be evaluated by several methods. The most common is probably modeling the residual effect by prisms. The bottom face of the prism has the elevation h^g and the top face has the elevation h. This method was described also in this thesis in subsection 2.3.11. However, this method has one significant issue: if the point P lies under MES, we have to evaluate the effect inside the masses, because the evaluation point P is inside MES. This problem is not handled automatically by using prism modeling as it is usually used and as it was described in Subsection 2.3.11; a so-called harmonic correction has to be added. This problem was pointed out already in [Forsberg, 1984]. In this work, the problem is solved by introducing the harmonic correction for gravity anomalies. However, the harmonic correction was developed only for gravity anomaly and no other corrections were derived for other gravity field quantities. This problem becomes again important after the release of EGM08, which gives more focus on RTM. Recently, the problem was recalled in [Forsberg, 2009] (the problem was pointed out, but not solved) and [Omang

et al., 2010]. In [Omang et al., 2010], the authors moved the evaluation point P above masses (MES), then they removed the topography (the moved point was already not inside) and finally they are analytically continued the value back to the point P.

We propose another solution to the harmonic reduction problem. We split the residual terrain effect on four parts: the Bouguer layer of thickness h and the corresponding terrain effect going through point $P(h)$ (see Figure 3.3) and to a Bouguer layer of thickness h^g and the corresponding terrain effect (see Figure 3.4). We will show that our method can easily handle the problem of harmonic correction.

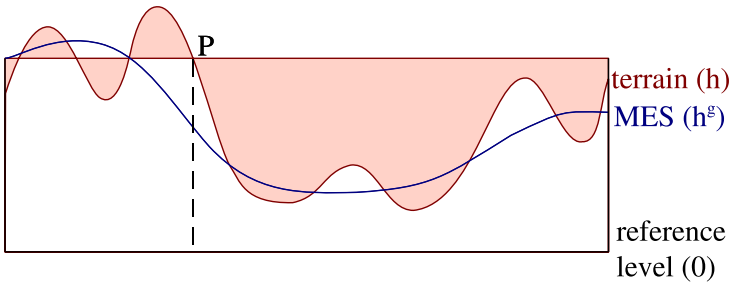

Figure 3.3: *Terrain effect in planar approximation*

The harmonic correction can be applied in cases, when we had model which is capable to model gravitation outside masses as a harmonic function and inside masses as a non-harmonic function as it is in the reality. However, global geopotential models given as series of spherical harmonics cannot handle non-harmonic functions. The values are from the mean elevation surface continued downward to the reference ellipsoid using analytical continuation. As a result, all values computed from GGM outside its reference ellipsoid act as harmonic functions, even for points which are in the reality inside

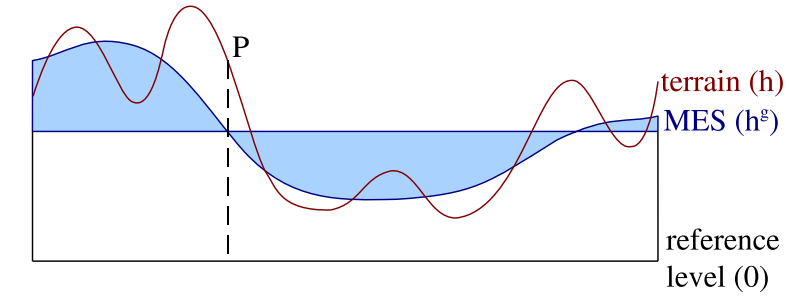

Figure 3.4: *Terrain effect of MES*

masses. The non-harmonicity of functions inside masses is not part of GGM and therefore should not be corrected.

Despite the last paragraph, we will derive a solution which includes the harmonic correction as it is more general. The expressions which will be derived for this more advanced concept, can be used also for evaluation of RTM without harmonic correction, as will be shown later.

3.1.4 Size of Bouguer layers

First, we would like to remind the terminology, which is used herein. The Bouguer layer has a shape of either a Bouguer plate (in planar approximation) or a Bouguer shell (in spherical approximation). The unlimited plate is an infinite plate, whereas the limited plate is truncated at radius R from the center so it has a shape of a cylinder. The unlimited Bouguer shell has not an infinite volume as the unlimited plate. It is a spherical layer. The limited Bouguer shell is again truncated at a certain distance from the computational point.

The traditional introduction of the Bouguer layers has one issue. The

gravitational effect of the Bouguer layers (plate or shell) is usually evaluated for the infinite plate or for the whole Bouguer shell, whereas the terrain effect is evaluated only up to a certain distance from the computational point. This can cause a significant discrepancy between the size of the terrain effect and the size of the gravitational effect of the Bouguer layer.

We can demonstrate it on a simple example: imagine a point P on a single mountain of the height $h(P) = 8000$ m above the sea level. For simplicity, we put $h^g(P) = 0$. The gravitational signal generated by topography of such a mountain is split to a Bouguer shell of thickness 8000 m, which generates a very large gravitational signal. Almost all of that signal would be canceled by the terrain correction, which would have above oceans exactly the same gravitational effect as the respective part of the Bouguer shell. The effect would be almost canceled also above land. However, once the evaluation of the terrain effect is limited, the huge part of this virtual effect remains uncompensated. The purpose of the terrain effect for such points is not only to model rough topography nearby the evaluational point, but it should also correct the large gravitational effect of the Bouguer layer so it cannot be limited.

This issue is well known and a lot of effort has been done to evaluate the omitted terrain effect, which is called the far-zone terrain effect, see, e.g., [Novák et al., 2001], [Mikuška et al., 2006] or [Makhloof and Ilk, 2008]. We propose in this thesis an alternative approach: instead of evaluation of the far-zone terrain effect, we can cut the effect of the Bouguer shell at the same distance as the terrain effect.

Our solution is based on truncation of the Bouguer plate or shell at the same distance from the computational point where we stop evaluation of the terrain effect. We use formulas derived for the limited Bouguer plate and the

limited Bouguer shell instead of formulas for the unlimited Bouguer plate or shell as it is usual in geodesy. In our approach, both the effect of terrain and of the Bouguer layer are omitted behind a certain distance.

We will now demonstrate our modification of the residual terrain modeling, which is able to fix both above mentioned issues. First, we will apply the method for the gravity anomaly Δg (as the original RTM was developed for the gravity anomaly in [Forsberg, 1984]). Then we will generalize the method also for the gravitational potential V and its second radial derivative V_{rr}.

3.2 Derivation of RTM effects

3.2.1 RTM for Δg in planar approximation

The residual terrain effect can be evaluated only up to a small distance of $10'$–$20'$ from the computational point [Forsberg, 1984]. In such a case, we can evaluate the terrain effect in planar approximation instead of spherical approximation with the sufficient accuracy. We will provide a more general solution for spherical approximation in Subsection 3.2.2.

Let us start with the definition of the RTM effect for the gravity anomaly Δg over some area S

$$\Delta g^{rtm}(P) = \Delta g^{rtm}(x, y, z) = -G\rho \iint_S \left(\int_{h^g}^{h} \frac{z - z'}{l^3} dz' \right) dS, \tag{3.3}$$

where h^g is the elevation of MES and h is the elevation of the actual topography (approximated by high-resolution DEM). Both h and h^g are illustrated on Figure 3.2. All the other constants have the same meaning as in Section 2.3.

The inner integral in Equation (3.3) can be split into four parts to introduce the classic terrain corrections and the effect of the Bouguer plates as was proposed in Subsection 3.1.3. We get

$$\int_{h^g}^{h} \frac{z-z'}{l^3}dz' = \int_{0}^{h} \frac{z-z'}{l^3}dz' - \int_{0}^{h^g} \frac{z-z'}{l^3}dz' =$$
$$\int_{0}^{h(P)} \frac{z-z'}{l^3}dz' + \int_{h(P)}^{h} \frac{z-z'}{l^3}dz' - \int_{0}^{h^g(P)} \frac{z-z'}{l^3}dz' - \int_{h^g(P)}^{h^g} \frac{z-z'}{l^3}dz', \qquad (3.4)$$

where $h(P)$ is the elevation of the real topography at the evaluation point P and $h^g(P)$ is the elevation of MES at the same point.

Integral boundaries of two of the integrals do not depend on h or h^g which are varying in the outer integral so they represent the effect of two layers with constant thickness of $h(P)$ and $h^g(P)$. The other integrals represent the classic terrain correction. Therefore the four integrals can be schematically rewritten as

$$\Delta g^{rtm} = \Delta g_{BP} + \Delta g_{TE} - \Delta g^g_{BP} - \Delta g^g_{TE}, \qquad (3.5)$$

where

$$\Delta g_{BP} = -G\rho \iint_S \left(\int_0^{h(P)} \frac{z-z'}{l^3}dz' \right) dS, \qquad (3.6)$$

$$\Delta g_{TE} = -G\rho \iint_S \left(\int_{h(P)}^{h} \frac{z-z'}{l^3}dz' \right) dS, \qquad (3.7)$$

$$\Delta g^g_{BP} = -G\rho \iint_S \left(\int_0^{h^g(P)} \frac{z-z'}{l^3}dz' \right) dS, \qquad (3.8)$$

$$\Delta g^g_{TE} = -G\rho \iint_S \left(\int_{h^g(P)}^{h^g} \frac{z-z'}{l^3}dz' \right) dS, \qquad (3.9)$$

where Δg_{TE} denotes the planar terrain effect of the real topography evaluated for the level h and Δg^g_{TE} denotes the terrain effect of MES (see Figure 3.4). The upper index "g" denotes parameters related to MES throughout this chapter. The lower indices "TE", "BS" and "BP" denote the terrain effects, the Bouguer shell and Bouguer plate. Limited and unlimited plates (and shells) can be clearly distinguished from the context, so we have not introduced further indexes to distinguish them. We denote $h(P)$ and $h^g(P)$ elevation of the evaluation point P ($h(P)$ at real surface and $h^g(P)$ on MES), whereas h and h^g are variable heights of the surface (and MES) around the point P.

There are no issues with evaluation of the terrain effects Δg_{TE} and Δg^g_{TE}. We can use for example the prism method described in Subsection 2.3.11 or any other method mentioned in Subsection 2.3.10. It should be mentioned, that the prisms are used only around the computational point P so they cannot touch it and no singularities may occur. If prisms are used for direct modeling of the residual terrain without introducing the Bouguer layer, singularities may occur and formulas from Subsection 2.3.11 cannot be used.

In the classic approach, Δg_{BP} and Δg^g_{BP} are analytically evaluated over the infinite Bouguer plate S. The analytical integration of Δg_{BP} and Δg^g_{BP} is quite simple and required relations were shown in Section 2.3.3. First, we will study the case $h(P) > h^g(P)$. We have

$$\Delta g_{BP} = -2\pi G\rho h(P), \tag{3.10}$$

according to (2.78), where we have put $h = h(P)$ because the point P is on the top of plate and

$$\Delta g^g_{BP} = -2\pi G\rho h^g(P) \tag{3.11}$$

according to (2.78) where $h = h^g(P)$ because point P is above the plate. The

total effect of the Bouguer plates is then given by

$$\Delta g_{BP}^{rtm} = -2\pi G\rho \left(h(P) - h^g(P)\right). \tag{3.12}$$

Next we will study the case $h(P) < h^g(P)$. We have

$$\Delta g_{BP} = -2\pi G\rho h(P), \tag{3.13}$$

according to (2.78) because the point P is still on the top of the plate and

$$\Delta g_{BP}^{g} = -2\pi G\rho \left(h^g(P) + 2\left(h(P) - h^g(P)\right)\right) = -2\pi G\rho \left(2h(P) - h^g(P)\right), \tag{3.14}$$

according to (2.79), where $z = h(P) - h^g(P)$ and $h = h^g(P)$, because the point P is now inside the Bouguer plate. We have to keep the position of the plate shown at Figure 2.2 at page 31, where the origin of the coordinate system is on the top of the cylinder and the cylinder of thickness h lies under the origin of the coordinate system. The total effect is then

$$\Delta g_{BP}^{rtm} = -2\pi G\rho \left(h(P) - \left(2h(P) - h^g(P)\right)\right) = 2\pi G\rho(h(P) - h^g(P)). \tag{3.15}$$

Easy comparison of Equations (3.12) and (3.15) gives

$$-2\pi G\rho(h(P) - h^g(P)) - (2\pi G\rho(h(P) - h^g(P))) = -4\pi G\rho(h(P) - h^g(P)) \tag{3.16}$$

which is the harmonic correction as was derived in [Forsberg, 1984] using a different approach.

We have derived in Subsection 2.3.3 also the general solution (2.77), which holds for any position of the computational point. We can use this equation instead of particular solutions (2.78) and (2.79) for evaluation of Δg_{BP}^{g}. Using the general expression has the advantage, that the size of $h(P)$ and $h^g(P)$ is not relevant. We can use only one general formula, which applies the

harmonic correction itself if required. We will again introduce $z = h(P) - h^g(P)$ and $h = h^g(P)$ so the general solution becomes

$$\Delta g_{BP}^{rtm} = -2\pi G\rho \left(h(P) - |h(P) - h^g(P)|\right), \tag{3.17}$$

where $|\cdot|$ is absolute value function.

We can use the formula in Equation (2.77) also for computing Δg_{BP} instead of that in Equation (2.78), but this generalization helps only in very special cases, e.g. when the point P is in the area of negative heights.

The expression in Equation (3.17) contains implicitly the harmonic correction, but it is still inconsistent with (3.5), because integrals (3.6) and (3.8) were evaluated for the unbounded area S (infinite plate), whereas the integrals in Equations (3.7) and (3.9) are evaluated only up to a certain threshold distance. This inconsistency can have even bigger impact on the potential V, which is for the unlimited plate infinite [Vaníček et al., 2001].

To solve this issue, we should keep the same integration area S for all integrals in Equations (3.6) – (3.9). We will choose the spherical distance ψ_0 as a parameter to keep consistency with spherical approximation which will be described later. The integration area S is then a circle with the center in the point P and radius $R = R_m\psi_0$. Bouguer layers are cylinders with radii R and height $h(P)$ and $h^g(P)$ so we can use the expressions derived for the limited cylinder in subsection 2.3.2 of this thesis. The gravitational effect of the limited Bouguer plate for a point on the top of the cylinder (2.62) can be used for evaluation of Δg_{BP}

$$\Delta g_{BP} = -2\pi G\rho \left(h(P) + R - \sqrt{h(P)^2 + R^2}\right), \tag{3.18}$$

and the general formula (2.60) should be used for evaluation of Δg^g_{BP}

$$\Delta g^g_{BP} = 2\pi G\rho\Big(|h(P) - h^g(P)| - |h(P)| + \sqrt{h(P)^2 + R^2} - \sqrt{h(P)^2 - 2h(P)h^g(P) + h^g(P)^2 + R^2}\Big). \tag{3.19}$$

We have just derived formulas for Δg_{BP} and Δg^g_{BP}, which can be introduced into (3.5). Evaluation of Equation (3.5) gives the total residual terrain effect which is free of both issues mentioned in the Subsection 3.1.1.

We have presented not only the results, but also some detailed steps and ideas in this subsection. We have chosen the gravity anomaly in planar approximation for this detailed explanation, because it is the most common quantity to be evaluated by using RTM. In the following sections, we will keep the same ideas, but we will not repeat all detailed steps again.

3.2.2 RTM for Δg in spherical approximation

The RTM effect Δg^{rtm} for the gravity anomaly Δg over a sphere σ is given in spherical approximation by

$$\Delta g^{rtm}(P) = \Delta g^{rtm}(r, \theta, \lambda) = -G\rho \iint_\sigma \left(\int_{R+h^g}^{R+h} \frac{r' - r\cos\psi}{\ell^3} dr' \right) d\sigma, \tag{3.20}$$

where ℓ is the spatial distance between the computational point and integration element.

We can again split the inner integral in Equation (3.20) to introduce the classic terrain corrections and Bouguer shells as in the former subsection. We get

$$\int_{R+h^g}^{R+h} \frac{r' - r\cos\psi}{\ell^3} dr' = \int_R^{R+h} \frac{r' - r\cos\psi}{\ell^3} dr' - \int_R^{R+h^g} \frac{r' - r\cos\psi}{\ell^3} dr' = \tag{3.21}$$

$$\int_{R}^{R+h(P)} \frac{r'-r\cos\psi}{\ell^3}dr' + \int_{R+h(P)}^{R+h} \frac{r'-r\cos\psi}{\ell^3}dr' - \int_{R}^{R+h^g(P)} \frac{r'-r\cos\psi}{\ell^3}dr' - \int_{R+h^g(P)}^{R+h^g} \frac{r'-r\cos\psi}{\ell^3}dr'. \tag{3.22}$$

This equation can be again schematically written as

$$\Delta g^{rtm} = \Delta g_{BS} + \Delta g_{TE} - \Delta g^g_{BS} - \Delta g^g_{TE} \tag{3.23}$$

where

$$\Delta g_{BS} = -G\rho \iint_{\sigma} \left(\int_{R}^{R+h(P)} \frac{r'-r\cos\psi}{\ell^3}dr' \right) d\sigma, \tag{3.24}$$

$$\Delta g_{TE} = -G\rho \iint_{\sigma} \left(\int_{R+h(P)}^{R+h} \frac{r'-r\cos\psi}{\ell^3}dr' \right) d\sigma, \tag{3.25}$$

$$\Delta g^g_{BS} = -G\rho \iint_{\sigma} \left(\int_{R}^{R+h^g(P)} \frac{r'-r\cos\psi}{\ell^3}dr' \right) d\sigma, \tag{3.26}$$

$$\Delta g^g_{TE} = -G\rho \iint_{\sigma} \left(\int_{R+h^g(P)}^{R+h^g} \frac{r'-r\cos\psi}{\ell^3}dr' \right) d\sigma. \tag{3.27}$$

There are again no issues with evaluation of terrain effects Δg_{TE} and Δg^g_{TE}. We can use for example TMV method described in Subsection 2.3.9 or any other method mentioned in Subsection 2.3.8.

We will now focus on evaluation of Δg_{BS} and Δg^g_{BS}. If the evaluation of Δg_{TE} and Δg^g_{TE} is not limited (e.g., when far-zone terrain effects are introduced), we can use relations for V_r derived in Subsection 2.3.5. Otherwise we should limit the integration for the Bouguer shell as well as integration of Δg_{BS} and Δg^g_{BS} and we should use relations derived in Subsection 2.3.4.

We will omit explicit (P) in $h(P)$ and $h^g(P)$ in further expressions for Bouguer layers. They never depend on h and h^g in their original meaning (see explanation under (3.9)) so it cannot cause any confusion and all expressions will be much shorter. But we will keep (P) in integrals such as in Equation (3.20), where is difference between h and $h(P)$ important.

We will start with the unlimited Bouguer shell. Δg_{BS} is computed by the particular expression for point on the shell in Equation (2.143). We get

$$\Delta g_{BS} = -4\pi G\rho h. \tag{3.28}$$

Δg^g_{BS} can be computed by using substitution $r_1 = R$, $r_2 = R + h^g$, $r = R + h$ into the general solution (2.141)

$$\begin{aligned}\Delta g^g_{BS} = -\frac{\pi G\rho}{3(h+R)^2}\Big(&- |h - h^g| \left(h^2 + 2hR + 2h^{g2} + 4h^gR + 3R^2\right) \\ &+ 2\left(h^3 + 3h^2R + 3hR^2 + h^g\left(h^{g2} + 3h^gR + 3R^2\right)\right) \\ &- (h - h^g)(h + R)(h + 2h^g + 3R)[h - h^g]\Big).\end{aligned} \tag{3.29}$$

Expressions in Equations (3.28) and (3.29) could be again inconsistent with the terrain effects Δg_{TE} and Δg^g_{TE}. The integration was done over the whole sphere σ so TE and TE^g have to be also evaluated over the whole sphere, otherwise we get significant errors in Δg^{rtm} in rough terrain where the heights $h(P)$ and $h^g(P)$ significantly differ. The layer of thickness $(h-h^g)$ generates big effect all around the globe which must be compensated by TE or TE^g, but is not because the evaluation of TE and TE^g stopped at some distance from the computational point.

Coming back to the original equation (3.20), the idea is to limit the outer integration area σ from the sphere to a spherical cap already at this place. Because the boundaries of the shell $R + h^g$ and $R + h$ are usually close to

each other (as the mean surface interpolates the real surface), the omitted residual effect is expected to be small. The limited integration area is then propagated to all four integrals (3.24)–(3.27) in a consistent way.

Now we will derive the effect of the limited Bouguer shell. For Δg_{BS} we can use a simplified (approximate) relation given by (2.115) for point on the top of the shell. We have

$$\Delta g_{BS} = \pi G\rho \left(\frac{h^2}{\ell_1} + (h+R)^2 \sin^2(\psi_0) \left(\frac{1}{\ell_1} - \frac{1}{\ell_2} \right) + \ell_1 - \ell_2 - 2h \right). \quad (3.30)$$

Variables and parameters used in (3.30) are described in Subsection 2.3.4.

For Δg^g_{BS} we have to use either the exact general formula (2.106) or the simplified formula (2.107), which is simpler, but still precise enough for our needs. Inserting $r_1 = R$, $r_2 = R + h^g$, $r = R + h$ into (2.107) gives

$$\begin{aligned} \Delta g^g_{BS} = \frac{1}{3}\pi G\rho \Bigg(& - \frac{6R^2|h| - 6R^2|h-h^g|}{(h+R)^2} + 3\left(\frac{h^2}{\ell_1} - \frac{(h-h^g)^2 + \ell_2^2}{\ell_2} + \ell_1 \right) \\ & + 6\psi_0^2 (h+R) \log\left(\frac{-h + h^g + \ell_2}{\ell_1 - h} \right) - \frac{6\left(\ell_2(h^g - h) + h\ell_1\right)}{h+R} \\ & + 3\left(\frac{1}{\ell_1} - \frac{1}{\ell_2} \right) \psi_0^2 (h+R)^2 + \frac{2\left(\ell_1^3 - \ell_2^3\right)}{(h+R)^2} \Bigg). \end{aligned} \quad (3.31)$$

The formulas (3.30) and (3.31) are not so simple as the formulas for unlimited plate, but these formulas need to be evaluated only once for each computational point (because all integrals in Equations (3.24) and (3.26) were evaluated analytically) so their complexity cannot affect the total computational time, which is driven by the time consuming evaluation of terrain corrections Δg_{TE} and Δg^g_{TE} (where the outer integrals have to be solved numerically).

3.2.3 RTM for potential V in spherical approximation

The RTM effect V^{rtm} for the gravitational potential V over a sphere σ is given in spherical approximation by

$$V^{rtm}(P) = V^{rtm}(r,\theta,\lambda) = G\rho \iint_{\sigma} \left(\int_{R+h^g}^{R+h} \frac{1}{\ell} r'^2 dr' \right) d\sigma. \tag{3.32}$$

The right-hand side can be rewritten to four parts

$$V^{rtm} = V_{BS} + V_{TE} - V^g_{BS} - V^g_{TE}, \tag{3.33}$$

where

$$V_{BS} = G\rho \iint_{\sigma} \left(\int_{R}^{R+h(P)} \frac{1}{\ell} r'^2 dr' \right) d\sigma, \tag{3.34}$$

$$V_{TE} = G\rho \iint_{\sigma} \left(\int_{R+h(P)}^{R+h} \frac{1}{\ell} r'^2 dr' \right) d\sigma, \tag{3.35}$$

$$V^g_{BS} = G\rho \iint_{\sigma} \left(\int_{R}^{R+h^g(P)} \frac{1}{\ell} r'^2 dr' \right) d\sigma, \tag{3.36}$$

$$V^g_{TE} = G\rho \iint_{\sigma} \left(\int_{R+h^g(P)}^{R+h^g} \frac{1}{\ell} r'^2 dr' \right) d\sigma. \tag{3.37}$$

The terms V_{TE} and V^g_{TE} are terrain effects. Their evaluation was described generally in Subsection 2.3.8, one particular method (TMV) in Subsection 2.3.9. The terms V_{BS} and V^g_{BS} should be again calculated using expressions for the potential of the limited Bouguer shell which was derived in Subsection 2.3.4. The general solution (2.98) was simplified to expression (2.105). Using (2.105) for V_{BS} gives

$$V_{BS} = \pi G\rho \left(-\frac{h^3}{3R} - h^2 + h\ell_1 + (h+R)^2 \sin^2\psi_0 \log\frac{\ell_2}{\ell_1 - h} \right), \tag{3.38}$$

where

$$\ell_1 = \sqrt{(h+R)^2 + R^2 - 2R(h+R)\cos\psi_0}, \tag{3.39}$$

$$\ell_2 = \sqrt{2(h+R)^2 - 2(h+R)^2\cos\psi_0}. \tag{3.40}$$

Now we have to evaluate V_{BS}^g. We again need the general solution valid for any r, because the evaluation point P may be located inside the shell, i.e.,

$$\begin{aligned} V_{BS}^g = \frac{1}{3}\pi G\rho\Bigg(& \frac{(h-h^g)|h-h^g|(h+2h^g+3R) - h|h|(h+3R)}{h+R} \\ & + 3\cos\psi_0\left(\ell_2^g\left(-(h+R)\cos\psi_0 + h^g + R\right) + \ell_1^g\left((h+R)\cos\psi_0 - R\right)\right) \\ & + 3(h+R)^2\sin^2\psi_0\cos\psi_0\log\left(\frac{-(h+R)\cos\psi_0 + h^g + R + \ell_2^g}{-(h+R)\cos\psi_0 + R + \ell_1^g}\right) \\ & + \frac{2\left(\ell_2^{g3} - \ell_1^{g3}\right)}{h+R}\Bigg), \end{aligned} \tag{3.41}$$

where

$$\ell_1^g = \sqrt{-2R(h+R)\cos\psi_0 + (h+R)^2 + R^2} \tag{3.42}$$

$$\ell_2^g = \sqrt{-2(h+R)(h^g+R)\cos\psi_0 + (h+R)^2 + (h^g+R)^2}. \tag{3.43}$$

3.2.4 RTM for potential V in planar approximation

$$V^{rtm}(P) = V^{rtm}(x,y,z) = G\rho \iint\limits_S \left(\int\limits_{h^g}^{h} \frac{1}{l} dz' \right) dS. \tag{3.44}$$

The right-hand side of Equation (3.44) can be again rewritten to four parts

$$V^{rtm} = V_{BP} + V_{TE} - V_{BP}^g - V_{TE}^g, \tag{3.45}$$

where

$$V_{BP} = G\rho \iint\limits_S \left(\int\limits_0^{h(P)} \frac{1}{l} dz' \right) dS, \tag{3.46}$$

$$V_{TE} = G\rho \iint\limits_S \left(\int\limits_{h(P)}^{h} \frac{1}{l} dz' \right) dS, \tag{3.47}$$

$$V_{BP}^g = G\rho \iint\limits_S \left(\int\limits_0^{h^g(P)} \frac{1}{l} dz' \right) dS, \tag{3.48}$$

$$V_{TE}^g = G\rho \iint\limits_S \left(\int\limits_{h^g(P)}^{h^g} \frac{1}{l} dz' \right) dS. \tag{3.49}$$

V_{TE} and V_{TE}^g are the terrain effects in planar approximation. Their evaluation was described in Subsections 2.3.10 and 2.3.11. For evaluation of V_{BP} and V_{BP}^g we need expressions derived in Subsection 2.3.2. According to (2.51) we get

$$V_{BP} = G\rho\pi \left(R^2 \log \frac{\sqrt{h^2 + R^2} + h}{R} - h^2 + h\sqrt{h^2 + R^2} \right), \tag{3.50}$$

and from general Equation (2.53) we get

$$\begin{aligned} V_{BP}^g = \pi G\rho \Big(& (h - h^g)|h - h^g| - h|h| + R^2 \log \left(\frac{l_h + h}{h - h^g + l_0} \right) \\ & + l_h(h - h^g) + h^g l_h - l_0(h - h^g) \Big), \end{aligned} \tag{3.51}$$

where

$$\ell_h = \sqrt{(h - h^g)^2 + 2h^g(h - h^g) + h^{g2} + R^2}, \tag{3.52}$$

$$\ell_0 = \sqrt{(h - h^g)^2 + R^2}. \tag{3.53}$$

3.2.5 RTM for gravity gradient V_{rr} in spherical approximation

The RTM effect V_{rr}^{rtm} for the second radial derivative of the gravitational potential V_{rr} over a sphere σ is given in spherical approximation by

$$V_{rr}^{rtm}(P) = G\rho \iint_{\sigma} \left[\int_{R+h^g}^{R+h} \frac{2r'^2 - 4\cos\psi rr' + (3\cos^2\psi - 1)r^2}{\ell^5} r'^2 dr' \right] d\sigma. \tag{3.54}$$

The right-hand side of Equation (3.54) can be as usual rewritten to four parts

$$V_{rr}^{rtm} = V_{rr\,BS} + V_{rr\,TE} - V_{rr\,BS}^{g} - V_{rr\,TE}^{g}, \tag{3.55}$$

where

$$V_{rr\,BS} = G\rho \iint_{\sigma} \left(\int_{R}^{R+h(P)} \frac{2r'^2 - 4\cos\psi rr' + (3\cos^2\psi - 1)r^2}{\ell^5} r'^2 dr' \right) d\sigma, \tag{3.56}$$

$$V_{rr\,TE} = G\rho \iint_{\sigma} \left(\int_{R+h(P)}^{R+h} \frac{2r'^2 - 4\cos\psi rr' + (3\cos^2\psi - 1)r^2}{\ell^5} r'^2 dr' \right) d\sigma, \tag{3.57}$$

$$V_{rr\,BS}^{g} = G\rho \iint_{\sigma} \left(\int_{R}^{R+h^g(P)} \frac{2r'^2 - 4\cos\psi rr' + (3\cos^2\psi - 1)r^2}{\ell^5} r'^2 dr' \right) d\sigma, \tag{3.58}$$

$$V_{rr\,TE}^{g} = G\rho \iint_{\sigma} \left(\int_{R+h^g(P)}^{R+h^g} \frac{2r'^2 - 4\cos\psi rr' + (3\cos^2\psi - 1)r^2}{\ell^5} r'^2 dr' \right) d\sigma. \tag{3.59}$$

Terms $V_{rr\,TE}$ and $V_{rr\,TE}^{g}$ are terrain effects for the second order radial derivatives of the potential. Their evaluation was described generally in Subsection 2.3.8, one particular method (TMV) in subsection 2.3.9. Terms $V_{rr\,BS}$

and $V^g_{rr\,BS}$ must be again calculated using expressions for the second radial derivative of the potential of the limited Bouguer shell, which were derived in Subsection 2.3.4. The general solution (2.116) was simplified for a point on the top of the shell to the expression given by Equation (2.134). The most important step in the simplification was using limit from right (i.e. from the outer space) on the surface of the limited cap, where the second derivative is not continuous. Using (2.134) for $V_{rr\,BS}$ gives

$$V_{rr\,BS} = \pi G\rho \left(-\frac{h^3}{\ell_1^3} - \frac{h\,(h+R)^2\,\psi_0^2}{\ell_1^3} + \frac{3h}{\ell_1} \right). \tag{3.60}$$

For $V^g_{rr\,BS}$ we have to use the general solution, which was unfortunately quite complicated. After usual substitutions we get

$$\begin{aligned}
V^g_{rr\,BS} = \frac{1}{3}\pi G\rho \Bigg(& \frac{2\,(|h|\,((h+R)^2+2R^2) - |h-h^g|\,((h+R)^2+2(h^g+R)^2))}{(h+R)^3} \\
& - \frac{2(|h| - |h-h^g|)}{h+R} + 3(h+R)^2 \sin^4\psi_0 \cos\psi_0 \\
& \cdot \Big(\frac{(h^g+R)\,((h+R)\cos\psi_0 + \ell_2^g) - (h+R)^2 + {\ell_2^g}^2}{m_2^2 {\ell_2^g}^2} \\
& - \frac{(-h-R)\,(h - R\cos\psi_0 + R) + R\ell_1^g + {\ell_1^g}^2}{m_1^2 {\ell_1^g}^2} \Big) \\
& + 6(h+R)\sin^2(\psi_0)\cos\psi_0 \Big(\frac{2\,(h - (h^g+R)\cos\psi_0 + R - \ell_2^g\cos\psi_0)}{m_2^g \ell_2^g} \\
& - \frac{2\,(h - R\cos\psi_0 + R - \ell_1^g\cos\psi_0)}{m_1^g \ell_1^g} \Big) + 3(h+R)^2 \sin^2\psi_0 \cos\psi_0 \\
& \cdot \Big(\frac{(h - (h^g+R)\cos\psi_0 + R)\,(-h + \cos(\psi_0)\,(h^g + R + \ell_2^g) - R)}{m_2^g {\ell_2^g}^3} \\
& + \frac{(h - R\cos\psi_0 + R)\,(h - R\cos\psi_0 + R - \ell_1^g\cos\psi_0)}{m_1^g {\ell_1^g}^3} \Big) \\
& - \frac{2\,((h+R)^2 - 2(h^g+R)^2)\,[h-h^g] - 2\,((h+R)^2 - 2R^2)\,[h]}{(h+R)^2} \\
& + \frac{6\,(\ell_1^g\,(h - (h^g+R)\cos\psi_0 + R)^{\,2} - \ell_2^g\,(h - R\cos(\psi_0) + R)^{\,2})}{\ell_1^g \ell_2^g (h+R)}
\end{aligned}$$

$$
\begin{aligned}
&+\frac{12\left(\ell_1^g\left(h-R\cos\psi_0+R\right)-\ell_2^g\left(h-\left(h^g+R\right)\cos\psi_0+R\right)\right)}{(h+R)^2}\\
&+3\cos\psi_0\Bigg(\frac{\left((h+R)\cos\left(\psi_0\right)-h^g-R\right)\left(h-\left(h^g+R\right)\cos\psi_0+R\right)^2}{\ell_2^{g3}}\\
&+\frac{3\left(\ell_2^g-\ell_1^g\right)(h+R)\cos\psi_0+\left(\cos\left(2\psi_0\right)+2\right)\left(\ell_1^g(h^g+R)-R\ell_2^g\right)}{\ell_1^g\ell_2^g}\\
&-\frac{\left((h+R)\cos\psi_0-R\right)\left(h-R\cos\left(\psi_0\right)+R\right)^2}{\ell_1^{g3}}\Bigg)+4[h-h^g]\\
&+\frac{6\left(\ell_2^g-\ell_1^g\right)}{h+R}-\frac{4\left(\ell_1^{g3}-\ell_2^{g3}\right)}{(h+R)^3}-4[h]+6\log\frac{m_2^g}{m_1^g}\sin^2\psi_0\cos\psi_0\Bigg), \quad (3.61)
\end{aligned}
$$

where ℓ_1^g, ℓ_2^g, m_1^g and m_2^g are defined by

$$\ell_1^g=\sqrt{-2R(h+R)\cos\psi_0+(h+R)^2+R^2}, \quad (3.62)$$

$$\ell_2^g=\sqrt{-2(h+R)(h^g+R)\cos\psi_0+(h+R)^2+(h^g+R)^2}, \quad (3.63)$$

$$m_1^g=-(h+R)\cos\psi_0+R+\ell_1^g, \quad (3.64)$$

$$m_2^g=-(h+R)\cos\psi_0+h^g+R+\ell_2^g. \quad (3.65)$$

Note that the general formula (3.61) is a general solution, but it contains two discontinuous points. The formula may fail in two cases: if $h(P)=h^g(P)$ the point is again on the cylinder. However, $V_{rr\,BS}^g$ and $V_{rr\,BS}$ cancels each other so we do not have to evaluate any of them; if $h(P)=0$, the formula may also fail. In this case, we should use the limit from right for the point P_4 as in Equation (3.60).

3.2.6 RTM for gravity gradient V_{rr} in planar approximation

The RTM effect V_{rr}^{rtm} for the second radial derivative of the gravitational potential V_{rr} is given in planar approximation by

$$V_{rr}^{rtm}(P) = G\rho \iint\limits_S \left(\int\limits_{h^g}^{h} \frac{3(z-z')^2 - l^2}{l^5} dz' \right) dS \tag{3.66}$$

We will (as in other cases) rewrite the right-hand side as

$$V_{rr}^{rtm} = V_{rr\,BP} + V_{rr\,TE} - V_{rr\,BP}^{g} - V_{rr\,TE}^{g}, \tag{3.67}$$

where

$$V_{rr\,BP} = G\rho \iint\limits_S \left(\int\limits_{0}^{h(P)} \frac{3(z-z')^2 - l^2}{l^5} dz' \right) dS, \tag{3.68}$$

$$V_{rr\,TE} = G\rho \iint\limits_S \left(\int\limits_{h(P)}^{h} \frac{3(z-z')^2 - l^2}{l^5} dz' \right) dS, \tag{3.69}$$

$$V_{rr\,BP}^{g} = G\rho \iint\limits_S \left(\int\limits_{0}^{h^g(P)} \frac{3(z-z')^2 - l^2}{l^5} dz' \right) dS, \tag{3.70}$$

$$V_{rr\,TE}^{g} = G\rho \iint\limits_S \left(\int\limits_{h^g(P)}^{h^g} \frac{3(z-z')^2 - l^2}{l^5} dz' \right) dS. \tag{3.71}$$

We have already shown solutions for all integrals in Equations (3.68)–(3.71). $V_{rr\,TE}$ and $V_{rr\,TE}^{g}$ are terrain effects in planar approximation. Their evaluation was described in Subsections 2.3.10 and 2.3.11. For evaluation of $V_{rr\,BP}$ and $V_{rr\,BP}^{g}$ we need expressions derived in subsection 2.3.2. Because V_{rr} is not continuous function, we have to choose between limit from right or limit from left for $V_{rr\,BP}$ which is on the top of the cylinder where the singularity

occurs. We have chosen the limit from right because it is a limit from outer space and that is the case which are we interested in. We get

$$V_{rr\,BP} = \lim_{z \to 0^+} V_{rr}(P_2) = 2G\rho\pi \frac{h}{\sqrt{R^2 + h^2}}. \tag{3.72}$$

For $V^g_{rr\,BP}$ we have to use the general formula

$$V^g_{rr\,BP} = 2\pi G\rho \left(\frac{h}{l^g_h} - \frac{h - h^g}{l^g_0} + [h - h^g] - [h] \right), \tag{3.73}$$

where

$$\ell_h = \sqrt{(h - h^g)^2 + 2h^g(h - h^g) + {h^g}^2 + R^2}, \tag{3.74}$$

$$\ell_0 = \sqrt{(h - h^g)^2 + R^2}. \tag{3.75}$$

We should pay special attention to two cases, where the general formula fails due to discontinuities in second vertical derivatives of the potential. For $h = h^g$ we should use Equation (3.72) instead of Equation (3.73), but in this case, $V_{rr\,BP}$ and $V^g_{rr\,BP}$ cancel each other. For $h = 0$ (evaluational point is on the bottom of the cylinder), we should use Equation (2.71) instead of Equation (3.72).

3.3 Numerical examples

We will now demonstrate the effect of various Bouguer layers with and also without the harmonic correction for one model situation. In our example, the mean elevation surface has elevation $h^g = 1000\ m$. The elevation $h(P)$ of the computational point P is in range $\langle 0\ m; 2000\ m \rangle$ and is plotted on axis x on all figures in this section. All figures in this section are showing the dependance of particular quantities on a position of point P with respect to MES $h^g = 1000\ m$. For $h(P) < 1000\ m$ the evaluational point P lies under

MES, for $h(P) = 1000\ m$ on MES and for $h(P) < 1000\ m$ above MES so the plots cover all possible positions of point P with respect to MES including the discontinuities for V_{rr}. Plots are evaluated for default value $\psi_0 = 5'$ if other value is not explicitly provided. These parameters can be treated as the worst case scenario for applications in the Czech Republic.

3.3.1 Effect on V_r

The total effect of Bouguer layers $V_{r\,BP} - V^g_{r\,BP}$ was evaluated for the unlimited plate, limited plate and limited shell. The result including the harmonic correction for our example is illustrated at Figure 3.5.

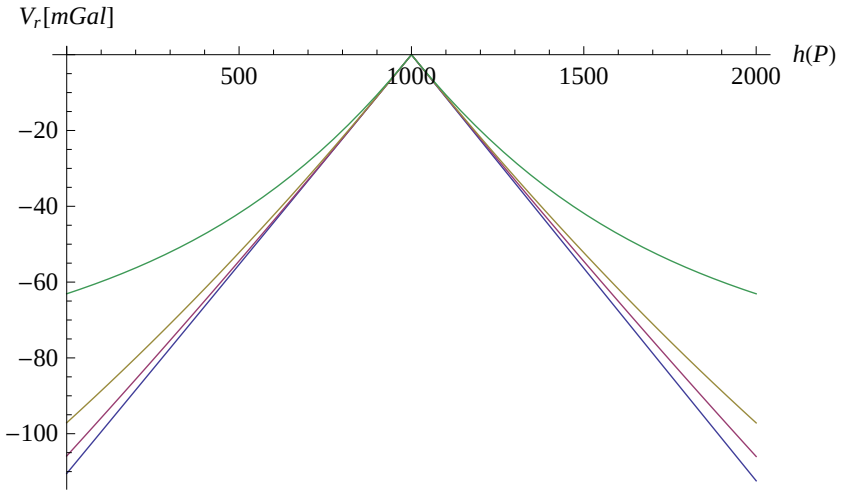

Figure 3.5: *Residual terrain effect for V_r.* Residual terrain effect evaluated as $V_{r\,BP} - V^g_{r\,BP}$ including the harmonic correction for $\psi_0 = 60'$ (blue line), $\psi_0 = 5'$ (violet line), $\psi_0 = 2'$ (brown line) and $\psi_0 = 60'$ (green line).

The same comparison of effects with and without the harmonic correction for the limited Bouguer shell is illustrated on Figure 3.6. We see that for

the point P above the mean elevation surface ($h^g = 1000$ m), the harmonic correction is zero, whereas under the mean elevation surface, it has almost the same size (in case of the unlimited plate exactly the same size), but opposite sign. The harmonic correction has the major effect on the total effect.

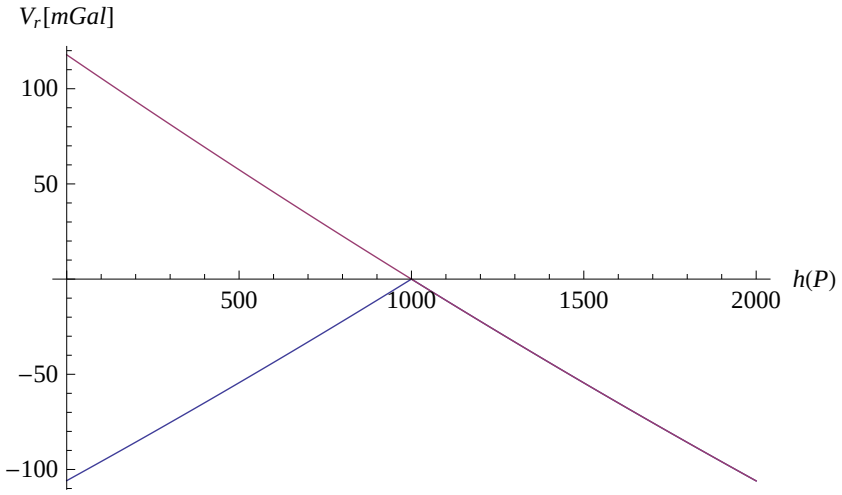

Figure 3.6: *Effect of harmonic correction on V_r.* Residual effect $V_{r\,BP} - V^g_{r\,BP}$ including the harmonic correction (blue line) and neglecting the harmonic correction (violet line).

The effect of the limited or unlimited Bouguer layer was studied already in Subsection 2.3.6 so we will not repeat the analysis again.

3.3.2 Effect on V

We will now show $V_{BP} - V^g_{BP}$ for our model. The Figure 3.7 shows the gravitational potential in planar approximation $V_{BP} - V^g_{BP}$. We have evaluated the effect again with and also without the harmonic correction. The harmonic correction itself is also plotted. As expected, the harmonic correction applies

only for P under the mean elevation surface.

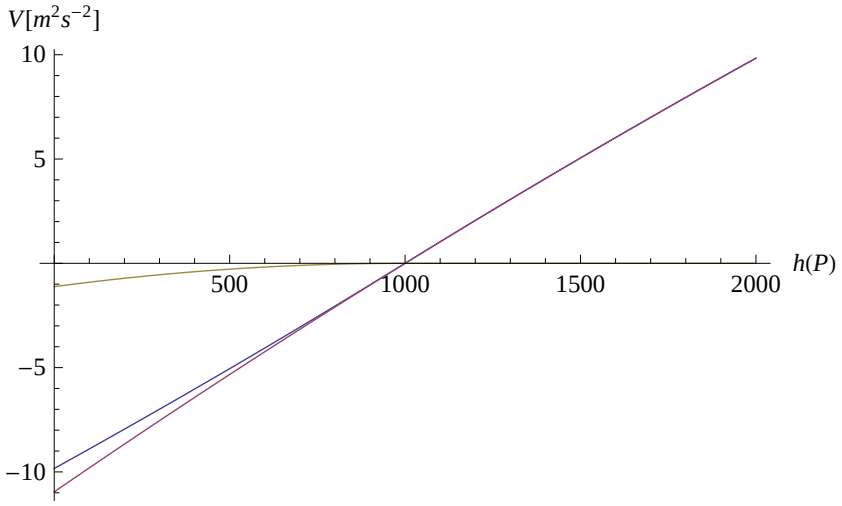

Figure 3.7: *Residual terrain effect for V.* Residual effect evaluated as $V_{BP} - V^g_{BP}$ including the harmonic correction (blue line) and neglecting the harmonic correction (violet line). The harmonic correction is also evaluated (brown line).

We can see that the effect of the harmonic correction on the potential is much smaller than on the gravitational attraction. The difference between the limited plate and limited shell is illustrated on Figure 3.8 for $\psi_0 = 5'$, $\psi_0 = 10'$ and $\psi_0 = 30'$. The effect may be significant particularly for larger ψ_0 and it cannot be omitted.

The effect of the unlimited Bouguer shell is unrealistically high and the effect of the unlimited Bouguer plate is infinite, so the use of the limited plate or better the limited shell is the best option. The use of the unlimited shell would be also an option, but it is necessary to evaluate the far-zone effect to reduce effect of distant masses, which is not required in our method.

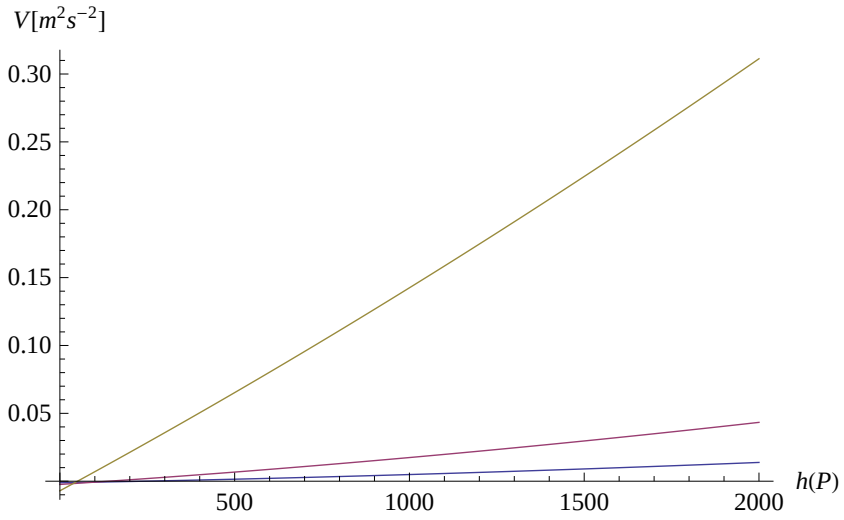

Figure 3.8: *Differences between the Bouguer plate and shell for* V. Differences between the residual effects of the Bouguer plate and shell were computed as $(V_{BP} - V^g_{BP}) - (V_{BS} - V^g_{BS})$ and evaluated for $\psi_0 = 5'$ in blue, $\psi_0 = 10'$ in violet and $\psi_0 = 30'$ in brown.

3.3.3 Effect on V_{rr}

The effect on the second radial derivative of potential V_{rr} is plotted on Figure 3.9. As usually, we have evaluated the effect $V_{rr\,BS} - V_{rr}{}^g_{BS}$ generated by the limited Bouguer shell and $V_{rr\,BP} - V_{rr}{}^g_{BP}$ generated by the limited Bouguer plate.

The difference between potentials $V_{rr\,BS} - V^g_{rr\,BS}$ (limited Bouguer shell) and $V_{rr\,BP} - V^g_{rr\,BP}$ (limited Bouguer plate) is illustrated on Figure 3.10. Values on Figure 3.10 are below 0.5 E, so the difference between planar and spherical approximation is not important. This behavior was also expected because V_{rr} is known to be influenced predominantly by the nearby masses.

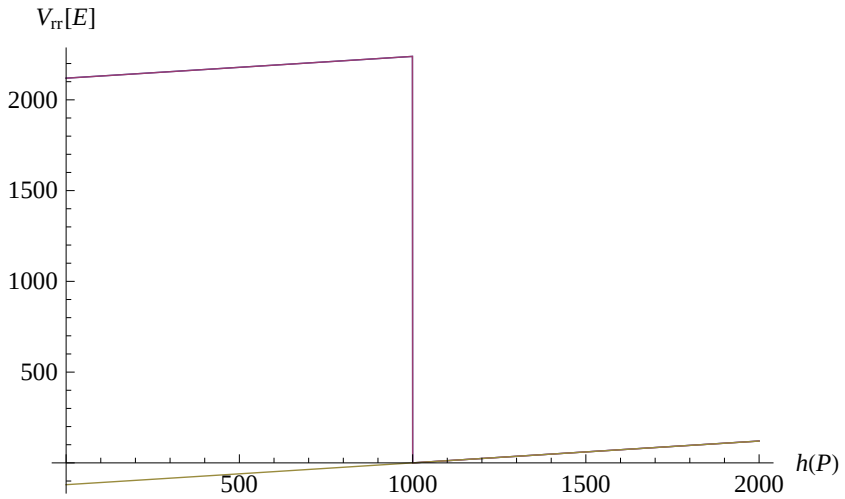

Figure 3.9: *Residual effect for* V_{rr}. The residual effect $V_{rr\,BS} - V^{g}_{rr\,BS}$ (blue line) and effect of the the limited Bouguer plate $V_{rr\,BP} - V^{g}_{rr\,BP}$ (violet line) including the harmonic correction. The brown line is $V_{rr\,BS} - V^{g}_{rr\,BS}$ neglecting the harmonic correction.

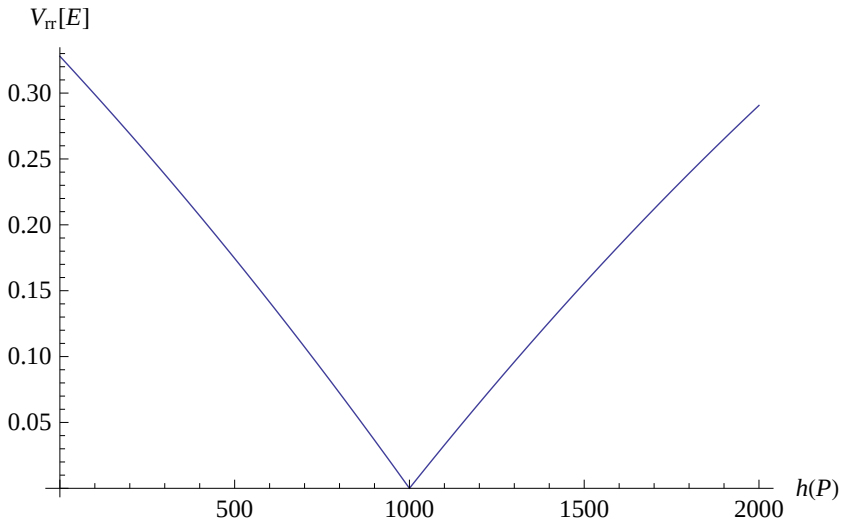

Figure 3.10: *Differences between Bouguer plate and shell for* V_{rr}. Differences are evaluated as $(V_{rr\,BP} - V^{g}_{rr\,BP}) - (V_{rr\,BS} - V^{g}_{rr\,BS})$.

Chapter 4

Numerical experiments

4.1 Methodology

We will now evaluate selected gravity field parameters for the area of the Czech Republic and its close neighborhood. The reference part for each parameter will be computed from EGM08 according to Section 2.2. This reference part will be supported by RTM computed from SRTM DEM with spatial resolution of $3''$, which is freely available. For evaluation of RTM, we will use computational formulas derived in Chapters 2 and 3.

There are four main options and parameters that should be set up. These options are:

1. maximal degree and order of EGM08 to be used,
2. terrain approximation: spherical or planar,
3. cut off distance for terrain effect (ψ_0),
4. harmonic correction: to be or not to be applied.

The maximal degree and order of EGM08 was chosen as the maximal available degree and order, i.e., to degree 2190 and order 2159. In the Czech Republic terrestrial gravity data were used with spatial resolution $5'$ and the quality of EGM08 in the Czech Republic was proven to be good several times ([Burša et al., 2009], [Novák et al., 2009a]), so there is no reason to stop the summation of series at lower degrees.

The advantages of planar and spherical approximation for terrain effects have been studied many times (also by the author of this thesis in [Tsoulis et al., 2009]). Also the differences for Bouguer plate or shell were already studied, for the unlimited plate and shell by [Vaníček et al., 2001] and for the limited plate and shell in Subsection 2.3.6 and also in Section 3.3, so the analysis of the differences will be not repeated again herein. We have chosen the

spherical approximation so all results in this section are provided in spherical approximation. We have derived all required formulas also in planar approximation and we have shown at several places in this thesis that the results are very similar, so the planar approximation may be used as well, especially for our maximal integration distance $\psi_0 = 10'$. However, the spherical approximation is still considered to be closer to the reality. The disadvantage of spherical approximation is that the computational formulas for effects of the Bouguer shell are more complicated than for the Bouguer plate, particularly for V_{rr}. For V_{rr}, the differences between planar and spherical approximation are so small, that we can even use planar approximation for the Bouguer layer and spherical approximation for the terrain effect without introducing any significant errors. One of important reasons was also computational time: evaluation of terrain effects using TMV method is much faster than evaluation of terrain effects using prism modeling by PAN method.

The spatial resolution of EGM08 is $5'$, so the RTM should cover only the terrain effect which is not included in EGM08. According to [Forsberg, 1984], we do not have to evaluate the effect for distances bigger than $10'$. However, this threshold was derived for evaluation under specific conditions: for gravitational attraction in medium rough terrain. Choosing the right cut-off distance for terrain effects on various quantities taking into consideration also the terrain roughness and real resolution of reference gravity data is still an open problem which is not solved in this thesis. We can expect that for the potential V the distance could be extended, especially in a rough terrain. For example at the Zugspitze mountain in Germany it was for recommended to use integration radius at least 200 km for the potential derived by RTM [Hirt et al., 2010]. However, we have two good reasons why we can afford using such a quite small distance of $10'$ in our area:

1. We are evaluating effects for the Czech Republic where is not too rough terrain.

2. EGM08 is known to have a good quality in the Czech Republic so its spatial resolution of $5'$ is trustworthy.

The last point to be decided is whether to use or not the harmonic correction for points which are under the mean elevation surface. We have discussed this topic in subsection 3.1.3 and we have concluded, that there is no reason to introduce the harmonic correction, when the reference part of gravity comes from GGM which gives implicitly harmonic quantities anywhere above its reference ellipsoid or sphere. Therefor, the harmonic correction will not be applied as it generally should not be applied for RTM when reference quantities were derived from EGM08. The evaluation of quantities without harmonic correction was not explicitly mentioned in section 2.3, but it is straightforward: Instead of evaluation of Δg_{BS} and Δg^g_{BS} separately, it is sufficient to evaluate Δg_{BS} where is the height $h(P)$ replaced by the elevation of residual topography $h(P) - h^g(P)$. The elevation $h(P) - h^g(P)$ must keep its sign even if it is negative. The same procedure is also applied for the other parameters V and V_{rr}.

4.2 Input data

In this section, we will shortly describe datasets which were used for evaluation of RTM quantities. We will describe two digital elevation models (DEM): SRTM and DEM2006 and three testing datasets for the area of the Czech Republic: a dataset of GNSS/leveling points, gravity stations from Czech Gravimetric Network and a set of gravity gradients measured at se-

lected gravity stations. We will not describe EGM08 again, as its description was provided already in Section 2.2.

4.2.1 SRTM3

SRTM3 is a global digital elevation model which comes from a Shuttle Radar Topography Mission [Farr et al., 2007] and covers 80 percent of the earth's surface. It has spatial resolution $3'' \times 3''$, which is about 60×90 meters in the Czech Republic.

The accuracy of SRTM for all continents was studied in [Rodriguez et al., 2006]. The accuracy of SRTM heights expressed as the standard deviation of heights in Europe is 6.2 m [Rodriguez et al., 2006]. Another study of the accuracy of SRTM heights for the territory of Poland was published in [Karwel and Ewiak, 2008]. This study shows similar results: the root mean square error of heights with comparison with GNSS measured heights was 5.4 m.

The position error of SRTM3 was also studied in [Rodriguez et al., 2006]: in Europe 90 % cells has the error in position better than 8.8 m. The standard deviation in [Rodriguez et al., 2006] is not provided, but can be easily computed from 90 % error value under assumption of normal distribution of errors in both directions: the standard deviation of the horizontal position then reads 4.1 m.

There are two versions of SRTM provided by NASA: SRTM V1 and SRTM V2. Even though the version V2 is significantly improved, it still contains lots of void cells and outliers and therefore cannot be easily used for our computations. However, the CGIAR-CSI organization (Consultative Group for International Agriculture Research – Consortium for Spatial Information) provides post-processed SRTM V2 data called SRTM V3 and

SRTM V4, where voids and outliers are fixed (usually by interpolation). In this thesis, we are using the newest SRTM V4 data.

Positional and height errors described above are related to SRTM V1 and SRTM V2, but newer versions only remove outliers and fills void values, the bulk of heights was not updated and therefore we can use standard deviations evaluated for older versions also for the newer version which was used.

The SRTM3 model serves as a detailed DEM from which the precise terrain effects are computed. SRTM3 model is shown at Figure 4.1.

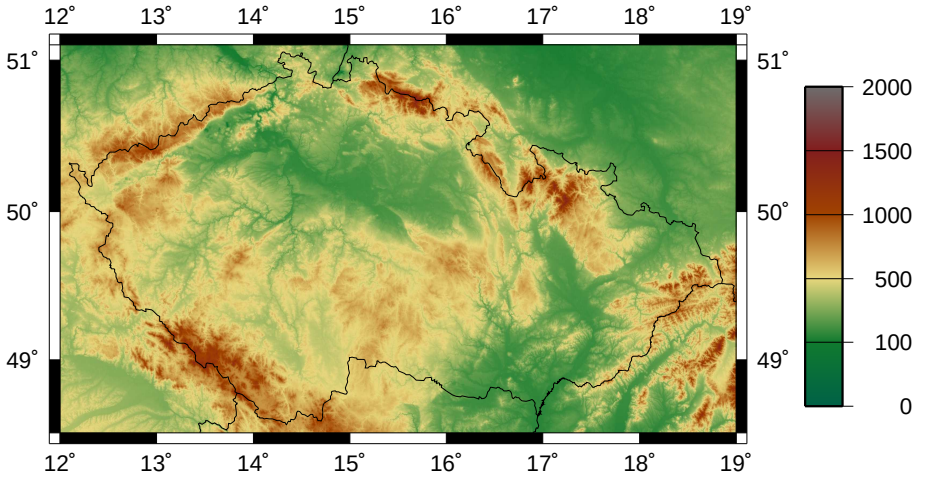

Figure 4.1: SRTM3 heights over the Czech Republic. [m]

4.2.2 DTM2006.0

The development of EGM08 required compilation of a very high-resolution global topographic database. Therefore, the National Geospatial-Intelligence Agency (NGA) of the USA has compiled a global database DTM2006.0. This database was used consistently in the computation of all terrain related quantities during pre-processing of gravity data and development of

the global model EGM08 [Pavlis et al., 2006]. Such quantities include analytical continuation terms, topographic/isostatic gravitational models and models necessary to convert height anomalies to geoid undulations.

The native resolution of DTM2006.0 is $30'' \times 30''$, but NGA has developed also a version which is provided in a form of coefficients of a spherical harmonic expansion up to degree 2160. This version of DTM2006.0 is provided by NGA together with EGM08.

We are using DTM2006.0 to define the mean level surface in the residual terrain modeling. DTM2006.0 evaluated up to degree 2160 in the area of the Czech Republic is shown at figure 4.2.

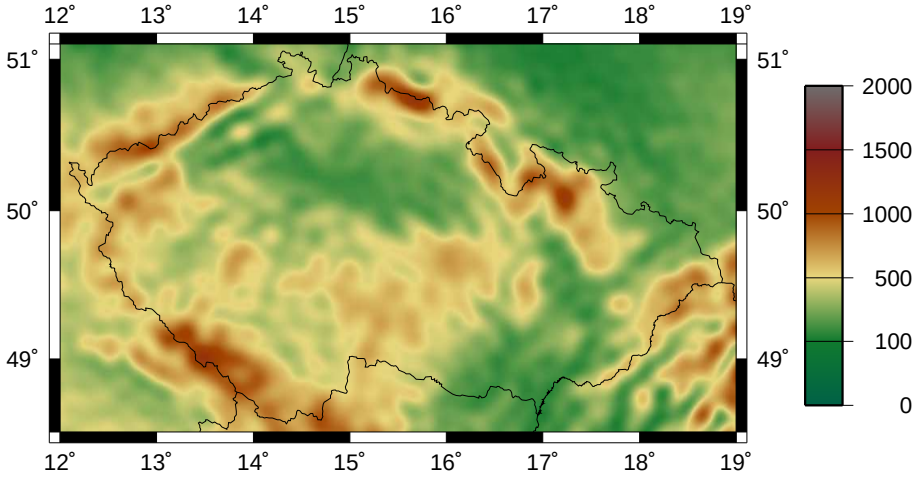

Figure 4.2: DTM2006.0 heights over the Czech Republic. [m]

4.2.3 GNSS/leveling points

In the Czech Republic a compound system is used as an official national coordinate reference system, which consists of two independent systems: Datum of Uniform Trigonometric Cadastral Network (S-JTSK) for 2D position (x, y) and Baltic Vertical Datum - After Adjustment (Bpv) for heights [VUGTK,

2010]. This system is not geocentric and there is no simple transformation rule between ETRS89 and S-JTSK/Bpv.

For transformation of coordinates from ETRS89 into S-JTSK/Bpv several identical points have to be used for which we know coordinates in both ETRS89 and S-JTSK/Bpv. The Land Survey Office in Prague (ZÚ) has measured ETRS89 coordinates (using GNSS) at almost 4000 JTSK points, see Figure 4.3. This number of points allows transformation of ETRS coordinates to S-JTSK with the accuracy required by national legislation.

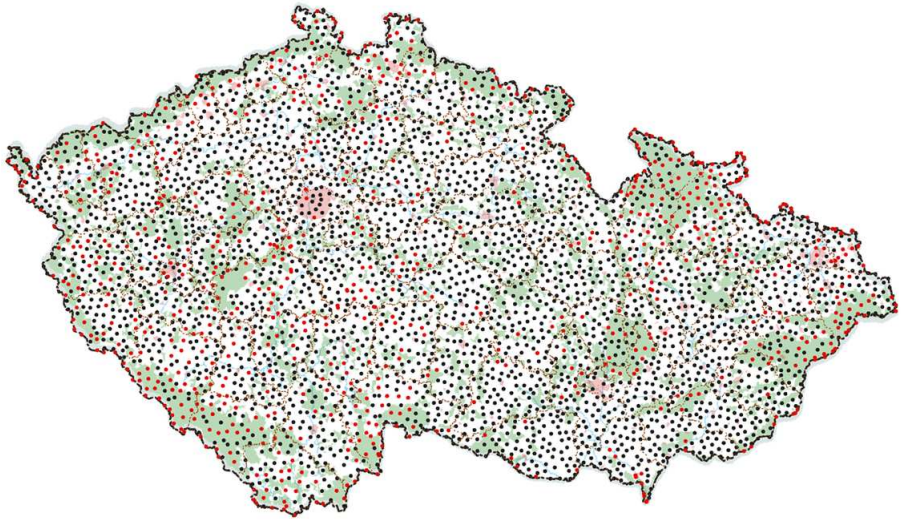

Figure 4.3: *All ETRS89/S-JTSK points.* The total number of points is 3950. After [CUZK, 2009].

Two methods were used to determine the ETRS89 coordinates: either the static method or the Real-time kinematic method (RTK). Bpv heights were determined either by spirit leveling or by trigonometric leveling. However, at some ETRS89/S-JTSK points the height was measured neither by spirit nor trigonometric leveling but it was computed only by transformation from

ETRS89 height. We have removed these points from the set because we are interested only in points whose height was determined in both systems (ETRS89 and Bpv) by independent methods.

Based on different methods of measurement and therefore different accuracy of the coordinates of the ETRS89/S-JTSK points, we can divide these points into two distinctive datasets. First dataset includes points which were measured by static GNSS method. Second dataset contains points which were measured by the RTK method. As we want to test our results by using the best available data, we will use only points with the height measured by spirit leveling.

We have a database of 1018 points which fulfill our conditions. This dataset is described in [Novák et al., 2009b] as CZTN dataset. The only difference between our dataset of 1018 points and dataset CZTN of 1024 points described in the above mentioned article is that we have removed 6 points which were duplicated in the CZTN dataset. These duplicate points have the same identification numbers and the same ellipsoidal (ETRS89) heights, but different normal (Bpv) heights. We have checked the actual heights provided by ZU to detect which point from each pair is wrong and we have removed the wrong point from each pair. This operation resulted in 1018 unique points.

From the set of 1018 points we have also removed additional two points which were obviously outliers. The final dataset of 1016 points is shown at figure 4.4.

The normal height (in Bpv system) of GNSS/leveling points was estimated using very precise leveling from the closest point of the Czech National Leveling Network (CSNS). The geometric height (in ETRS89) was measured by static 8-hours GNSS observation campaigns with an average length of

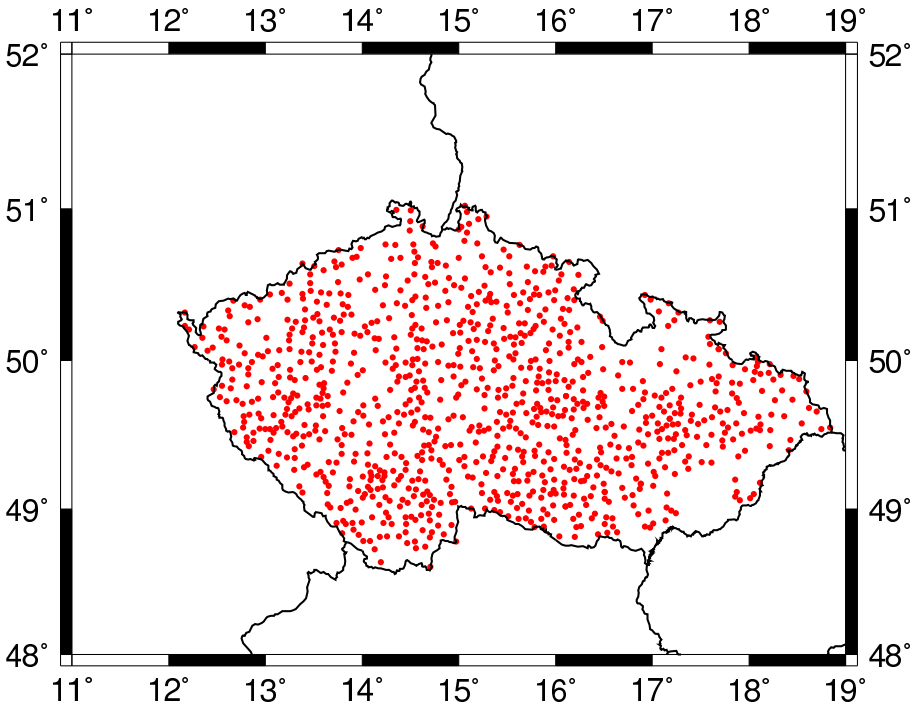

Figure 4.4: *Selected ETRS89/S-JTSK points.* Subset of 1016 ETRS89/S-JTSK points with leveled heights.

baseline between the stations at the level of 10 km.

The analysis of the accuracy of coordinates of GNSS/leveling points was also studied in [Novák et al., 2009b] with following results:

- Accuracy of ellipsoidal heights $\approx \pm 10$ mm.
- Accuracy of spirit leveled heights with respect to CSNS $\approx \pm 5$ mm. However, the accuracy of these heights may be affected also by systematic errors in CSNS. Repeated observations in the CSNS showed a small tilt in the NW-SE direction. The range of the tilt is from +5 to -3 cm at the boundaries of the country. The estimated rate of change

is within -1 to +5 mm per year.

This facts have to be kept in mind when working with the GNSS/leveling points, but we will use these points and their coordinates in this thesis "as they are".

4.2.4 CGS gravimetric points

The Czech Gravimetric Network consist of more than 400 points which are equally distributed over the area of the Czech Republic. At each of these points are known magnitude of gravity g and normal height H with very high accuracy. The standard deviation of g (computed from the adjustment of the CGS network made by Czech Land Survey Office) varies between $0.003 - 0.020$ mGal [Olejník, 1997], [Träger, 2004]. The gravity system is S-Gr95.

The g values were re-adjusted using least squares adjustment by Martin Lederer from the Czech Land Survey Office. For the re-adjustment not only points from CGS, but also gravimetric points from the neighborhood countries were used. The total amount of used gravimetric points was 720. From this adjustment not only the results (gravity g) were obtained, but also their covariance matrix C_g.

In this thesis we use a set of 455 CGS points, which were readjusted by Martin Lederer. This set consists of CGS points of 0., 1. and 2. order as well as points of the Czech gravimetric base and available absolute gravimetric points (see figure 4.5).

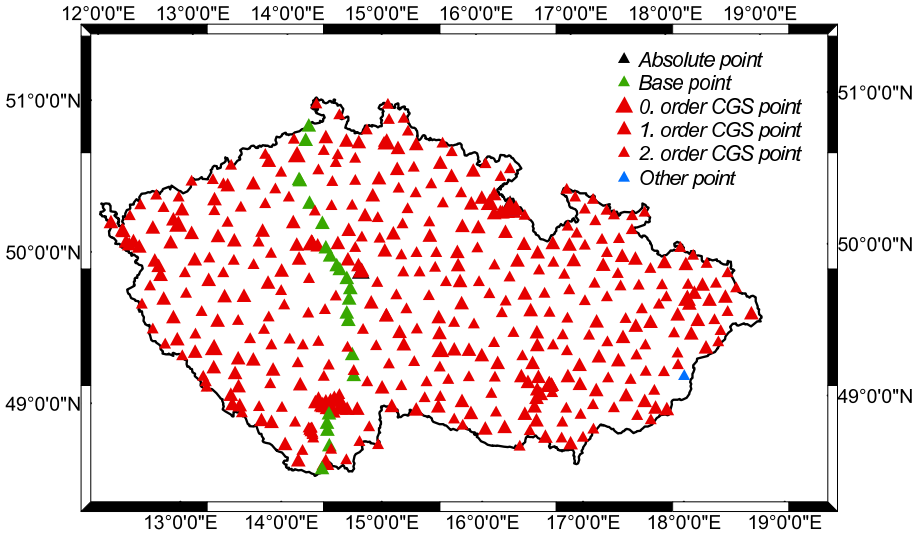

Figure 4.5: *CGS points in Czech Republic.*

4.2.5 Vertical gravity gradients

CGS contain 15 absolute points measured with the FG5 absolute gravimeter with a very high accuracy ($\approx 2\ \mu Gal$). At these 15 absolute points not only gravity was measured, but also the gravity gradient. The gradients were evaluated from gravity measurements in several vertical levels from 0 m to 1.5 m above each point. Gravity was measured independently by two or three gravimeters (Scintrex CG-5, La Coste & Romberg G (LCR) and ZLS Burris). For details about the procedure and gradients on these points see [Lederer and Pálinkáš, 2007]. The standard deviation of the gradient estimates is about 1 E.

Despite the high accuracy of the estimated gradients at the absolute points, these points are not ideal for comparison with other gravity gradient models, because they are usually situated in buildings (often in subbasements), whereas the gravity gradient from other models is computed on a

free surface.

We have used also 61 points, where the gravity gradient was also measured by ZÚ, and which were kindly provided us by Martin Lederer and Otakar Nesvatba. Some of these points overlap with points mentioned above.

4.3 Height anomaly

4.3.1 Model for height anomaly

First quantity that will be computed by our combination approach is the height anomaly ζ. The computational formula for height anomaly (Brun's formula) is

$$\zeta = \frac{T}{\gamma}, \tag{4.1}$$

where T is the disturbing gravity potential on the surface of the earth and γ is normal gravity on telluroid. The disturbing potential T for a point P on the surface of the earth with elevation h is computed as

$$T(P) = T^g + T^{rtm}, \tag{4.2}$$

where T^g is the disturbing potential computed from GGM and T^{rtm} is the disturbing potential computed from residual terrain. T^g is computed by Equation (2.21) and T^{rtm} is computed as the gravitational potential of the residual terrain given by V^{rtm}. We can replace T^g by V^{rtm} because the normal potential V_n was already subtracted in T^g.

We will now insert Equation (3.33) for V^{rtm} into Equation (4.2)

$$\begin{aligned} T(P) &= T^g + V_{BS} + V_{TE} - V^g_{BS} - V^g_{TE} \\ &= T^g + V^{rtm}_{BS} + V^{rtm}_{TE} \end{aligned} \tag{4.3}$$

where $V_{BS}^{rtm} = V_{BS} - V_{BS}^{g}$ is the effect of the Bouguer layer for residual terrain, which can be computed in one step, because we do not apply harmonic correction, and $V_{TE}^{rtm} = V_{TE} - V_{TE}^{g}$ is the residual terrain effect (without Bouguer layer effect).

Potentials V_{TE}, V_{TE}^{g} and V_{TE}^{rtm} are plotted at Figure 4.7. Potentials V_{BS}^{rtm} and height anomalies ζ^{g} and the final model ζ are plotted at Figure 4.8.

4.3.2 Testing height anomalies

We have tested our model of the height anomalies on 1016 GNSS/leveling points in the Czech Republic. Results are shown in Table 4.1.

	ζ^{*}	ζ^{g}	ζ_{BS}^{rtm}	ζ_{TE}	ζ_{TE}^{g}	$\Delta\zeta_0$	$\Delta\zeta_1$	$\Delta\zeta_2$
mean	45.042	45.493	0.048	0.040	0.017	0.450	0.499	0.501
std	1.341	1.341	0.053	0.471	0.181	0.031	0.057	0.031
min	42.125	42.557	-0.218	-2.831	-0.947	0.355	0.288	0.410
max	47.495	47.898	0.332	2.259	0.873	0.549	0.787	0.605
range	5.370	5.341	0.550	5.090	1.820	0.194	0.499	0.195

Table 4.1: *Statistics of* ζ $[m]$

The quantities are denoted as follows:

- ζ^{*} is the observed value at GNSS/leveling points,
- ζ^{g} is the value computed from EGM08,
- ζ_{BS}^{rtm} is the gravitational effect of limited Bouguer shell computed for $\psi_0 = 10'$,
- ζ_{TE} is the terrain effect,

- ζ^g_{TE} is the terrain effect computed from mean elevation surface.

The differences are defined as follows:

$$\Delta\zeta_0 = \zeta^* - \zeta^g, \tag{4.4}$$

$$\Delta\zeta_1 = \zeta^* - (\zeta^g + \zeta^{rtm}_{BS}), \tag{4.5}$$

$$\Delta\zeta_2 = \zeta^* - (\zeta^g + \zeta^{rtm}_{BS} + \zeta_{TE} - \zeta^g_{TE}). \tag{4.6}$$

We can see that there is a very good agreement even for ζ^* and ζ^g as the standard deviation of $\Delta\zeta_0$ is only 3.1 cm. The systematic shift of 45 cm is known to be caused by different height and gravity reference systems. Adding the effect of the Bouguer layer without any compensation brings decrease of the fit to almost 6 cm as is shown for $\Delta\zeta_1$. The column $\Delta\zeta_1$ can be treated as a gravitational potential equivalent of simple Bouguer reduction as is usually used for gravitational acceleration. When we finish RTM by adding terrain effects (see $\Delta\zeta_2$), we get slightly different results from $\Delta\zeta_2$ in terms of the mean, minimal and maximal values, but the standard deviation remains the same. Therefore, we cannot decide which results are better and whether the application of RTM improved the pure EGM08 solution. The problem is that 3 cm is the expected accuracy of GNSS/leveling points and the total accuracy cannot be better than accuracy of ζ^*.

4.4 Gravity

4.4.1 Model for gravity

The second quantity, which will be computed by our combinational approach, is the magnitude of gravity acceleration g. Our computational formula will

be

$$g(P) = g^g + \Delta g^{rtm}, \tag{4.7}$$

where g^g is gravity computed from GGM and Δg^{rtm} is the effect of residual terrain on the gravity anomaly, which is the same as on gravity. Evaluation of g^g from GGM is not so easy, because we should also take into account ellipsoidal correction and manually add centrifugal acceleration because it is not included in GGM (it is not harmonic and cannot be expanded into spherical harmonics). These issues can be solved using formulas shown in subsection 2.2.4.

We will again split Δg^{rtm} into four parts

$$\begin{aligned} g(P) &= g^g + \Delta g_{BS} + \Delta g_{TE} - \Delta g^g_{BS} - \Delta g^g_{TE} \\ &= g^g + \Delta g^{rtm}_{BS} + \Delta g^{rtm}_{TE} \end{aligned} \tag{4.8}$$

where $\Delta g^{rtm}_{BS} = \Delta g_{BS} - \Delta g^g_{BS}$ is the effect of the Bouguer layer for residual terrain without the harmonic correction, and $\Delta g^{rtm}_{TE} = \Delta g_{TE} - \Delta g^g_{TE}$ is the residual terrain effect (here without the Bouguer layer).

Gravity anomalies Δg_{TE}, Δg^g_{TE} and Δg^{rtm}_{TE} are plotted at Figure 4.9. Δg^{rtm}_{BS} is plotted at Figure 4.10. We have not plotted g^g and the final model of g, because these quantities have strong correlation with height and latitude and local differences remain hidden in plots of g. Instead, we have plotted T^g_r and T_r. However, we have evaluated the model of g, which will be used in next subsection to test the effect of RTM on gravitational attraction. T^g_r and T_r are plotted also at Figure 4.10. We can see considerably more details in the final model which contains RTM induced gravitation compared to EGM08 solution, which is much smoother.

4.4.2 Testing gravity

We have tested our model of gravity g on 455 GNSS/leveling points in the Czech Republic. Results are shown in Table 4.2.

	g^*	g^g	Δg_{BS}^{rtm}	Δg_{TE}^{rtm}	$\delta\Delta g_0$	$\delta\Delta g_1$	$\delta\Delta g_2$
mean	980909.961	980920.212	-13.098	0.971	10.251	-3.003	-3.974
std	49.481	53.469	12.692	0.718	12.930	2.545	2.491
min	980805.245	980793.973	-27.886	0.068	-11.273	-8.086	-8.432
max	980979.501	980978.262	11.303	1.889	28.178	0.212	-0.539
range	174.255	184.289	39.189	1.821	39.451	8.297	7.893

Table 4.2: *Statistics of g.* [*mGal*]

The quantities in the Table 4.2 are

- g^* is the observed value at gravity stations,
- g^g is the value computed from EGM08,
- Δg_{BS}^{rtm} is the effect of limited Bouguer shell,
- Δg_{TE}^{rtm} is the terrain effect (already reduced by the effect of the mean elevation surface).

The differences are:

$$\delta\Delta g_0 = \Delta g^* - \Delta g^g, \tag{4.9}$$

$$\delta\Delta g_1 = \Delta g^* - (\Delta g^g + \Delta g_{BS}^{rtm}), \tag{4.10}$$

$$\delta\Delta g_2 = \Delta g^* - (\Delta g^g + \Delta g_{BS}^{rtm} + \Delta g_{TE} - \Delta g_{TE}^{g}). \tag{4.11}$$

Table 4.2 shows, that it is possible to predict gravity in the Czech Republic only from EGM08 with accuracy 13 mGal (standard deviation of column $\delta\Delta g_0$) with a systematic shift -13 mGal. Adding the effect of the limited Bouguer plate causes decrease of the standard deviation to 2.55 mGal, the mean value is reduced to -3 mGal as well. After adding also terrain corrections, we get standard deviation of 2.49 mGal and mean difference -4 mGal. The main part of the mean value of the differences is again caused by differences in height and gravity reference systems. What is interesting is the fact that the Bouguer shell plays much bigger role in this case than the terrain correction. This is caused by the fact that the free air gravity gradient and gradient inside masses are significantly different. This difference cannot be incorporated into EGM08, which provides only harmonic continuation from quantities which are defined on its reference sphere by its coefficients. EGM08 cannot handle steps in gravity gradients and these steps have to be added manually. We want to remind that adding of these gradient changes is accomplished by the term Δg_{BS}^{rtm}. No special harmonic correction needs to be applied for points under the mean elevation surface. The harmonic correction as is explained in [Forsberg, 1984] covers the problem, when the model contains such gradient step at the mean elevation surface. In such a case, this step should be removed by Δg_{BS}^{g} including the harmonic correction and then again added at the real terrain height by Δg_{BS}.

We will now show also empirically that no additional harmonic correction should be applied to EGM08 gravity. The effect of the harmonic correction is twice as large as the effect of the Bouguer plate (or shell) as it was shown in Subsection 3.3.1. The harmonic correction causes that the RTM correction has the same size, but the opposite sign for points under the mean elevation surface (see figure 3.5). We have a balance set of positive and negative

elevation differences between real surface and mean elevation surface at our gravity stations so if there is any need to apply harmonic correction, half of our corrections Δg_{BS}^{rtm} would have a wrong sign. These corrections are so large, that mistakes in half of their signs would have been clearly visible in the column $\delta\Delta g_1$, which would have larger standard deviation (or the same in the best case) than $\delta\Delta g_0$. Instead, there is a significant improvement in the standard deviation, which proves that our methodology is correct and the harmonic correction as proposed in [Forsberg, 1984] should not be applied for quantities computed from EGM08.

4.5 Gravity gradient

4.5.1 Model for gravity gradient

The third and last quantity which will be computed by our combination method is the gravity gradient g_r. The computational formula is

$$g_r(P) = g_r^g + V_{rr}^{rtm}, \tag{4.12}$$

where g_r^g is gravity computed from GGM and V_{rr}^{rtm} is the effect of residual terrain on the second vertical derivation of the gravitational potential, which can serve us as the effect on the gravity gradient as well. Evaluation of g_r^g was described in Subsection 2.2.5. We will again split V_{rr}^{rtm} into four parts

$$\begin{aligned} g_r(P) &= g_r^g + V_{rrBS} + V_{rrTE} - V_{rrBS}^g - V_{rrTE}^g \\ &= g_r^g + V_{rrBS}^{rtm} + V_{rrTE}^{rtm}, \end{aligned} \tag{4.13}$$

where $V_{rrBS}^{rtm} = V_{rrBS} - V_{rrBS}^g$ is the effect of Bouguer layer for residual terrain without the harmonic correction, and $V_{rrTE}^{rtm} = V_{rrTE} - V_{rrTE}^g$ is the residual terrain effect (here without the Bouguer layer).

Quantities V_{rrTE}, V^g_{rrTE} and V^{rtm}_{rrTE} are plotted at Figure 4.11. V^{rtm}_{rrBS} is plotted at Figure 4.12. We have again plotted the disturbing quantity T_{rr} instead of g^g_r as it is better for visualization. T^g_{rr} and the T_{rr} (including all corrections) are also plotted at Figure 4.12. In this case the RTM signal has not only much larger spatial variability, but it has also larger absolute values. Most of the total RTM effect V_{rrTE} is now caused by terrain effects V^{rtm}_{rrTE} and only the minor part by the Bouguer layer V^{rtm}_{rrBS}.

4.5.2 Testing gravity gradient

We have tested our model of gravity gradient g_r on 61 gravimetric points in the Czech Republic, where also gravity gradient was measured. Results are shown in Table 4.3. Because the total number of test points is not large, we provide also Figure 4.6 with all points including their observed and predicted values. Each column represents one point, green mark is the gravity gradient predicted only from EGM08, red mark is the observed gravity gradient and blue mark is the gravity gradient evaluated by combination of EGM08 and RTM. The plot shows that EGM08 is absolutely not capable of representing the complex behavior of g_r and the value remains almost constant. The RTM method provides significant improvements, as is clear from the plot. In most columns of the plot, the blue marks (gradient predicted by EGM08+RTM) are significantly closer to the observed values (red) than the green marks (EGM08 only solution).

The quantities in the Table 4.3 are defined as follows:

- g^*_r is the observed gravity gradient,
- g^g_r is the value computed from EGM08,
- V^{rtm}_{rrBS} is the effect of the limited Bouguer shell,

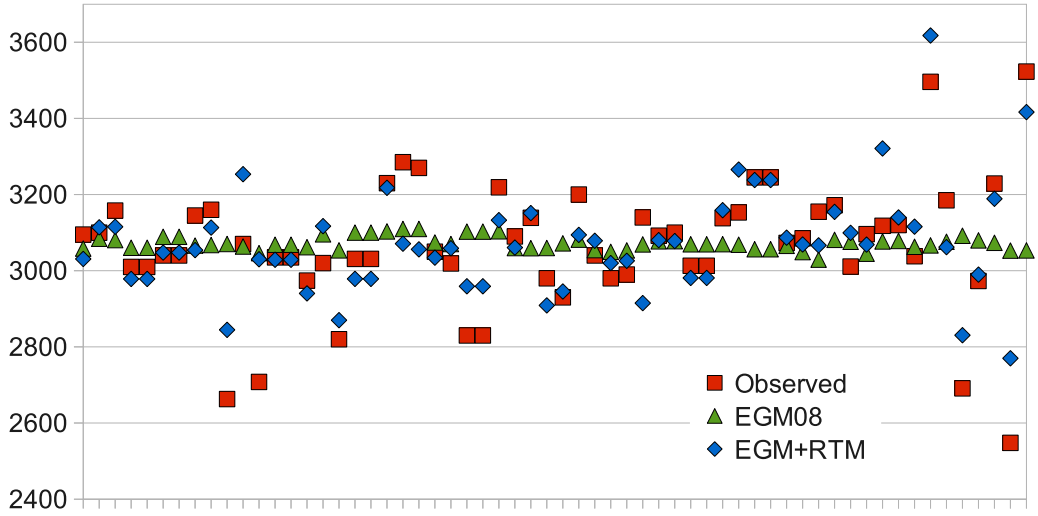

Figure 4.6: *Gravity gradient at test points in CZ.* [E]

	g_r^*	g_r^g	V_{rrBS}^{rtm}	V_{rrTE}^g	V_{rrTE}	Δg_{r0}	Δg_{r1}	Δg_{r2}
mean	3064.7	3072	5.2	-3.50	-15.0	-7.3	-12.5	-1.0
std	169.2	17.6	13.8	6.97	91.9	168.9	162.7	138.7
min	2548.0	3029.1	-31.2	-14.8	-306.0	-504.9	-491.4	-283.0
max	3523.0	3109.7	33.9	11.9	194.7	469.7	475.7	551.4
range	975.0	80.6	65.01	26.7	500.7	974.6	967.0	834.3

Table 4.3: *Statistics of* g_r. [*E*]

- V_{rrTE} is the terrain effect,
- V_{rrTE}^g is the terrain effect of the mean elevation surface.

The differences are:

$$\Delta g_{r0} = g_r^* - g_r^g, \tag{4.14}$$

$$\Delta g_{r1} = g_r^* - (g_r^g + V_{rrBS}^{rtm}), \tag{4.15}$$

$$\Delta g_{r2} = g_r^* - (g_r^g + V_{rrBS}^{rtm} + V_{rrTE} - V_{rrTE}^g). \tag{4.16}$$

The statistics in Table 4.3 also show the significant improvement of gravity gradients after introducing RTM effects: the standard deviation has decreased from 169 E (for $\delta\Delta g_0$) to 138 E (for $\delta\Delta g_2$). The mean value has decreased also, but its size is small with respect to the standard deviation so its decrease is not statistically significant. We believe that the fit could be even better if we could use DEM with higher resolution.

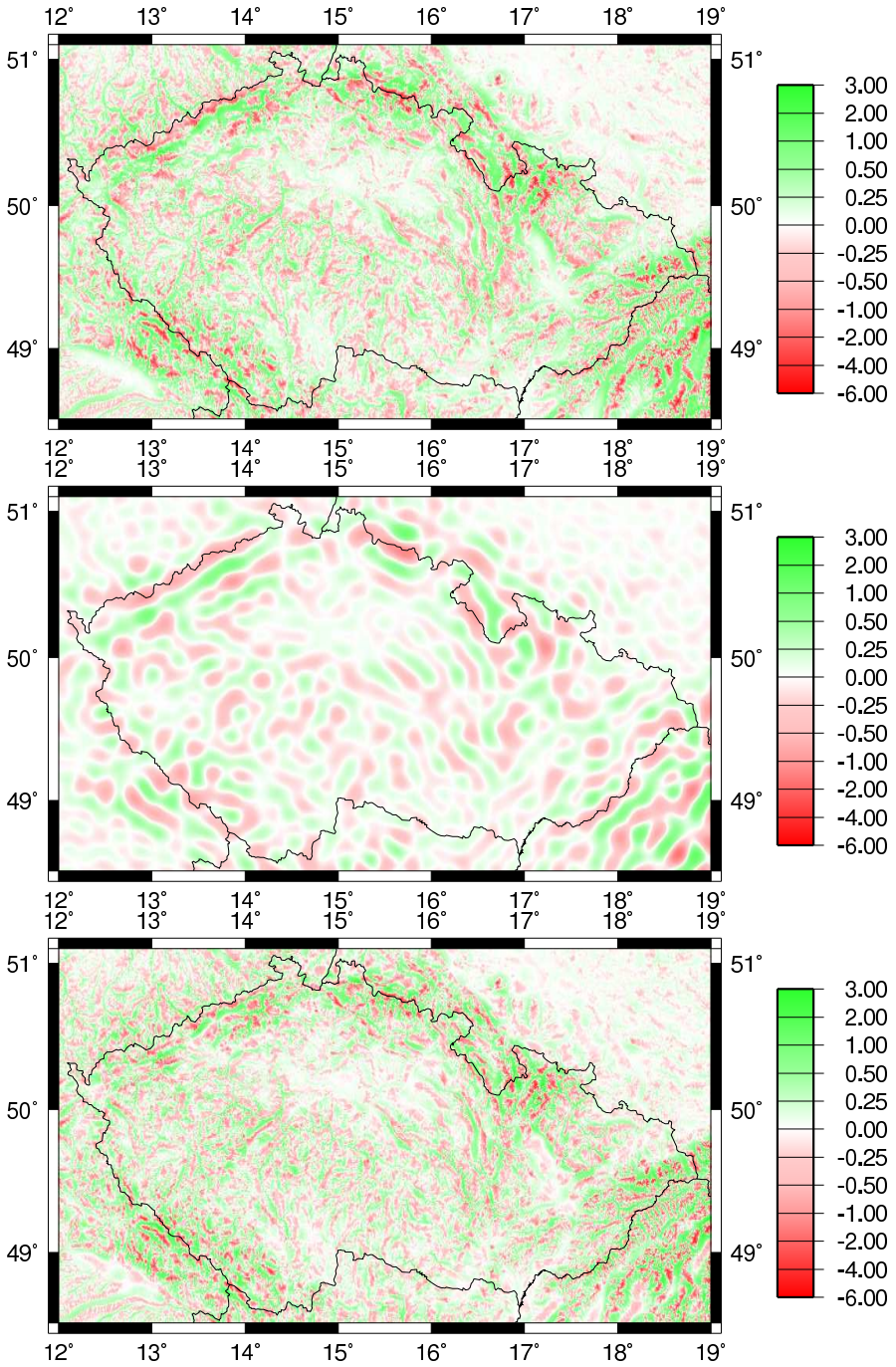

Figure 4.7: *Terrain effects for V in CZ.* From top: V_{TE} / V_{TE}^{g} / V_{TE}^{rtm}. $[m^2/s^2]$

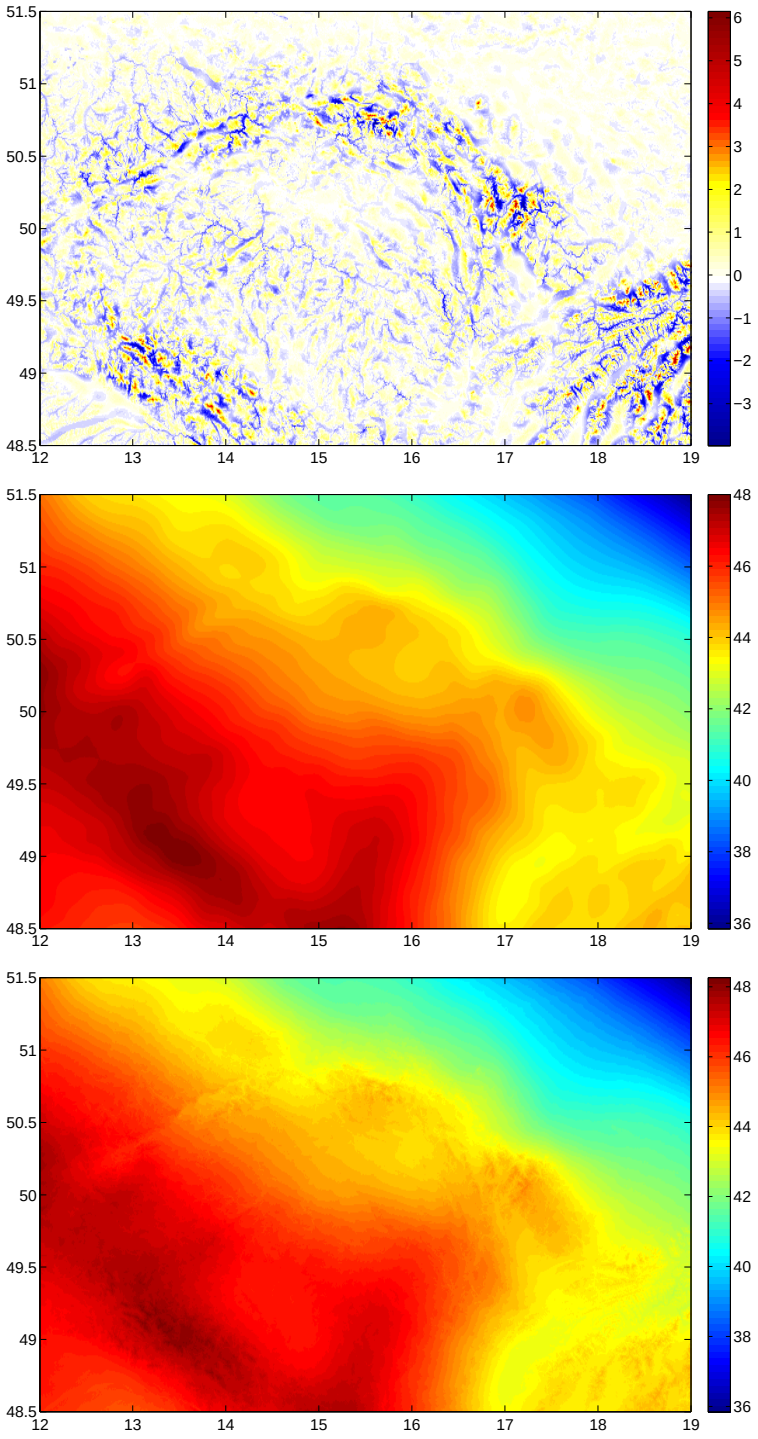

Figure 4.8: *V_{BS}^{rtm} and height anomalies in CZ.*
From top: V_{BS}^{rtm} $[m^2/s^2]$ / ζ^g $[m]$ / ζ $[m]$

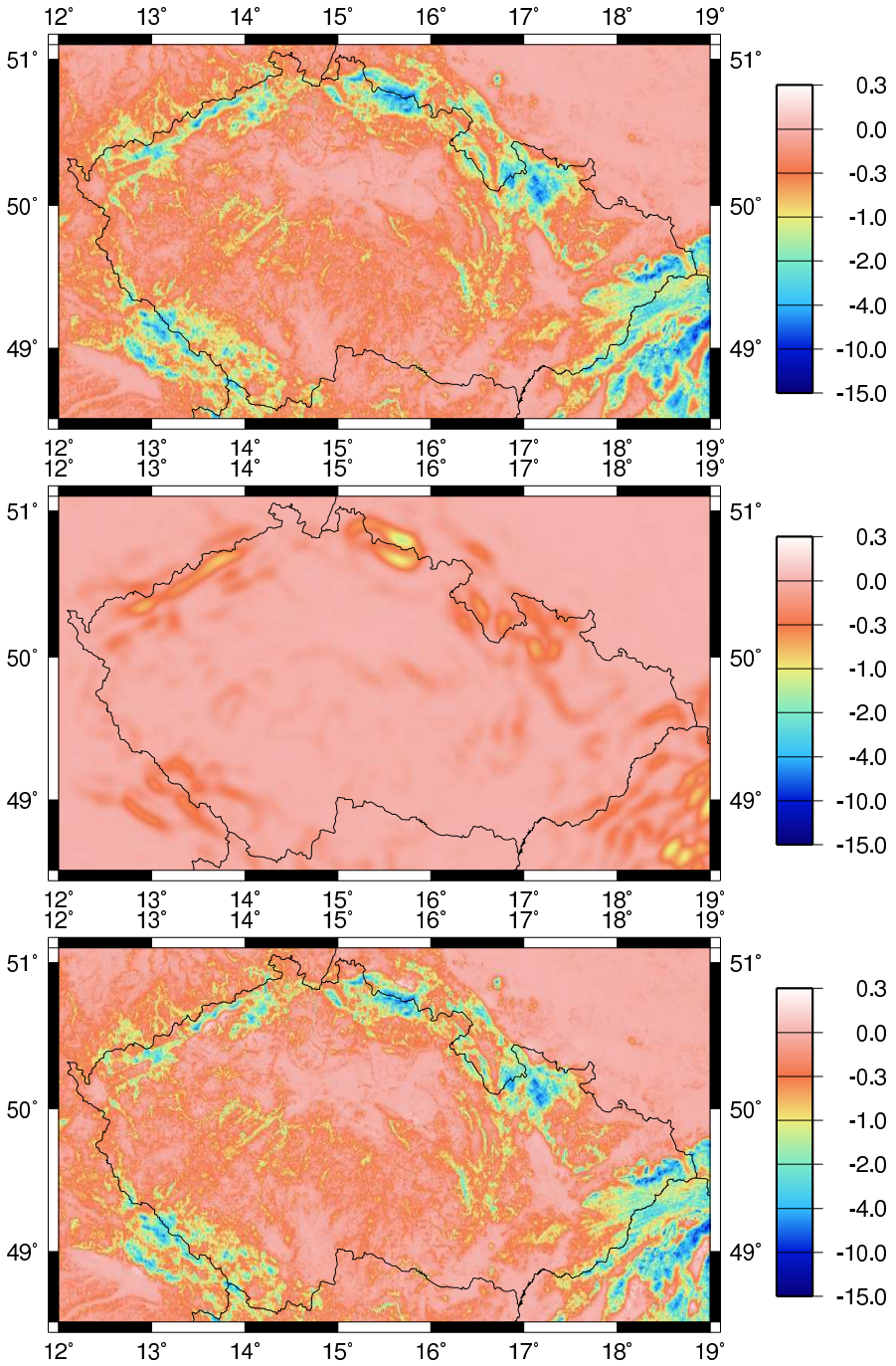

Figure 4.9: *Terrain effects for Δg in CZ.*
From top: Δg_{TE} / Δg^{g}_{TE} / Δg^{rtm}_{TE}. $[mGal]$

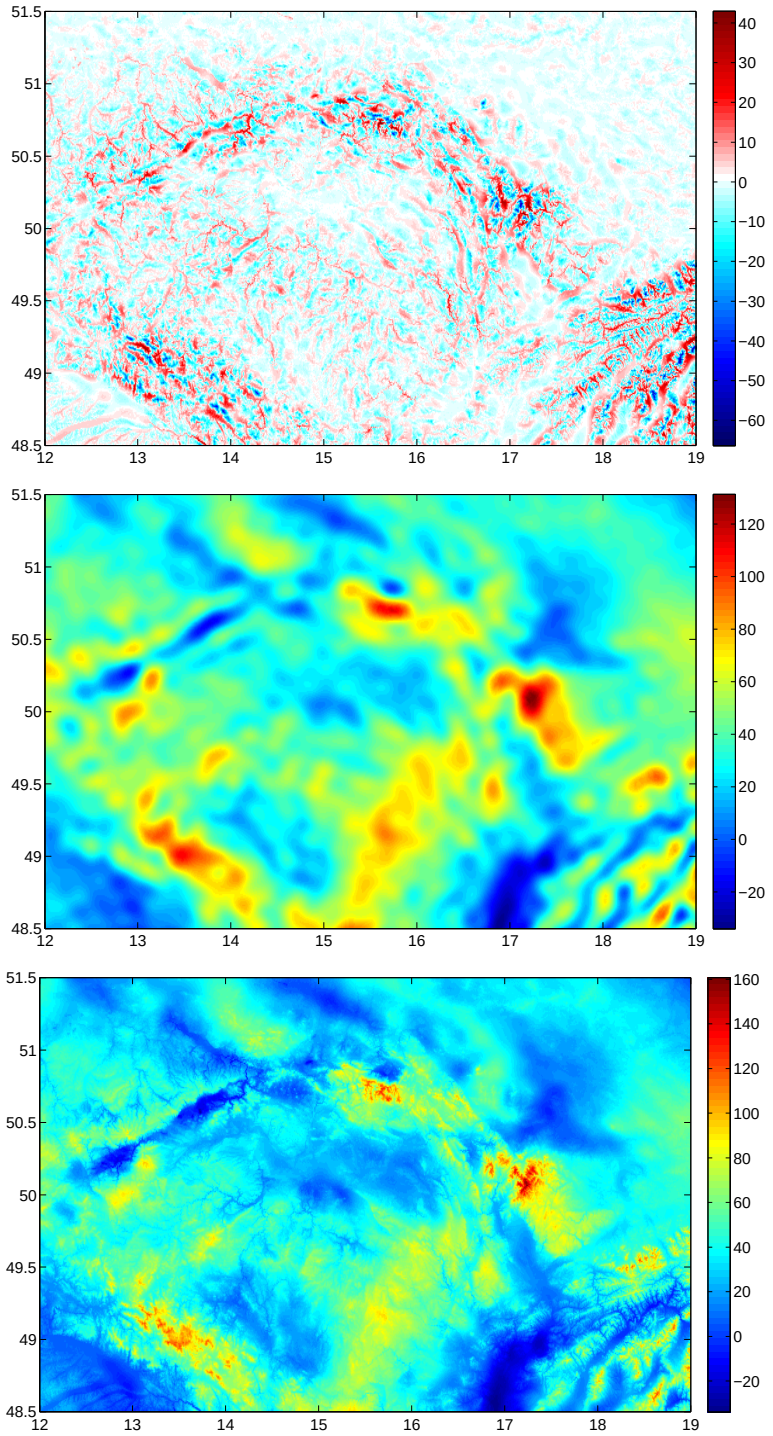

Figure 4.10: Δg_{BS}^{rtm} *and gravity disturbance in CZ.*
From top: Δg_{BS}^{rtm} $[mGal]$ / T_r^g $[mGal]$ / T_r $[mGal]$

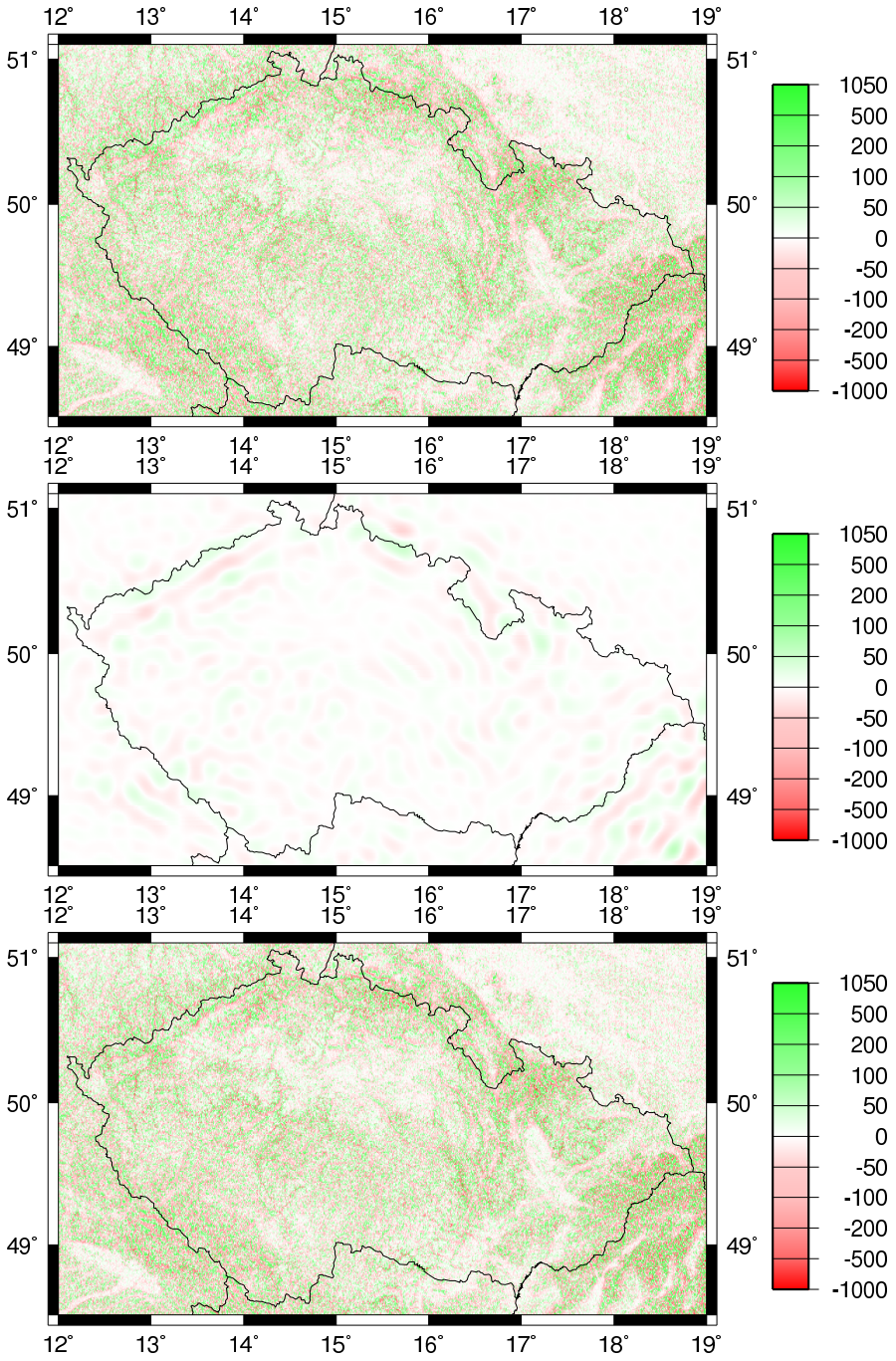

Figure 4.11: *Terrain effects for V_{rr} in CZ.*
From top: V_{rrTE} / V^{g}_{rrTE} / V^{rtm}_{rrTE}. All $[E]$

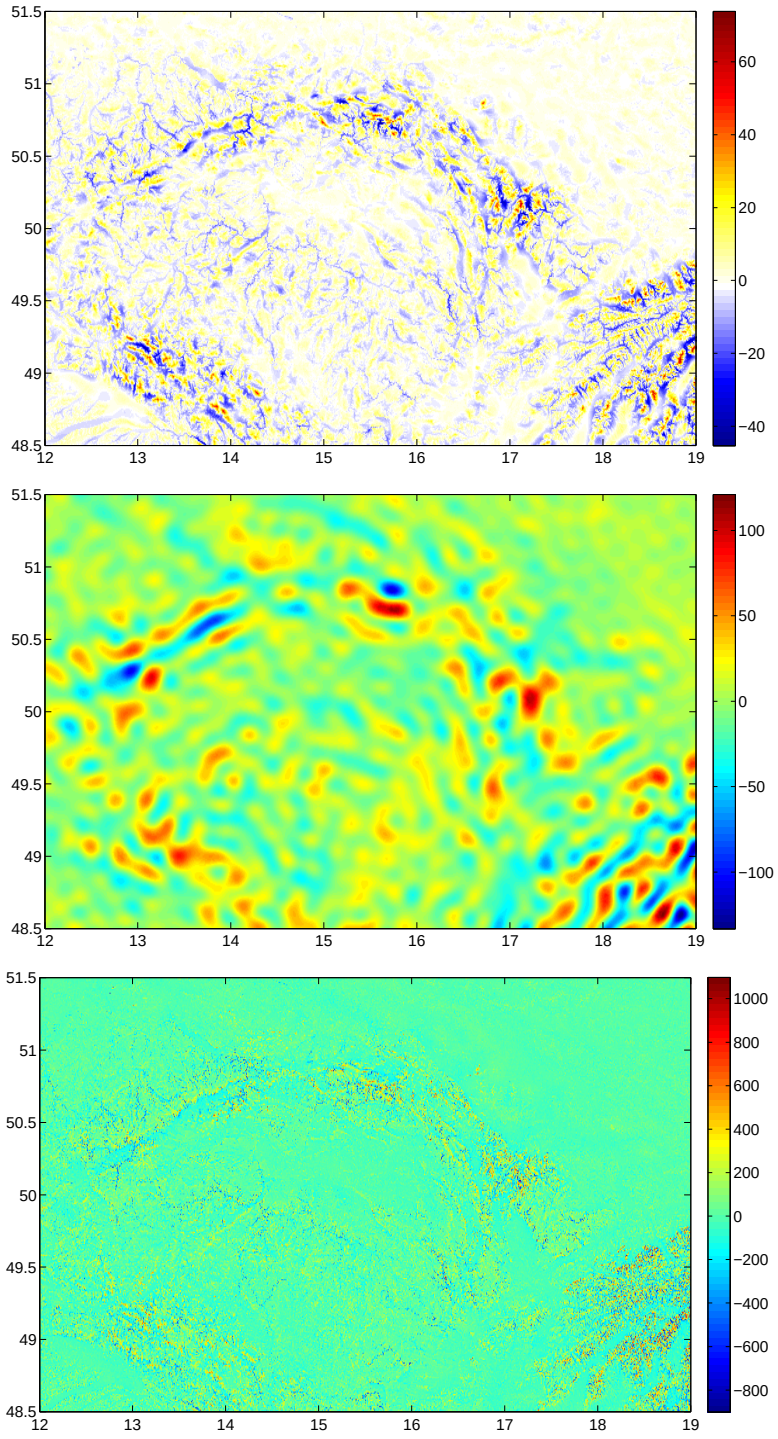

Figure 4.12: V^{rtm}_{rrBS} *and* T_{rr} *in CZ.* From top: V^{rtm}_{rrBS} / T^{g}_{rr} / T_{rr}. All $[E]$

Chapter 5

Conclusions

5.1 Summary

The main goal of this thesis was fulfilled. We have successfully set up the new combination method based on residual terrain modeling, which can predict gravity field quantities from EGM08 and digital elevation models. We have evaluated the height anomalies, magnitude of the gravity acceleration and the gravity gradient in the Czech Republic and we have also compared computed values with observations.

In Chapter 2, we have reviewed basic theory required for evaluation of gravity field quantities from EGM08 in Section 2.2. An important Subsection 2.2.6 contains evaluation of mean omission errors for EGM08. The omission error for height anomaly is about 3 cm. For gravity anomaly the mean omission errors is about 10-15 mGal (depends on used degree variance model). The same value holds also for magnitude of the gravity acceleration. The degree variance models have shown very different results for the gravity gradient, the Tscherning/Rapp model 75 E and Flurry (2006) model 512 E. However, both models show only very little dependence of the mean omission error on the maximal degree of GGM for the omission error of the gravity gradient.

In Section 2.3, we have derived formulas for gravitational potential and its first and second radial derivatives for four types of geometric bodies: the unlimited and limited Bouguer shell and the unlimited and limited Bouguer plate. The formulas for limited and unlimited plate were derived also by other authors, i.e., [Burša, 2004], but we are providing original generalized version of formulas, which do not depend on the relative position of the evaluation point to the Bouguer plate. Also most formulas for the effects of Bouguer shell were already published, but the solution for the gravity gradient of the

limited Bouguer shell is our original result, yet very complex. Despite the fact that most effects can be computed also by other already published formulas, we have derived all formulas using unified approach and they can be found at one place.

Moreover, we have derived also simplified formulas when the general formulas were too complex, especially for the effects of the limited Bouguer shell. During the derivation of simplified formulas, we have sometimes used approximation and we have neglected some parts of expressions. The effect of each neglected term has been carefully considered during the derivation, either analytically using the Wolfram Mathematica software package for manipulating algebraic expressions or numerically in more complicated cases. Unfortunately it was not possible to explain each algebraic step in detail. To support the credibility of derived expressions, we have provided some plots and tables in Subsection 2.3.6 with numerical comparison of all important approximate formulas with their exact counterparts.

Derived formulas are then applied in residual terrain modeling (Chapter 3) of height anomalies, gravity anomalies and gravity gradients. Because we have derived general formulas for points above the Bouguer layer, on the Bouguer layer or even inside it, our formulas can be used in a way which implicitly includes the harmonic correction. This is achieved by splitting the gravitational effect of terrain into four parts, see Subsections 3.2.1–3.2.6.

The harmonic correction is discussed in Subsection 3.1.3. Contrary to assumptions and results results in [Forsberg, 1994] and [Omang et al., 2010], we are showing that no harmonic correction is required for evaluation of any gravity field quantities from EGM08, when the RTM effect is properly computed.

Chapter 4 contains description of used datasets and evaluation of the

height anomaly, gravity and gravity gradient models for the Czech Republic by our combination approach. All three quantities are tested at GNSS/leveling points (height anomaly), gravimetric points (gravity) and also the gravity gradient is tested at few gradiometric points. The accuracy expressed by the standard deviation of the differences between observed and computed values values is quite good: for height anomaly it is 3 cm, for gravity 2.5 mGal and for the gravity gradient 140 E. These results are discussed in the following section.

5.2 Accuracy of numerical results

The accuracy of obtained results is limited by the accuracy of input data and by the used methodology. We have shown in the introduction, that proper evaluation of the RTM effects has major impact on the accuracy of the gravity anomalies. We will now compare accuracy of our results, which is expressed as a standard deviation of differences between observed and computed height anomalies, gravity anomalies and gravity gradients with results provided by the other authors and also with the expectations coming from the estimated EGM08 omission errors.

In case of the height anomaly, we have achieved the same standard deviation of 3 cm as quasigeoid models derived from terrestrial gravimetric measurements. However, the height anomalies computed from EGM08 without any terrain correction have the same standard deviation. The problem is that the testing points have the accuracy also about 3 cm [Novák et al., 2009b] so the GNSS/leveling points cannot be used to judge if there was any improvement in accuracy after applying the residual terrain effect. The estimated omission error is also about 3 cm.

For the gravity anomalies, we have achieved the standard deviation of 12.9 mGal before applying the RTM effect. This standard deviation agrees very well with the estimated omission error which was estimated to be in a range 10–15 mGal. After applying the full RTM effect (the Bouguer layer and the terrain correction), the standard deviation was reduced to 2.49 mGal. If we neglect the terrain correction and evaluate only the effect of the Bouguer layer, we get the standard deviation of 2.55 mGal. This shows that the proper evaluation of the effect of the Bouguer layer is crucial in this case and it proves that our methodology and derivations provided in Chapters 2 and 3 are valid. The best result publicated in [Huang and Kotsakis, 2009] for terrestrial gravimetry was 4.9 mGal in [Claessens et al., 2009] for Australia. The best result we have found in available publications was 3.5 mGal in [Forsberg, 2009] for the area of Auvergne, France. Our result 2.55 mGal is very good in comparison with the other standard deviations, but we should note that the roughness of the terrain plays very important role and results for different areas cannot be directly compared. The best results published in [Huang and Kotsakis, 2009] was reported in Florida [Roman et al., 2009], where were used for comparison gravity anomalies from aerial gravimetry and the reported standard deviation was 2.3 mGal. This result is slightly better, but the gravity signal from aerial gravimetry is spectrally limited so it does not require so precise evaluation of terrain effects, particularly in Florida as it is a flat country with maximum height about 100 m.

We have tested also the accuracy of a local model of mean values of terrestrial gravity anomalies [Kadlec et al., 2007], which is available for the Czech Republic with the spatial resolution of $30''$. The accuracy of gravity anomalies from this model which has been evaluated at the same testing points was 1 mGal so our RTM method cannot give as accurate results as a

database of terrestrial gravity anomalies. This result was expected, but we can see that the RTM method is only 2.5× worse.

All numerical results were computed without applying the harmonic correction for points lying under the mean elevation surface as proposed in [Forsberg, 1984], because we have shown in Subsection 3.1.3 that such correction is not required. To test our conclusion, we have tried to evaluate the gravity anomaly also with the harmonic correction and we have received the standard deviation 20.8 mGal, which is a clear empirical proof that our approach do not need the harmonic correction. Because the methodology is same also for other gravity field quantities, our methodology does not require derivation of new harmonic corrections for all the other gravity field quantities as it is proposed in [Omang et al., 2010].

The standard deviation of gravity gradients has decreased from 169 E (without RTM effect) to 138 E (including the RTM effect). The expected omission error was between 75 (Tscherning/Rapp degree variance model) and 512 (Flury 2006 degree variance model). The numerical results show, that EGM08 generates almost constant gravity gradient between 3030 E and 3110 E, whereas the observed gravity gradients have quite wide range 2550-3520 E. In this case, almost the whole effect is generated by RTM and EGM08 has not played important role — we can use the mean value of 3080 E instead and get almost the same accuracy. To evaluate the gravity gradient, the resolution and accuracy of the terrain effect is crucial.

5.3 Conclusions

Going back to section 1.2, we will provide a short review of achieved goals.

The main goal was to develop a method for precise computation of height

anomalies, gravity anomalies and gravity gradient from GGM and DEM. We think that this goal was fulfilled, including its partial steps:

- The omission error of selected gravity field quantities was computed in Subsection 2.2.6.

- A method based on RTM was described and successfully used. The key original idea behind our method is that a limited Bouguer shell or limited Bouguer plate should be used for reduction of the gravity anomalies instead of using unlimited plate or shell as it is now common. The same stands also for the other gravity field parameters. All required formulas have been originally derived, even though most of them are already known.

- The harmonic reduction problem was studied in Subsection 3.1.3 and it was concluded that it is not required in our method. Achieved results, particularly for the gravity anomalies, show that this hypothesis is right.

- Three gravity field quantities (the height anomaly, magnitude of gravity and gravity gradient) were evaluated by the proposed method in the Czech Republic and results were compared with observed values. The standard deviations between observed and computed values are at least as good as were reported by other authors or even better, particularly for the gravity anomaly. The standard deviations were for 3 cm for the height anomaly, 2.5 mGal for gravity anomaly and and 140 E for the gravity gradient.

Even though we have tested the method in the Czech Republic, we should note, that the methodology is general and may be used anywhere. The

datasets used for evaluation of all quantities were EGM08, SRTM3 and DTM2006.0, which are also available globally. Therefore, our method can be used anywhere in the world to increase the accuracy of values predicted from EGM08.

5.4 Recommendations for future work

We would like to point out some issues, which have not been solved in this thesis and which should be studied in the future.

The biggest issue is the cut-off distance for the terrain modeling, which is in our method used also as a cut-off distance for the limited Bouguer plate or shell. We have kept the cut-off distance of $10'$as is proposed in [Forsberg, 1984]. However, may not be enough in a rough terrain, as was pointed in [Hirt et al., 2010].

Another issue is the credibility of degree variance models for estimation of omission errors for the gravity gradient. Two models which were used in subsection 2.2.6 give totaly different results.

The last but not least issue is required resolution of digital elevation model used for evaluation of residual terrain effects. We have used SRTM3 in this thesis, which is globally available, but at least for estimation of gravity gradients, digital elevation models with higher resolution should be considered.

Bibliography

[Anderson, 1976] Anderson, E. G. (1976). The effect of topography on solutions of Stokes's problem. Unisurv Report S14. Technical report, University of New South Wales, Kensington.

[Ardalan and Safari, 2004] Ardalan, A. A. and Safari, A. (2004). Ellipsoidal terrain correction based on multi-cylindrical equal-area map projection of the reference ellipsoid. *Journal of Geodesy*, 78:114–123.

[Blakely, 1996] Blakely, R. J. (1996). *Potential Theory in Gravity and Magnetic Applications.* Cambridge University Press.

[Blitzkow and de Matos, 2009] Blitzkow, D. and de Matos, A. C. O. C. (2009). EGM2008 and PGM2007A evaluation for South America. In Huang, J. and Kotsakis, C., editors, *Newton's Bulletin: External Quality Evaluation Reports of EGM08*, number 4, pages 73–78. Bureau Gravimétrique International and International Geoid Service.

[Burša, 2004] Burša, M. (2004). *Geopotenciál : teoretické základy a modely.* Ministerstvo obrany ČR, Geografická služba AČR, Dobruška.

[Burša et al., 2009] Burša, M., Kenyon, S., Kouba, J., Šíma, Z., Vatrt, V., and Vojtíšková, M. (2009). Results of EGM08 geopotential model testing

and its comparison with EGM96. In Huang, J. and Kotsakis, C., editors, *Newton's Bulletin: External Quality Evaluation Reports of EGM08*, number 4, pages 50–56. Bureau Gravimétrique International and International Geoid Service.

[Claessens et al., 2009] Claessens, S. J., Featherstone, W. E., Anjasmara, I. M., and Filmer, M. S. (2009). Is Australian data really validating EGM2008, or is EGM2008 just in/validating Australian data? In Huang, J. and Kotsakis, C., editors, *Newton's Bulletin: External Quality Evaluation Reports of EGM08*, number 4, pages 207–251. Bureau Gravimétrique International and International Geoid Service.

[CUZK, 2009] CUZK (2009). Zhuštění bodů se souřadnicemi ETRS89 na území ČR [in czech]. [online], [cit. 2.7.2009], `http://www.cuzk.cz/Dokument.aspx?PRARESKOD=998&MENUID=0&AKCE=DOC:10-GPS_TRANS`.

[Farr et al., 2007] Farr, T. G., Rosen, P. A., Caro, E., and et al., R. C. (2007). The Shuttle Radar Topography Mission. *Rev. Geophys.*, 45.

[Flury, 2006] Flury, J. (2006). Short-wavelength spectral properties of the gravity field from a range of regional data sets. *Journal of Geodesy*, 79:624–640.

[Forsberg, 1984] Forsberg, R. (1984). A study of terrain reductions, density anomalies and geophysical inversion methods in gravity field modelling. Technical report, The Ohio State University.

[Forsberg, 1994] Forsberg, R. (1994). *International School for the determination and use of the geoid – lecture notes*, chapter Terrain effects in geoid computations. International geoid service.

[Forsberg, 2009] Forsberg, R. (2009). Terrain modelling with ultra-high resolution spherical harmonic geopotential models. Presented at Geodesy for planet Earth, IAG, Buenos Aires.

[Gruber, 2009] Gruber, T. (2009). Evaluation of the EGM08 gravity field by means of GPS-levelling and sea surface topography solutions. In Huang, J. and Kotsakis, C., editors, *Newton's Bulletin: External Quality Evaluation Reports of EGM08*, number 4, pages 3–17. Bureau Gravimétrique International and International Geoid Service.

[Heck and Seitz, 2007] Heck, B. and Seitz, K. (2007). A comparison of the tesseroid, prism and point-mass approaches for mass reductions in gravity field modelling. *Journal of Geodesy*, 81:121–136.

[Heiskanen and Moritz, 1967] Heiskanen, W. A. and Moritz, H. (1967). *Physical Geodesy*. W. H. Freeman and Company, San Francisco and London.

[Hirt, 2010] Hirt, C. (2010). Prediction of vertical deflections from high-degree spherical harmonic synthesis and residual terrain model data. *Journal of Geodesy*, 84:179–190.

[Hirt et al., 2010] Hirt, C., Featherstone, W. E., and Marti, U. (2010). Combining EGM2008 and SRTM/DTM2006.0 residual terrain model data to improve quasigeoid computations in mountainous areas devoid of gravity data. *Journal of Geodesy*, 84:557–567.

[Hoffmann-Wellenhof and Moritz, 2005] Hoffmann-Wellenhof, B. and Moritz, H. (2005). *Physical Geodesy*. Springer, Wien and New York.

[Huang and Kotsakis, 2009] Huang, J. and Kotsakis, C., editors (2009). *Newton's Bulletin: External Quality Evaluation Reports of EGM08*. Number 4. Bureau Gravimétrique International and International Geoid Service.

[ICGEM, 2008] ICGEM (2008). International Center for Global Gravity Field Models -Global Gravity Field Models. [online], [cit. 1.7.2011], `http://icgem.gfz-potsdam.de/ICGEM/`.

[Jekeli et al., 2009] Jekeli, C., Yang, H. J., and Kwon, J. H. (2009). Using gravity and topography-implied anomalies to assess data requirements for precise geoid computations. *Journal of Geodesy*, 83:1193–1202.

[Kadlec et al., 2007] Kadlec, M., Kostelecký, J., and Novák, P. (2007). Database for local gravity field modelling over the area of Central Europe. *Geodetický a kartogrfický obzor*, (12).

[Karwel and Ewiak, 2008] Karwel, A. K. and Ewiak, I. (2008). Estimation of the Accuracy of the SRTM Terrain Model on the Area of Poland. In *The international archives of the photogrammetry, remote sensing and spatial information sciences*, pages 169–172. ISSN 1682-1750.

[Lederer and Pálinkáš, 2007] Lederer, M. and Pálinkáš, V. (2007). Precise Determination of Vertical Gravity Gradients in the Czech Gravity Network. In *Proceedings of the International Symposium on Terrestrial Gravimetry: Static and Mobile Measurements*, pages 167–172, Saint Petersburg.

[Lemoine et al., 1998] Lemoine, F. G., Kenyon, S. C., Factor, J. K., Trimmer, R., Pavlis, N. K., Chinn, D. S., Cox, C. M., Klosko, S. M., Luthcke,

S. B., Torrence, M. H., Wang, Y. M., Williamson, R. G., Pavlis, E. C., Rapp, R. H., and Olson, T. R. (1998). The development of the joint NASA GSFC and NIMA geopotential model EGM96. NASA Goddard Space Flight Center, Greenbelt, Maryland, 20771 USA.

[Li et al., 2009] Li, J. C., Ning, J. S., Chao, D. B., and Jiang, W. P. (2009). Evaluation of the Earth Gravitational Model 2008 using GPS-leveling and gravity data in China. In Huang, J. and Kotsakis, C., editors, *Newton's Bulletin: External Quality Evaluation Reports of EGM08*, number 4, pages 252–274. Bureau Gravimétrique International and International Geoid Service.

[Macmillan, 1930] Macmillan, W. D. (1930). *The theory of the potential*. McGraw-Hill. New York.

[Mader, 1951] Mader, K. (1951). Das Newtonsche Raumpotential prismatischer Körper und seine Ableitungen bis zur dritten Ordnung. *Österreichische Zeitschrift für Vermessungswesen*, Sonderheft 11.

[Makhloof and Ilk, 2008] Makhloof, A. A. and Ilk, K.-H. (2008). Far-zone effects for different topographic-compensation models based on a spherical harmonic expansion of the topography. *Journal of Geodesy*, 82:93–111.

[Martinec, 1998] Martinec, Z. (1998). *Boundary value problems for gravimetric determination of a precise geoid*, volume 73 of *Lecture notes in Earth sciences*. Springer, Berlin Heidelberg New York.

[Mayer-Gürr, 2009] Mayer-Gürr, T. (2009). ITG-Grace03s: The latest GRACE gravity field solution computed in Bonn. Presented at Joint International GSTM and DFG SPP Symposium, 15. October 2007, Potsdam.

[McCarthy and Petit, 2004] McCarthy, D. D. and Petit, G. (2004). IERS Conventions. IERS Technical Note 32, Institution, Frankfurt am Main: Verlag des Bundesamts für Kartographie und Geodäsie.

[Merry, 2009] Merry, C. L. (2009). EGM2008 evaluation for Africa. In Huang, J. and Kotsakis, C., editors, *Newton's Bulletin: External Quality Evaluation Reports of EGM08*, number 4, pages 200–206. Bureau Gravimétrique International and International Geoid Service.

[Mikuška et al., 2006] Mikuška, J., Pašteka, R., and Marušiak, I. (2006). Estimation of distant relief effect in gravimetry. *Geophysics*, 71.

[Moritz, 1980a] Moritz, H. (1980a). *Advanced Physical Geodesy*. Wichmann, Abacus Press.

[Moritz, 1980b] Moritz, H. (1980b). Geodetic Reference System 1980. *Bulletin Géodésique*, 54(3).

[Nagy et al., 2000] Nagy, D., Papp, G., and Benedek, J. (2000). The gravitational potential and its derivatives for the prism. *Journal of Geodesy*, 74:552–560.

[Nagy et al., 2002] Nagy, D., Papp, G., and Benedek, J. (2002). Corrections to "The gravitational potential and its derivatives for the prism". *Journal of Geodesy*, 76:475.

[Novák and Grafarend, 2005] Novák, P. and Grafarend, E. W. (2005). Ellipsoidal representation of the topographical potential and its vertical gradient. *Journal of Geodesy*, 78(11-12):691–706.

[Novák et al., 2009a] Novák, P., Klokočník, J., Kostelecký, J., and Zeman, A. (2009a). Testing EGM08 using Czech GPS/leveling data. In Huang,

J. and Kotsakis, C., editors, *Newton's Bulletin: External Quality Evaluation Reports of EGM08*, number 4, pages 126–132. Bureau Gravimétrique International and International Geoid Service.

[Novák et al., 2009b] Novák, P., Kostelecký, J., and Klokočník, J. (2009b). Testing global geopotential models through comparison of a local quasi-geoid model with GPS/leveling data. *Studia Geophysica and Geodetica*, 53(1):39–60.

[Novák et al., 2001] Novák, P., Vaníček, P., Martinec, Z., and Véronneau, M. (2001). Effects of the spherical terrain on gravity and the geoid. *Journal of Geodesy*, 75(9):491–504.

[Olejník, 1997] Olejník, S. (1997). *Evolution of gravity control points on territory of the Czech Republic*. Land Survey Office.

[Omang et al., 2010] Omang, O. C. D., Tscherning, C. C., and Forsberg, R. (2010). Generalisation of the harmonic reduction procedure in residual topographic modeling. In *Proceedings Hotine-Marussi Symposium*, Rome, Italy.

[Pavlis et al., 2006] Pavlis, N. K., Factor, J. K., and Holmes, S. A. (2006). Terrain-Related Gravimetric Quantities Computed for the Next EGM. Presented at the 1st International Symposium of the International Gravity Field Service 2006, Istanbul, Turkey.

[Pavlis et al., 2008] Pavlis, N. K., Holmes, S. A., Kenyon, S. C., and Factor, J. K. (2008). An Earth Gravitational Model to degree 2160: EGM2008. Presented at the 2008 General Assembly of the European Geosciences Union, Vienna, Austria, April 13-18, 2008.

[Rapp, 1973] Rapp, R. (1973). Geoid information by wavelength. *Bulletin Géodésique*, 110:405–411.

[Rapp, 1998] Rapp, R. H. (1998). Past and future developments in geopotential modeling. In Forsberg, R., Feissel, M., and Dietrich, R., editors, *Geodesy on the Move*. Springer-Verlag, Berlin New York.

[Rodriguez et al., 2006] Rodriguez, E., Morris, C. S., and Belz, E. J. (2006). A global assessment of the SRTM performance. *Photogrammetric engineering and remote sensing*, 72(3):249 – 260. ISSN: 0099-1112.

[Roman et al., 2009] Roman, D. R., Saleh, J., Wang, Y. M., Childers, V. A., Li, X., , and Smith, D. A. (2009). EGM08 comparisons with GPS/leveling and limited aerogravity over the United States of America and its Territories. In Huang, J. and Kotsakis, C., editors, *Newton's Bulletin: External Quality Evaluation Reports of EGM08*, number 4, pages 73–78. Bureau Gravimétrique International and International Geoid Service.

[Rózsa and Tóth, 2005] Rózsa, S. and Tóth, G. (2005). The determination of the effect of topographic masses on the second derivatives of gravity potential using various methods. In Tregoning, P. and Rizos, C., editors, *Dynamic planet: Monitoring and understanding a dynamic planet with geodetic and Oceanographic Tools*, volume 130 of *International Association of Geodesy Symposia*, pages 391–397, Cairns, Australia.

[Shen, 2009] Shen, W. (2009). Convergence of spherical harmonic series expansion of the Earth's gravitational potential. *Geo-Spatial Information Science*, 12:1–6.

[Sjöberg, 2011] Sjöberg, L. E. (2011). Quality Estimates in Geoid Computation by EGM08. *Journal of Geodetic Science*, 4(1):361–366.

[Torge, 2001] Torge, W. (2001). *Geodesy*. Walter de Gruyter, Berlin and New York, 3., completely rev. and extended ed. edition.

[Träger, 2004] Träger, L. (2004). Development of the gravimetric network on the territory of former Czechoslovakia. In Holota, P. and Slaboch, V., editors, *50 years of the Research Institute of Geodesy, Topography and Cartography*, volume 50(36), pages 131–141. VUGTK.

[Tscherning and Rapp, 1974] Tscherning, C. C. and Rapp, R. H. (1974). *Closed covariance expressions for gravity anomalies, geoid undulations, and deflections off the vertical implied by anomaly degree variance model.* The Ohio State University.

[Tsoulis, 1999a] Tsoulis, D. (1999a). *Analytical and numerical methods in gravity field modeling of ideal and real masses.* PhD thesis, Deutsche Geodätische Kommission, Reihe C, No 510, München.

[Tsoulis, 1999b] Tsoulis, D. (1999b). Multipole expressions for the gravitational field of some finite bodies. *Bolletino di Geodesia e Scienze Affini*, 58(4):353–381.

[Tsoulis, 2003] Tsoulis, D. (2003). Terrain modeling in forward gravimetric problems: a case study on local terrain effects. *Journal of applied geophysics*, 54:145–160.

[Tsoulis et al., 2009] Tsoulis, D., Novák, P., and Kadlec, M. (2009). Evaluation of precise terrain effects using high-resolution digital elevation models. *Journal of Geophysical Research*, (114).

[Vaníček et al., 2001] Vaníček, P., Novák, P., and Martinec, Z. (2001). Geoid, topography, and the Bouguer plate or shell. *Journal of geodesy*, 75(4):210–215. DOI: 10.1007/s001900100165.

[VUGTK, 2010] VUGTK (2010). Terminologický slovník zeměměřictví a katastru nemovitostí [in Czech]. [online], [cit. 29.8.2010], `http://www.vugtk.cz/slovnik/index.php`.

[Wenzel, 1999] Wenzel, G. (1999). *International School for the determination and use of the geoid – lecture notes*, chapter Global models of the gravity field of high and ultra-high resolution. International geoid service.

[WGS84, 2010] WGS84 (2010). World Geodetic System 1984. [online], last actualization 26. 3. 2010, [cit. 29. 8. 2010], `http://earth-info.nga.mil/GandG/wgs84/index.html`.

[Wild-Pfeiffer, 2008] Wild-Pfeiffer, F. (2008). A comparison of different mass elements for use in gravity gradiometry. *Journal of Geodesy*, 82:637–653. DOI 10.1007/s00190-008-0219-8.

[Zhu, 2007] Zhu, L. (2007). *Gradient modelling with gravity and DEM*. PhD thesis, The Ohio State University, Ohio.

[Zhu and Jekeli, 2009] Zhu, L. and Jekeli, C. (2009). Gravity gradient modeling using gravity and DEM. *Journal of Geodesy*, 83:557–567.

[Ågren, 2004] Ågren, J. (2004). *Regional geoid determination methods for the era of satellite gravimetry*. PhD thesis, Royal Institute of Technology, Stockholm.

[Ågren, 2009] Ågren, J. (2009). Evaluation of EGM2008 and PGM2007A over Sweden. In Huang, J. and Kotsakis, C., editors, *Newton's Bulletin:*

External Quality Evaluation Reports of EGM08, number 4, pages 99–109. Bureau Gravimétrique International and International Geoid Service.

List of authors publications

- Minár, J., Jenčo, M., Kadlec, M., Evans, I. S. et al. (submited 2011) Third-order geomorphometric variables (derivatives) – definition, computation and utilization. Submited to Journal of GIS.

- Pacina, J., Kadlec, M. (2010) Elementary forms recognition. Geomorfologický sborník, 9: 11. International conference: Stav geomorfologických výzkumů v roce 2010, Branná, 11.-13. 5. 2010. Praha : Univerzita Karlova, Přírodovědecká fakulta, 2010.

- Tsoulis D, Novák P, Kadlec M. (2009) Evaluation of precise terrain effects using high-resolution digital elevation models. Journal of Geophysical Research 114, B02404, doi:10.1029/2008JB005639.

- Kadlec M., Novák P. (2008) Porovnání metod pro výpočet terénních korekcí pro území střední Evropy. GEOS 2008 Conference Proceedings. Vydal VÚGTK v.v.i. Zdiby. Editor Milan Talich.

- Kadlec M., Kostelecký J. jr., Novák P. (2007) Databáze pro výpočty parametrů tíhového pole Země pro střední Evropu. Geodetický a kartografický obzor, č. 12/2007.

Cited publications

- Tsoulis D, Novák P, Kadlec M. (2009) Evaluation of precise terrain effects using high-resolution digital elevation models. Journal of Geophysical Research 114

  - C. Hirt, U. Marti, B. Bürki, W. E. Featherstone (2010) Assessment of EGM2008 in Europe using accurate astrogeodetic vertical deflections and omission error estimates from SRTM/DTM2006.0 residual terrain model data. Journal of Geophysical Research 115